

**University of Alberta**

Activation of Fluid Coke for Mercury Removal from Gases

by

Mihaela Bratu



A thesis submitted to the Faculty of Graduate Studies and Research  
in partial fulfillment of the requirements for the degree of

Master of Science  
in  
Chemical Engineering

Department of Chemical and Materials Engineering

Edmonton, Alberta  
Spring, 2008



Library and  
Archives Canada

Bibliothèque et  
Archives Canada

Published Heritage  
Branch

Direction du  
Patrimoine de l'édition

395 Wellington Street  
Ottawa ON K1A 0N4  
Canada

395, rue Wellington  
Ottawa ON K1A 0N4  
Canada

*Your file* *Votre référence*  
*ISBN: 978-0-494-45780-1*  
*Our file* *Notre référence*  
*ISBN: 978-0-494-45780-1*

**NOTICE:**

The author has granted a non-exclusive license allowing Library and Archives Canada to reproduce, publish, archive, preserve, conserve, communicate to the public by telecommunication or on the Internet, loan, distribute and sell theses worldwide, for commercial or non-commercial purposes, in microform, paper, electronic and/or any other formats.

The author retains copyright ownership and moral rights in this thesis. Neither the thesis nor substantial extracts from it may be printed or otherwise reproduced without the author's permission.

**AVIS:**

L'auteur a accordé une licence non exclusive permettant à la Bibliothèque et Archives Canada de reproduire, publier, archiver, sauvegarder, conserver, transmettre au public par télécommunication ou par l'Internet, prêter, distribuer et vendre des thèses partout dans le monde, à des fins commerciales ou autres, sur support microforme, papier, électronique et/ou autres formats.

L'auteur conserve la propriété du droit d'auteur et des droits moraux qui protègent cette thèse. Ni la thèse ni des extraits substantiels de celle-ci ne doivent être imprimés ou autrement reproduits sans son autorisation.

---

In compliance with the Canadian Privacy Act some supporting forms may have been removed from this thesis.

Conformément à la loi canadienne sur la protection de la vie privée, quelques formulaires secondaires ont été enlevés de cette thèse.

While these forms may be included in the document page count, their removal does not represent any loss of content from the thesis.

Bien que ces formulaires aient inclus dans la pagination, il n'y aura aucun contenu manquant.

  
**Canada**

## Abstract

The treatments required to convert fluid coke, produced by Syncrude Canada,, into high-surface areas activated coke and the ability of activated fluid coke to remove mercury from gas streams were studied. Physical activation methods, using mostly H<sub>2</sub>O-CO<sub>2</sub> mixtures at T≤800°C and P=100 to 620 kPa, were investigated. Surface areas >500 m<sup>2</sup>/g were obtained for some treatments; the average pore diameter for all activated cokes was about 2 nm. The Hg capture ability of activated fluid coke was evaluated using a pulse adsorption apparatus. Activated fluid coke particles with surface areas above 200 m<sup>2</sup>/g captured Hg from an argon stream at temperatures up to 150°C. Vapour impregnation of activated fluid coke with sulphur at temperatures above 400 to 600°C increased the amount of and temperature at which Hg was adsorbed. The optimum temperature for sulphur impregnation was 500°C; this sample strongly adsorbed Hg at temperature up to 250°C.

## **ACKNOWLEDGEMENTS**

I would like to express my deep gratitude to my supervisor Dr. Sieg E. Wanke for his guidance and financial support throughout this research. His patience and encouragement were essential for the accomplishment of this work. It was a privilege to work with him.

I would also like to thank to Dr. Long Wu who assisted me throughout my research. His advices and suggestions were a great help.

I extend my appreciation to the Advanced Coal Cleaning and Combustion Technology research group for facilitating the use of their equipment for the mercury adsorption experiments.

Finally I would like to thank the AERI/ASRA Industrial Research Chair for the financial support that made this thesis project possible. Scholarship support was also received from Chemical and Materials Engineering Department.

# TABLE OF CONTENTS

CHAPTER 1 INTRODUCTION .....	1
CHAPTER 2. LITERATURE REVIEW .....	4
2.1. Activated carbon - properties and production .....	4
2.1.1. Properties of activated carbon.....	4
2.1.2. Production of activated carbon .....	5
2.2. Syncrude fluid coke from Athabasca oil sands bitumen .....	8
2.2.1. Production of Syncrude fluid coke.....	8
2.2.2. Properties of Syncrude fluid coke.....	9
2.2.3. Applications of Syncrude fluid coke .....	11
2.3. Activated carbon from petroleum coke.....	11
2.4. Activated carbon for Hg control emissions.....	14
CHAPTER 3. MATERIALS, EQUIPMENT AND PROCEDURES.....	19
3.1. Materials.....	19
3.2. Treatment of fluid coke.....	19
3.2.1. Classification of fluid coke.....	19
3.2.2. Equipment and procedure for thermal treatment of fluid coke.....	20
3.3. Equipment and procedure used for mercury capture by fluid coke.....	25
3.4. Equipment and procedure used for sulfur impregnation of activated coke.....	32
3.5. Characterization methods.....	33
3.5.1. Particle size distribution analysis.....	33
3.5.2. Surface area, micropore volume and mesopore size distribution .....	34
3.5.3. SEM and EDX analyses.....	34

3.5.4. XPS analysis.....	35
3.5.5. Gas chromatography analysis.....	35
3.5.6. Sulphur analysis.....	36
CHAPTER 4. RESULTS OF FLUID COKE CHARACTERIZATION AND ACTIVATION.....	37
4.1. Properties of untreated fluid coke.....	37
4.2. Effect of treatment time on surface area, porosity and mass loss.....	49
4.3. Effect of treatment temperature on surface area, porosity and mass loss .....	55
4.4. Effect of treatment gas composition on surface area, porosity and mass loss ....	62
4.4.1. Activation of fluid coke with CO <sub>2</sub> /H <sub>2</sub> O mixture.....	62
4.4.2. Activation of fluid coke with N <sub>2</sub> /H <sub>2</sub> O mixture.....	66
4.4.3. Activation of fluid coke with mixtures containing O <sub>2</sub> .....	68
4.5. Effect of particle size on surface area, porosity and mass loss.....	69
4.6. Effluent gas composition.....	70
4.6.1. Effluent gas composition as a function of treatment temperature.....	71
4.6.2. Effluent gas composition as a function of treatment gas composition.....	75
CHAPTER 5. MERCURY ADSORPTION BY ACTIVATED FLUID COKE.....	78
5.1. Mercury adsorption as a function of surface area.....	79
5.2. Mercury adsorption as a function of sorption temperature .....	82
5.3. Mercury adsorption on H <sub>2</sub> -treated samples.....	87
5.4. Mercury adsorption on sulphur impregnated samples.....	88
CHAPTER 6. SUMMARY, CONCLUSIONS AND RECOMMENDATIONS.....	96
References.....	100

APPENDIX A.....105

## LIST OF TABLES

Table 2-1. Properties of Syncrude coke from stockpiles.....	9
Table 3-1. Identification designations for various fluid coke samples.....	20
Table 4-1. Particle size distribution from sieve analysis for Coke 1 and Coke 2.....	37
Table 4-2. Comparison of surface areas and pore volumes for Coke 1 and Coke 2 size fractions .....	48
Table 4-3. Properties of activated fluid coke as a function of treatment time .....	49
Table 4-4. Properties of activated fluid coke as a function of treatment temperature.....	55
Table 4-5. Equilibrium constants for main overall reactions during activation of coke.....	58
Table 4-6. Results of activation with N <sub>2</sub> /H <sub>2</sub> O mixture.....	66
Table 4-7. Results of activation with N <sub>2</sub> /O <sub>2</sub> /H <sub>2</sub> O mixture.....	69
Table 4-8. Surface area and pore volume of different size fractions of Coke 2 before and after activation.....	70
Table 5-1. Activation conditions and properties of activated carbons.....	83
Table 5-2. The influence of heat treatment in argon of activated carbon on mercury adsorption .....	84
Table 5-3. XPS results for various activated and cross-sectioned fluid coke samples.....	86
Table 5-4. Mercury adsorption results of activated and H <sub>2</sub> -treated activated coke samples .....	88



Table 5-5. Molar composition of saturated sulphur vapour at various temperatures.....	94
---	----

## LIST OF FIGURES

Figure 3-1. Schematic diagram of the apparatus used for thermal treatment of fluid coke .....	21
Figure 3-2. Pressure and temperature profiles for Run IC10494 showing typical various in pressure and temperature with treatment time.....	23
Figure 3-3. Pressure and temperature profiles for Run MB10465 showing above average variations in pressure and temperature with treatment time.....	24
Figure 3-4. Pressure and temperature profiles for Run IC10473 showing pressure and temperature spikes during treatment.....	24
Figure 3-5. Schematic diagram of the apparatus used for mercury capture by fluid coke.....	25
Figure 3-6. Output of the Hg detector for activated coke IC10481 (BET SA= 489 m <sup>2</sup> /g).....	27
Figure 3-6a Expanded output of the Hg detector for activated coke IC10481 (BET SA= 489 m <sup>2</sup> /g).....	27
Figure 3-7. Output of the Hg detector for activated coke IC10490 (BET SA = 22.4 m <sup>2</sup> /g).....	28
Figure 3-7a. Expanded output of the Hg detector for activated coke IC10490 (BET SA = 22.4 m <sup>2</sup> /g).....	28
Figure 3-8. Calibration curves of mercury detector done on Sept 20/06 and Oct 24/06.....	30
Figure 3-9. Calibration curves of mercury detector done on Nov 20/06 and Nov 24/06.....	31

Figure 3-10. Calibration curves of mercury detector done on Jan 09/06 and Jan 19/06.....	31
Figure 3-11. Schematic diagram of the apparatus used for sulphur impregnation of activated fluid coke .....	32
Figure 4-1. Particle size distribution for smaller size fractions of Coke 1.....	38
Figure 4-2. Particle size distribution for larger size fractions of Coke 1.....	38
Figure 4-3. Particle size distribution for smaller size fractions of Coke 2.....	39
Figure 4-4. Particle size distribution for larger size fractions of Coke 2.....	39
Figure 4-5. Scanning electron microscope images of Coke 101 (<53µm fraction).....	41
Figure 4-6. Scanning electron microscope images of Coke 101 (100-125µm fraction) .....	41
Figure 4-7. Scanning electron microscope images of Coke 105 (100-125µm fraction).....	42
Figure 4-8. Scanning electron microscope images of Coke 105 (100-125µm fraction).....	42
Figure 4-9. Scanning electron microscope image of Coke 101 (<53µm fraction) and EDX line scan of sulphur concentration.....	43
Figure 4-10. Scanning electron microscope image of Coke 104 (100-125µm fraction) and EDX line scan of sulphur concentration.....	43
Figure 4-11. Scanning electron microscope image of Coke 105 (125-180µm fraction) and EDX line scan of sulphur concentration.....	44
Figure 4-12. Scanning electron microscope image of Coke 107 (>250µm fraction) and EDX line scan of sulphur concentration.....	44

Figure 4-13. Sulphur content as a function of coke particle size for Coke 1 and Coke 2.....	45
Figure 4-14. Carbon content as a function of coke particle size for Coke 1 and Coke 2.....	45
Figure 4-15. Carbon/Sulphur mass ratio as a function of particle size for Coke 1 and Coke 2.....	46
Figure 4-16. Sulphur content as a function of coke mass used for analysis, for Coke 1.....	47
Figure 4-17. Effect of treatment time on surface area at different treatment times in CO <sub>2</sub> (flow rate: 100 ml/min).....	50
Figure 4-18. Effect of treatment time on surface area using different activating agents.....	51
Figure 4-19. Effect of treatment time on pore volume.....	52
Figure 4-20. Relationship between total pore volume and surface area for Coke 104 activated for various times.....	53
Figure 4-21. Relationship between mass loss and surface area .....	54
Figure 4-22. Effect of treatment temperature on the surface area (treatment time was 4h unless indicated otherwise).....	56
Figure 4-23. Effect of treatment temperature on the pore volume (micro and meso) (treatment time was 4h unless indicated otherwise).....	58
Figure 4-24. Effect of treatment temperature on the mass loss (treatment time was 4h unless indicated otherwise).....	59
Figure 4-25. Relationship between pore volume (micro and meso) and surface area (treatment time was 4h unless indicated otherwise).....	60

Figure 4-26. Relationship between mass loss and surface area (treatment time was 4 h unless indicated otherwise).....	61
Figure 4-27. Effect of H <sub>2</sub> O flow rate on the surface area and mass loss (treatment conditions: 800°C, 345 kPa).....	63
Figure 4-28. Effect of H <sub>2</sub> O flow rate on the pore volumes (treatment conditions: 800°C, 345 kPa).....	64
Figure 4-29. Relationship between the pore volume and surface area (treatment conditions: 800°C, 345 kPa, flow rate from 2.3 to 18 ml/h).....	64
Figure 4-30. Effect of H <sub>2</sub> O flow rate on the CO concentration (treatment conditions: 800°C, 345 kPa).....	65
Figure 4-31. Effect of H <sub>2</sub> O flow rate on the CH <sub>4</sub> and H <sub>2</sub> S concentrations (treatment conditions: 800°C, 345 kPa).....	66
Figure 4-32. Comparison of the effects of N <sub>2</sub> /H <sub>2</sub> O and CO <sub>2</sub> /H <sub>2</sub> O mixtures on the surface area of activated fluid coke.....	67
Figure 4-33. Comparison of the effects of N <sub>2</sub> /H <sub>2</sub> O and CO <sub>2</sub> /H <sub>2</sub> O mixtures on the pore volume of activated fluid coke.....	67
Figure 4-34. Variations in CO concentration in effluent gas as a function of treatment temperature (composition on a H <sub>2</sub> and H <sub>2</sub> O-free basis).....	72
Figure 4-35. Variations in CO <sub>2</sub> concentration in effluent gas as a function of treatment temperature (composition on a H <sub>2</sub> and H <sub>2</sub> O-free basis).....	72
Figure 4-36. Variations in CH <sub>4</sub> concentration in effluent gas as a function of treatment temperature (composition on a H <sub>2</sub> and H <sub>2</sub> O-free basis).....	73
Figure 4-37. Variations in H <sub>2</sub> S concentration in effluent gas as a function of treatment temperature (composition on a H <sub>2</sub> and H <sub>2</sub> O-free basis).....	73

Figure 4-38. Average effluent composition (on H <sub>2</sub> and H <sub>2</sub> O-free basis) as a function of water feed rate (T=760°C, P=345 kPa, and CO <sub>2</sub> feed rate=188 ml/min) .....	76
Figure 4-39. Average effluent gas composition (on H <sub>2</sub> and H <sub>2</sub> O-free basis) as a function of water feed rate without any CO <sub>2</sub> in the feed (T=760°C, P=345 kPa and N <sub>2</sub> feed rate 42.5 mL/min).....	77
Figure 5-1. Effect of surface area on mercury adsorption by activated fluid coke.....	79
Figure 5-2. Results of repeat mercury capture experiments.....	81
Figure 5-3. Variation of mercury adsorption capacity at 140°C as a function of surface area.....	82
Figure 5-4. Mercury adsorption from first injected pulse as a function of adsorption temperature.....	83
Figure 5-5. XPS spectrum of oxygen 1s line for Sample SS10421.....	87
Figure 5-6. XPS spectrum of oxygen 1s line for Sample SS10421.....	87
Figure 5-7. Sulphur content of sulphur-impregnated activated fluid coke (IC10474-Sxxx as a function of impregnation temperature compared to sulphur content of unactivated (Coke 104) and activated fluid coke (IC10474).....	89
Figure 5-8. Variation of sulphur vapour pressure with temperature .....	90
Figure 5-9. Effect of sulphur addition on Hg capture as a function of sorption temperature (for samples IC10474-Sxxx).....	91
Figure 5-10. Mercury adsorption capacities as a function of adsorption temperature for sulphur-treated samples of activated fluid coke IC10474.....	92

## Chapter 1. Introduction

Mercury and its compounds are well known as ones of the most toxic pollutants due to its toxic effects on the environment and human health that have attracted public health and environmental attention recently. Human exposure to mercury can lead to serious health problems such as paralysis, urinary and intestinal complications, dysfunction of the central nervous system and in severe cases of intoxication, death (Nabais et al., 2006).

Although emissions of mercury occur naturally, major mercury pollution comes from anthropogenic activities. Two types of combustion processes that are major sources of mercury emissions are municipal waste combustors and coal-fired power plants. Mercury is a natural constituent of coal. It is reported that the mean mercury concentrations of Hg in coal ranges from 0.12 to 0.28  $\mu\text{g/g}$  (Carpi, 1997). When the coal is burned, mercury is released from the feed material to the flue gases in the form of elemental Hg and oxidized Hg. The concentration of mercury in flue gas is correlated with the mercury speciation, the flue gas temperature and the type of air pollution control device employed at the facility.

Mercury emission control measures in coal fired power plants are mainly based on the existing air pollution devices which include multiple cyclones, electrostatic precipitators, fabric filters, wet scrubbers, and wet and dry flue gas desulphurization systems. Performance of these control technologies depend on the differences in coal, plant design, and operation. While these devices are able to capture oxidized forms of Hg to some extent, they showed low efficiency for the control of elemental Hg emissions. (Liu et al., 2000).

The Canadian Council of Ministers of the Environment (CCME) is committed to reducing mercury releases to the environment. Therefore, in October 2006 CCME set mercury Canada-wide Standards for mercury emissions from coal-fired electric power plants. The goal is to reduce the mercury emissions from Canadian coal-fired power plants by 60% until 2010 and an 80% reduction by 2018.

New technologies have been developed for the control of mercury emissions. Among them, activated carbon adsorption is a technology that offers great prospective for

the control of gas-phase mercury emissions. Injection of activated carbon upstream of a particulate-control system has the potential of providing a low-cost option for control of mercury emissions from flue gases in coal-fired power plants. In carbon injection processes, a large carbon/mercury ratio is required to achieve Hg removal efficiency higher than 90%. To reduce the operating cost of the carbon injection process, it is required a high efficient adsorbent which can operate at a smaller C/Hg ratio or a lower-cost sorbent (Hsi et al, 1998). Another option is the use of specially treated activated carbons i.e. bromine containing activated carbons. One of the problems with these special activated carbons is their cost. A potential lower-cost alternative to activated carbon is activated petroleum coke.

Syncrude Canada Ltd. produces fluid petroleum coke as a result of the bitumen upgrading process, in its oil sands plant in northern Alberta. Fluid coke is a by-product, which is presently discharged. Fluid coke has a high calorific content but due to its high sulfur content, the use of this fluid coke as solid fuel would result in SO<sub>2</sub> emissions in excess of environmentally acceptable levels. On the contrary, its high carbon content and low inorganic and volatile matter makes it an excellent precursor to activated carbon. Its high sulfur content might have a significant impact on the use of generated activated carbon for Hg removal. This fluid coke is abundant and readily available, at practically no cost, which might positively affect the price of final product.

Fluid coke can be converted into activated carbon through physical or chemical activation. Physical activation involves devolatilization of raw material followed by activation, where the carbonaceous char is partially gasified with an oxidizing agent (i.e. CO<sub>2</sub>, steam, O<sub>2</sub>) in order to develop an adequate porous structure. Chemical activation involves the impregnation of the precursor with a chemical agent (i.e. alkaline hydroxides, ZnCl<sub>2</sub>, H<sub>3</sub>PO<sub>4</sub>) followed by heat treatment. Literature indicates that petroleum coke can be activated through both methods, yielding to activated carbons with high surface areas and excellent sorption properties from liquid phase as well as from gas phase.

The primary objectives of this thesis are to examine the production of activated carbon from Syncrude fluid coke and the feasibility of using this activated fluid coke for elemental Hg removal. The use of physically activated fluid coke for the removal of



mercury from gases has not been studied previously. In Chapter 2, a literature review on production of activated carbon from petroleum coke and applicability of activated carbon on Hg removal are presented. Chapter 3 provides the details on materials and experimental setup for thermal treatment of fluid coke and for Hg capture, respectively. The characterization techniques used to determine the properties of raw and activated coke are also covered in this chapter. Experimental results of fluid coke activation and the effect of treatment time, treatment temperature, treatment gas composition and effect of particle size on the properties of activated coke are the main subjects of Chapter 4. In Chapter 5, the results from Hg capture experiments are discussed. Also Hg removal capacity of sulfur-impregnated activated fluid cokes are presented in this chapter. Conclusions and recommendations are given in Chapter 6.

## **Chapter 2. Literature Review**

A brief review of activated carbons and manufacture of activated carbons is presented in this chapter. This is followed by a discussion of Syncrude fluid coke and use of activated carbons and coke for the capture of mercury from gas streams.

### **2.1. Activated carbon – properties, production and applications**

#### **2.1.1. Properties of activated carbon**

Activated carbon (AC), also called active carbon or activated coal, or activated charcoal, is a general term, which covers processed carbon materials with well developed porous structures and high internal surface areas. They consist principally of carbon (87-97%), but also contain such elements as hydrogen, oxygen, sulphur and nitrogen, as well as various mineral substances either originating from the raw material used or added during its manufacture (Jankowska et al., 1991).

Activated carbons are excellent adsorbents used in the treatment of drinking, domestic and industrial waste water for the removal of color, odor, taste and undesirable organic impurities, in solvent recovery, for air purification from inhabited spaces, in air pollution control, and for the purification of many chemical, food and pharmaceutical products, as well as for a variety of gas-phase applications (Bansal et al., 1988). The most important applications of activated carbon are the purification of air and water; large quantities of ACs are used in these applications and significant increases in their use is anticipated in these areas in the future.

The excellent adsorbent properties of ACs are attributed to their large surface area and a high degree of surface reactivity. The surface area is generally greater than 400 m<sup>2</sup>/g and often exceeds this value significantly reaching 1000-2500 m<sup>2</sup>/g (Jankowska et al., 1991). Most of this surface area is contained within micropores which have effective diameters of less than 2 nm. A particle of activated carbon is made up of a complex network of pores, with pore diameter ranging from 0.3 to several thousands nanometers. According to Dubinin (1966), pores can be classified in micropores ( $d < 2$  nm), mesopores ( $2 < d < 50$  nm) and macropores ( $d > 50$  nm); this classification of pores has been adopted by the Union of Pure and Applied Chemistry. Most of the adsorption takes

places in micropores, which represents ~90-95% of the total surface area of an activated carbon. However, meso and macropores play a very important role in the adsorption process since they serve as passage for the adsorbate into the micropores (Menendes-Diaz and Martin-Gullon, 2006).

An adequate pore structure is a necessary but not a sufficient condition for the optimization of the adsorption capacity of activated carbon. The nature and the amount of surface groups present on the carbon surfaces play an important role in the adsorption process. The presence or the absence of surface groups, formed by heteroatoms bonded to the carbon atoms of activated carbon, determine the chemical properties of activated carbon (e.g. hydrophobic/ hydrophilic character, acidic/basic character), and influence the interactions of activated carbon with different adsorbates. Therefore, by modifying the nature and the amount of surface functional groups activated carbon can be tailored for specific applications, e.g. basic carbons are preferred for adsorption of acidic molecules and acidic carbons for basic compounds (Menendes-Diaz and Martin-Gullon, 2006).

Oxygen containing surface groups are, by far, the most common in carbons (Bansal et al., 1988). They can originate from the starting material from which a particular activated carbon is produced or can be introduced during the manufacture process itself (e.g. during activation by oxidizing gases such as water vapor and air). Hydrogen-containing species are also found as chemisorbed water, as part of the surface groups such as carboxylic groups, phenolic groups, amines, or hydrogen directly bonded to carbon atoms. Treatment with ammonia or urea can be used to introduce nitrogen containing groups. Sulphur can be naturally present in carbon materials or can be introduced by the reaction of carbon materials with sulphur containing compounds such as:  $\text{H}_2\text{S}$ ,  $\text{CS}_2$  or  $\text{SO}_2$ . However, not all these groups are present at the same time on a carbon surface (Bansal et al., 1988).

### ***2.1.2. Production of activated carbon***

The production of activated carbon consists of two basic steps: carbonization followed by activation. Carbonization involves thermal decomposition of carbonaceous material, at temperatures below  $800^\circ\text{C}$ , eliminating non-carbon species and producing a

fixed carbon mass and an incipient porous structure (Bansal et al. 1988). Due to the evolution of the volatile matter, the material becomes richer in carbon and initial porous structure develops. This step is critical in the case of raw materials with a high content of volatile matter.

The parameters that determine the quality and the yield of the carbonization product are: the rate of heating, the final temperature, the soaking time at the final temperature, and the nature of the raw material. Among these, the heating rate is very important in the development of the final structure of the carbonization product. A high heating rate produces a very quick devolatilization, giving rise to a product with a well developed meso and macropore network, a low density and a low abrasion and hardness index. On the other hand, a low heating rate favors the formation of micropores and consequently, both density and hardness are higher than in the case of high heating rate (Menendes-Diaz and Martin-Gullon, 2006). In industrial processes, carbonization is carried out in direct heated kilns, in an oxidant atmosphere (steam with exhausted air from burners, operated at very low stoichiometric ratios), at low heating rate, at temperatures of 400-600°C, and long soaking times (Jankowska et al. 1991).

Activation has the objective to enhance the pore volume and to enlarge the diameters of the pores created during carbonization and to create new porosity. The factors that have the greatest influence on the properties of activated carbon obtained are: temperature of activation and the reactivity of the carbonaceous material towards the activating agent.

At low temperatures, the rate of chemical reaction of carbon with the oxidizing agent is small. With increases in the oxidation temperature, the rate of the chemical reaction increases and then the overall rate of the process becomes limited by the rate of transport of the oxidizing agent into the particle. At very high temperatures, the oxidation reaction rate becomes so high, that the whole oxidizing agent reacts with carbon on the external surface of the granule. In such a case significant losses of the material occur due to superficial burn-off, and a porous structure is not formed. The rate of oxidation process is limited by the reactivity of the initial carbonaceous material towards the oxidizing agent. The greater the reactivity of the substrates the lower the optimal temperature of the process at which uniform formation of pores is observed (Jankowska et al, 1991).

The activation methods are broadly divided into two main types: physical activation and chemical activation. Physical activation is carried out at temperatures between 800 and 1000°C, in the presence of suitable oxidizing agents such as H<sub>2</sub>O, CO<sub>2</sub>, air or any mixture of these gases. The gases react with the carbon atoms and remove some of the mass of the internal surface of the solid, in the incipient micropores, creating a well developed microporous material. The most reactive agent is oxygen, while the lowest reactive is CO<sub>2</sub> (Menendes-Diaz and Martin-Gullon, 2006). Activation of carbonized char with oxygen is highly exothermic, and the reaction temperature is very difficult to control. Consequently, oxygen activation is not applied at an industrial scale (Bansal et al., 1988).

Steam activation is the most widely used method for producing activated carbons in the world. Direct fire-heated systems are used in steam activation. At industrial scale, in a continuous operation, both steam and air are fed into the kiln. As steam activation is endothermic, the heat required is provided by the exothermic gas phase reaction of CO and H<sub>2</sub> (steam gasification products) with the appropriate amount of air. Air must be fed into the reactor at different reactor points in order to prevent carbon-oxygen gasification, so that they react only in gas phase. In this way, heat supplied by gas phase oxidation can balance the steam gasification requirements, and no fuel is needed by the fire burners except for the non-stationary starting operations (Menendes-Diaz and Martin-Gullon, 2006).

The main reactions occurring during activation are:



Activation with CO<sub>2</sub> is more endothermic than with steam and therefore requires a higher temperature. In actual industrial processes, the activating agent used is generally

flue gas to which a certain amount of steam is added so that a combined activation with steam and CO<sub>2</sub> can occur (Bansal et al., 1988).

A second commercial route for producing activated carbon involves the reaction of the carbon precursor with a chemical reagent and is known as chemical activation. The reagents that have been most used by industry are ZnCl<sub>2</sub>, H<sub>3</sub>PO<sub>4</sub> and KOH. Each reagent produces a different porosity in the carbon precursor. The common feature of these activating agents is that they are dehydrating agents which influence pyrolytic decomposition and inhibit formation of tar (Bansal et al., 1988).

Chemical activation is usually carried out at temperatures between 400 and 800°C. The starting material is impregnated with the activating agent in the form of concentrated solution. The chemical impregnated material is then heated to the desired temperature in an inert atmosphere. The product is cooled and washed to remove the activating agent, which is recycled. The feasibility of chemical activation processes is strongly dependent on efficiently recovering the reagent for recycling. This involves subsequent leaching stages, followed by an additional operation consisting of drying the washed carbon (Menendes-Diaz and Martin-Gullon, 2006).

Any carbonaceous material, with high carbon content, a low inorganic content, cheap and readily available can be used as an activated carbon precursor. Activated carbon can be obtained from a variety of raw materials such as: wood, nut shells, fruit stones, peat, sawdust, coals, petroleum coke, and various kinds of natural coals.

## **2.2. Syncrude fluid coke from Athabasca oil sands bitumen**

### ***2.2.1. Production of Syncrude fluid coke***

Coke is a by-product of the oil refining and bitumen upgrading. Fluid coke is obtained in the process of bitumen upgrading to synthetic crude oil employed by Syncrude Canada, in Alberta. Currently, about 5,000 tonnes of fluid coke are produced per day and this amount is expected to increase, due to the increasing production of synthetic crude oil. The fluid coking process is a continuous process. A fluid coking unit consists primarily of two vessels: the coking vessel and the burner vessel. The coke particles are heated up in the burner vessel after which they are recirculated to the coking

vessel to supply heat. Bitumen, previously pre-heated is sprayed into the fluidized bed of fluid coke particles in the coking vessel, which operates at temperatures  $\geq 500^{\circ}\text{C}$ . Bitumen is thermally cracked into lighter fractions which are recovered as liquid and vapor products, and the fluid coke particles get coated with layers of coke as they are recirculated through the coker. Part of the coke is continuously withdrawn from the coker vessel and transferred to the burner vessel for partial combustion. To maintain a constant mass of coke in the burner, part of the coke is withdrawn at the bottom of the burner and transported to the storage area (Furimsky, 2000).

### ***2.2.2. Properties of Syncrude fluid coke***

Fluid coke is a black, fine granular material, consisting of approximately spherical particles ranging in size from a few microns to 2 cm with a bulk specific gravity of 0.95 and a particle specific gravity of 1.6; Syncrude fluid coke is not soluble in water or oil (Bérubé, 2006). The study on leachability of coke samples taken from stockpiles, confirmed that the fluid coke is virtually non-leachable with respect to the regulated elements, as well as the volatile matter (Chung et al., 1996). The results of proximate and ultimate analysis of the coke are summarized in Table 2-1. The dates in brackets indicate years during which the coke was produced.

Analysis of Syncrude fluid coke from stockpiles indicates a uniform composition of the coke over more than 15 years of operation. Very little variation was observed for the carbon content, sulphur content and ash content. Fluid coke derived from oil sands has high sulphur content in comparison with the sulphur content of the coke obtained from conventional oil (~2%). Most of the sulphur is of organic type, and is buried in the coke matrix as a result of prolonged exposure at high temperature during the coking process. Fluid coke has a high calorific value of 33 MJ/kg, comparable with that of high rank coals, such as anthracites (Majid and Sparks, 1999).

Scanning electron microscopy reveals a smooth, non-porous surface (Jack et al., 1979). It has a graphite-like structure, which results from prolonged exposures at temperatures  $\geq 500^{\circ}\text{C}$ . BET surface areas, using nitrogen adsorption, increased from 1 to 22  $\text{m}^2/\text{g}$ , with decreasing particle size, reaching the maximum at a particle diameter of 69

µm (Fairbridge et al., 1986; 1987). The surface area of particles smaller than 69 microns does not increase with decreasing size, probably due to a different fractal dimension of the small particles compared to the large ones. The fractal dimension of a surface is a measure of the ability of a solid surface to fill a three-dimensional volume: a higher value of fractal dimension indicates a more irregular surface (Fairbridge et al., 1986).

Table 2-1. Properties of Syncrude coke from stockpiles (wt. %) (Chung et al., 1996)

Coke (years)	1(79/80)	2(80/82)	3(82/83)	4(83/85)	5(85/95)
<b>Proximate Analyses</b>					
Moisture	0.44	0.60	0.50	0.69	0.25
Ash	5.40	7.21	5.18	7.52	4.83
Volatiles	4.85	5.11	6.23	6.10	4.99
Fixed carbon	89.31	87.08	88.09	85.69	89.95
<b>Ultimate Analyses</b>					
Carbon	82.73	80.73	81.80	80.94	83.74
Hydrogen	1.72	1.63	1.66	1.56	1.77
H/C	0.25	0.24	0.24	0.23	0.25
Nitrogen	1.75	1.70	1.98	1.73	2.03
Sulphur	6.78	6.63	6.84	6.15	6.52
Oxygen	1.18	1.50	2.04	1.41	0.88

Syncrude fluid coke is difficult to gasify. It was determined that long residence times or temperatures higher than 1000°C were required to achieve high carbon conversion (Furimsky, 1985). The coke gasification rate is affected by the nature and concentration of the active sites and by the accessibility to the active sites, in other words by the surface structure of the coke. The rate of oxygen adsorption may be directly related to the accessibility to the active sites. Oxidation rate was shown to increase with decreased coking temperature, soaking time and particle size (Fairbridge et al.1986).



### **2.2.3. Applications of Syncrude fluid coke**

Currently, fluid coke made by Syncrude is stockpiled on the site. The high sulphur content and low reactivity have prohibited its use as a source of energy generation by direct combustion or gasification. Various desulphurization processes such as: steam treatment, alone or in presence of alkali compounds, hydrodesulphurization, and preoxidation followed by hydrodesulphurization, and impregnation with alkali compounds, carbonates or sulphides prior to combustion, have been reported in the literature. Hall et al. (1982) found that impregnation of fluid coke with small quantities of NaOH resulted in increased hydrodesulphurization of the product. Wet and dry impregnation of fluid coke with  $\text{CaCO}_3$ ,  $\text{Ca(OH)}_2$ ,  $\text{CaO}$ ,  $\text{NaHCO}_3$ , prior to combustion has been studied by Majid et al. (1988) and Otaigbe and Egiebor (1991). The results indicated that treatment with sulphur sorbents resulted in high sulphur removal, at temperature above  $600^\circ\text{C}$ . Ityokumbul (1994) has shown that molten caustic leaching of fluid coke at relatively low temperatures ( $200\text{--}400^\circ\text{C}$ ) also reduced the sulphur content of fluid coke. However, none of these processes have been proven feasible for large-scale application.

Gasification of fluid coke in fixed and fluidized beds has been evaluated. Because of its low reactivity, high severity conditions are required to achieve high gasification conversion. Commercial gasification is being delayed because of the availability of natural gas on the site of the upgrading plants. The current technologies cannot compete with the price of natural gas in the region (Furimsky, 1998).

### **2.3. Activated carbon from petroleum coke**

Production of activated carbon from petroleum coke has been investigated by several groups, mostly on delayed coke, rather than fluid coke, and involved chemical activation as the main route of activation.

Very high surface areas were obtained by chemical activation of petroleum coke, using KOH as activating agent, at a KOH/carbon mass ratio varying from 1 to 4 and final activation temperature of  $800^\circ\text{C}$ . O'Gady et al. (1986) reported a surface area as high as

3400 m<sup>2</sup>/g, while Ottawa et al. (1993) obtained an activated coke with an area of 3100 m<sup>2</sup>/g. In both cases, the activation was carried out in two heating steps: first the impregnated material was heated up to 400-500 °C, for dehydrating purpose. The product was next pyrolysed at 800-900 °C, in an inert atmosphere. The product was washed to remove the excess KOH and containing salts. The activated cokes obtained exhibited excellent adsorptive capacities, suitable for numerous applications, such as potable and waste water treatment. According to Ottawa et al. (1993), intercalation or enlargement of the carbon matrix by the potassium compounds in the course of forming carbonate, during activation process, may act as spacer to create the pores.

A high surface area activated coke was reported by Lee et al. (2000), using a delayed petroleum coke with 7 wt.% sulphur content, as starting material. The effects of NaOH and KOH on the development of surface area were evaluated. Activating agent/coke ratio was varied from 2 to 4, and the final temperature was 400-600 °C. It has been found that KOH was more effective for the development of surface area than NaOH. Surface areas up to 1980 m<sup>2</sup>/g were obtained during activation with KOH, in comparison with 1350 m<sup>2</sup>/g, obtained by NaOH activation. They claimed that desulphurisation plays a role in the development of surface area. The breakage of C-S bonds followed by the evolution of sulphur from carbon matrix leads to the formation of pores and sites where activation can occur. They reported that surface area did not increase significantly until the residual sulphur content was reduced to < 0.1% S. (Lee et al., 2000).

Surface areas between 1000-1750 m<sup>2</sup>/g were obtained by Wu et al. (2005) during activation of two petroleum cokes when KOH was used as the activating agent. They also evaluated the affect of physical activation and co-activation (KOH/water vapour) on the development of surface area. KOH/carbon ratio was 2, and activation temperature was 800 °C. Activated carbon with a surface area less than 1000 m<sup>2</sup>/g was obtained by physical activation, while a surface area as high as 3000 m<sup>2</sup>/g was obtained with the co-activation method. The co-activation method was more efficient in terms of surface area, but a much lower yield (29%) compared to chemical activation (63%) was obtained (yield is defined as the ratio of the mass of the activated coke to the initial mass of carbonaceous material). They claimed that the presence of Ni and Cr species in the coke

matrix may play a role in the development of surface area, acting as catalysts for the reaction between carbon and activation agents. More research has to be done to confirm this supposition.

Effect of carbonization, prior to KOH activation was studied by Chunlan et al. (2005). Petroleum coke was heated up to different temperatures: 500, 800 and 1200°C, followed by the activation, at KOH/carbon ratio of 3 and temperature of 730°C. The highest surface area was obtained from raw petroleum coke (1997 m<sup>2</sup>/g), while the lowest surface area was obtained from the petroleum coke carbonized at 1200°C (12 m<sup>2</sup>/g). They stated that alcoholic, phenolic, carboxylic and hydroxyl groups on the surface of raw coke might serve as 'active sites' in the chemical activation with KOH. Depleting the coke surface of these functional groups resulted in a less porosity development in activated product.

Very low surface areas were obtained when NaOH, H<sub>3</sub>PO<sub>4</sub> and ZnCl<sub>2</sub> were used as activating agents by Zamora et al. (2000). The starting material was petroleum coke with 6 wt.% sulphur. Activating agent/carbon ratio was 1, final temperature was 700°C. Surface areas of 16.3 – 35.4 m<sup>2</sup>/g were obtained, with NaOH being the most efficient activating agent.

Physical activation of Syncrude fluid coke, containing 6 mass % sulphur, with steam was used by DiPanflio and Egiebor (1996) to obtain an activated carbon with a maximum surface area of 318 m<sup>2</sup>/g. They also report results of chemical activation of fluid coke impregnated with KOH. KOH treated coke was prepared by mixing a specific quantity of raw coke with a solution of KOH, in which KOH content was equivalent to 4 wt.% of the coke used; the activation temperature was 850°C. Surface area increased with the increasing activation time, for the untreated raw coke. Addition of KOH did not have any effect on the development of surface area but increased the activation rate.

Delayed petroleum coke from Suncor Canada Ltd. has been activated, following the physical activation path, using steam, as activating agent, at temperature of 850°C (Shawwa et al., 2001). Unfortunately, no surface areas were reported. The quality of the product was determined by liquid-phase adsorption of methylene blue.

## 2.4. Activated carbon for Hg emissions control

Mercury is a toxic pollutant that has attracted significant public health and environmental attention recently. Although air emissions of mercury occur naturally, major mercury pollution comes from anthropogenic activities. Coal-fired power plants have been identified as the largest source of mercury emissions in USA and Canada. In USA, the amount of mercury released annually from coal-fired power plants is ~ 50 tonnes (Pavlish et al., 2003). In Canada, it is reported that in 2003 the coal-fired power plants emitted an estimated 2,695 kg of mercury from an estimated 3,725 kg of mercury in coal burned. The Canada-wide standard for mercury emissions includes caps on mercury emissions from new and existing coal-fired power plants so that 60% of mercury will be captured by 2010 (Canadian Council of Ministers of the Environment, 2006). Alberta is the largest emitter of mercury from coal fired power plants because it produces more electricity from coal-fired plants than other provinces. According to the Canada-wide standard for mercury emissions, Alberta must reduce mercury emissions from estimated 1,180 kg/yr in 2005 to 590 kg/yr in 2010.

Hg emissions from coal-fired power plants exist in three typical forms: elemental mercury ( $\text{Hg}^{\circ}$ ), oxidized mercury, ( $\text{Hg}^{2+}$ ) such as  $\text{HgCl}_2$  and  $\text{HgO}$ , and particle-bound mercury,  $\text{Hg}(p)$ . In general, the variability in Hg concentration and speciation depends on many factors, including mercury concentration in the coal, flue gas temperature, chemical constituents present in flue gas and type of air pollution control equipment employed (Carpi, 1996). Test data show that low-rank coals (sub bituminous and lignite coals) produce primarily elemental mercury, which is more challenging to control (Pavlish et al., 2005).

During combustion, at temperatures of 1200-1400°C in the combustion zone, mercury in coal is vaporized and exists as  $\text{Hg}^{\circ}$  (Hall et al., 1991). As the flue gas temperature decreases,  $\text{Hg}^{\circ}$  is partially oxidized to  $\text{Hg}^{2+}$ , by reacting with  $\text{HCl}$ ,  $\text{Cl}_2$ ,  $\text{NO}_2$  or  $\text{O}_2$  present in flue gas. Oxidation of mercury to chloro-mercury compounds will occur to a substantial degree in the presence of high concentrations of  $\text{HCl}$  and  $\text{Cl}_2$  (Hall et al, 1991). Many forms of  $\text{Hg}^{2+}$  are highly soluble in water (e.g.  $\text{HgCl}_2$  : 6.9 g/L at 25°C) and

are likely to be removed by precipitation or may exist in part adsorbed to particulate carbon in the exhaust stream (Capri, 1996). Hg<sup>0</sup> is difficult to remove from the flue gas streams due to its high equilibrium vapour pressure ( 0.25 Pa at 25°C) and low solubility in water ( $6 \times 10^{-5}$  g/L, at 25°C) (Hsi et al., 1998).

Current technologies for mercury emissions control in coal-fired power plants are based on the existing air pollution control devices, which include cold and hot electrostatic precipitators, fabric filters, wet and dry flue gas desulphurization systems, wet scrubbers, or combination of these. There is no single technology that can be broadly applied. Combinations of available methods may be able to provide up to 90% control for some plants but not others. This is due to factors, such as operating conditions, flue gas composition, mercury content in coal and differences in coal rank (Pavlish et al., 2003).

While adsorption by raw activated carbon can be effective in removing mercury at high sorbent /mercury ratios, impregnation of functional groups, can significantly improve the adsorption capacity. Chemically impregnated activated carbons were found to have several times higher Hg adsorption capacity than virgin activated carbons. Iodine, chlorine and sulphur compounds are most commonly used as impregnation agents to improve mercury adsorption (Krishnan et al., 1994). Bromine treatment of activated carbon has also been used to improve mercury adsorption and bromine, and field test in power plants have shown that bromine-treated activated carbon is effective in removing mercury from the coal-fired power plant flue gases (Lockert, et al., 2006).

For the manufacture of impregnated activated carbon, a precursor of a suitable quality for a specific application is impregnated (or sprayed) with solutions of salts or dry chemicals which, after drying remain on the internal surface of the activated carbon. Homogenous distribution of the impregnating agent on the internal surface has a very important effect on the adsorption capacity of the resulted activated carbon, since adsorption takes place inside the micropores.

In recent years, considerable attention has been devoted to develop sulphur-impregnated activated carbons for the removal of elemental mercury. Sulphur-impregnated activated carbons perform better than virgin carbons. The main reason is that while physisorption dominates the capacity of a virgin carbon, chemisorption,

facilitated by the formation of HgS, controls the adsorption capacity of sulphur-impregnated carbons. Different sulphur impregnation methods have been employed and the effect of sulphur impregnation on mercury adsorption capacity has been evaluated.

Sinha and Walker (1972) impregnated a Saran carbon by oxidation of H<sub>2</sub>S by O<sub>2</sub> at 140°C. They found that at 25°C, the adsorption capacity was greatest for the virgin carbon and decreased with increasing sulphur loading. At 150°C, the adsorption of mercury by virgin carbons was negligible compared with that of sulphur-impregnated carbon, due to the mercury reacting with sulphur, to form HgS.

Otani et al (1998) carried out sulphur impregnation on an activated carbon by soaking an activated carbon in a CS<sub>2</sub> solution followed by evaporating the solvent in nitrogen gas. They found that Hg adsorption capacity, tested at 36°C, increased with increasing sulphur content, an opposite effect observed to the previous study done by Sinha and Walker. Sinha and Walker reported that the surface area of Saran carbon was reduced from 875 to 1 m<sup>2</sup>/g, at a sulphur content of 11.8 wt. %, while the decrease in surface area was only from 1250 to 710 m<sup>2</sup>/g, at a sulphur impregnation of 13.8 wt. % according to Otani et al (1988). The differences in the methods by which sulphur was added to the activated carbons might be reason for the differences in the changes in BET surface areas.

Impregnation of activated carbon with elemental sulphur was studied by Korpiel and Vidic, (1997), Liu et al, (1998), Liu et al. (2000), Kwon and Vidic, (2000). A bituminous-activated carbon (BPL), commercialized by Calgon Carbon Corporation was used as starting material, for elemental sulphur impregnation. Mercury adsorption capacity was tested at different temperatures, from 25 to 140°C, and low influent Hg concentration of 55 µg/m<sup>3</sup>, at a N<sub>2</sub> flow rate of 1 L/min. They found that in the case of impregnation with elemental sulphur, the impregnation temperature employed was more important than sulphur content, in terms of mercury adsorption capacity of impregnated activated carbon. The results showed that carbons impregnated at high temperature (400-600°C) exhibited the highest efficiency for mercury removal. Higher treatment temperature produced relatively high surface areas, stronger bonding between sulphur and carbon and a larger fraction of mesopores which were believed to contribute to improved mercury capture.

The dependence of mercury capture on sulphur impregnation temperature can be explained by the fact that at high temperature, the vapour pressure of sulphur increases rapidly, and the nature of the sulphur vapour molecules change with temperature. Sulphur exists in several allotropes, including  $S_\lambda$  ( $S_8$  rings),  $S_\pi$  ( $S_8$  chains), and  $S_\mu$  (chains of variable length) with  $S_8$  rings being the only form at room temperature. At high temperature, sulphur gas possesses a significant fraction of  $S_6$  and  $S_2$ , which are smaller and more reactive than  $S_8$  because they possess a greater fraction of sulphur terminal atoms (Korpiel and Vidic, 1997). Consequently, the smaller and more reactive sulphur molecules will migrate easier inside the microporous structure of activated carbon, resulting in a more uniform sulphur distribution, with a greater reactivity compared with those impregnated at lower temperature. At low impregnation temperature, the predominant form of sulphur is  $S_8$  molecules, in the form of rings or long chains which could only enter large pores and easily form clusters. Therefore, these clusters will block pore entrances and reduce the total surface area (Liu and Vidic, 1998).

The sulphur/carbon ratio and the method of sulphur impregnation were also studied. When sulphur/carbon ratio was varied from 4:1 to 1:2, the sulphur content slightly decreased, which resulted in a small decrease in mercury uptake capacity (Liu and Vidic, 2000). Also, two sulphur impregnation methods were compared. In one method, which was also used in the previous studies, activated carbon and sulphur were placed in two different ceramic holders, one for the activated carbon and one for sulphur. On the other hand, in the second method, sulphur flakes were finely grounded and mixed with the activated carbon in a single holder. Direct contact between sulphur and activated carbon, during impregnation resulted in a reduced amount of sulphur necessary to reach the same sulphur concentration in the final product, compared with the method in which sulphur and activated carbon were placed separately. Also maintaining a stagnant, inert atmosphere during impregnation process improved sulphur deposition resulting in the increased capacity of the adsorbent when compared to that obtained under continuous flow of nitrogen (Liu and Vidic, 2000).

The influence of impregnation temperature and surface area on mercury removal capacity was confirmed by Kwon and Vidic (2000). Treatment with  $H_2S$ , at  $150^\circ C$  was compared with elemental sulphur impregnation, at  $600^\circ C$ , by means of Hg adsorption

capacity. The same activated carbon (BPL) was used as precursor and identical conditions were used for Hg adsorption. Treatment with H<sub>2</sub>S in place of elemental sulphur yielded comparable sulphur content but a significant lower mercury capacity.



## **Chapter 3. Materials, Equipment and Procedures**

Experimental work in this study consisted of physical activation of Syncrude fluid coke and evaluation of mercury adsorption capacity of activated fluid coke, by using pulse injection of air saturated with mercury. The effect of time, temperature, pressure treatment and of gas composition on the development of surface area and pore size distribution of activated coke was studied. Mercury capture of activated coke was evaluated as a function of operating temperature and properties of activated fluid coke: surface area, particle size, chemical composition. A description of materials, equipment and procedures used in activation and characterization of fluid coke and mercury capture experiments is presented in this chapter.

### **3.1. Materials**

Fluid coke used in this study was provided by Syncrude Canada Ltd. A 20 L sample, identified as Coke 1 was received in April 2005. Another sample, identified as Coke 2 was supplied in July 2005. These two coke samples were produced at different times. The samples were stored in metallic containers, at room temperature. No additional treatment (e.g. washing, degassing) was applied prior to use. No proximate or ultimate analyses were carried out.

Compressed gases used in the experiments: CO<sub>2</sub> (bone dry), air (extra dry), N<sub>2</sub> (UHP), He (PP), H<sub>2</sub> (UHP) and Ar (UHP) were obtained from Praxair. NaOH (beads, 1) and precipitated sulphur (powder/USP) were obtained from Fisher Scientific. All the water used was deionised water.

### **3.2. Treatment of fluid coke**

#### ***3.2.1. Classification of fluid coke***

Coke was separated into various size ranges by sieving using standard Canadian Metric sieves, ranging from 53 to 250 µm (Tyler mesh sizes from 270 to 60). The sieving procedure consisted of placing 200 g of coke on the 250 µm sieve and shaking the set of sieves for 15 min in a mechanical shaker. Coke of different particle size ranges were stored at room temperature in closed plastic containers. The 100-125 µm size fraction of

Coke 1 was used for most of the experiments. The identification codes for the different raw coke samples are listed in Table 3-1.

Table 3-1. Identification designations for various fluid coke samples.

Sample Identification	Sample Description
Coke 1	The fluid coke sample (20 L) obtained from Syncrude on April 14, 2005
Coke 2	The fluid coke sample (10 L) obtained from Syncrude on July 28, 2005
Coke 101	The <53 $\mu\text{m}$ fraction of Coke 1
Coke 102	The 53 – 80 $\mu\text{m}$ fraction of Coke 1
Coke 103	The 80 – 100 $\mu\text{m}$ fraction of Coke 1
Coke 104	The 100 - 125 $\mu\text{m}$ fraction of Coke 1
Coke 105	The 125 - 180 $\mu\text{m}$ fraction of Coke 1
Coke 106	The 180 – 250 $\mu\text{m}$ fraction of Coke 1
Coke 107	The >250 $\mu\text{m}$ fraction of Coke 1
Coke 201	The <53 $\mu\text{m}$ fraction of Coke 2
Coke 202	The 53 – 80 $\mu\text{m}$ fraction of Coke 2
Coke 203	The 80 – 100 $\mu\text{m}$ fraction of Coke 2
Coke 204	The 100 - 125 $\mu\text{m}$ fraction of Coke 2
Coke 205	The 125 - 180 $\mu\text{m}$ fraction of Coke 2
Coke 206	The 180 – 250 $\mu\text{m}$ fraction of Coke 2
Coke 207	The >250 $\mu\text{m}$ fraction of Coke 2

### ***3.2.2. Equipment and procedure for thermal treatment of fluid coke***

A schematic diagram of the apparatus used to activate the coke is presented in Figure 3-1. The activation reactions were carried out in a vertical reactor, located in a custom-made furnace. The furnace, with an operating temperature from 0 to 900°C, was used to heat up the samples. The reactor consisted of a 500 mm long, 12.5 mm O.D. 316 stainless steel tube. This 316 stainless tube was replaced with a 560 mm long, 10 mm O.D. Inconel tube, for the runs carried out at elevated pressures. The temperature was controlled with a proportional-integral-derivative (PID) controller using Thermocouple T2 as controller input. The actual temperature in the reactor was measured with

Thermocouple T1 which was inserted in the reactor such that its tip was just above the sample. The output from T1 was logged by the data acquisition system.

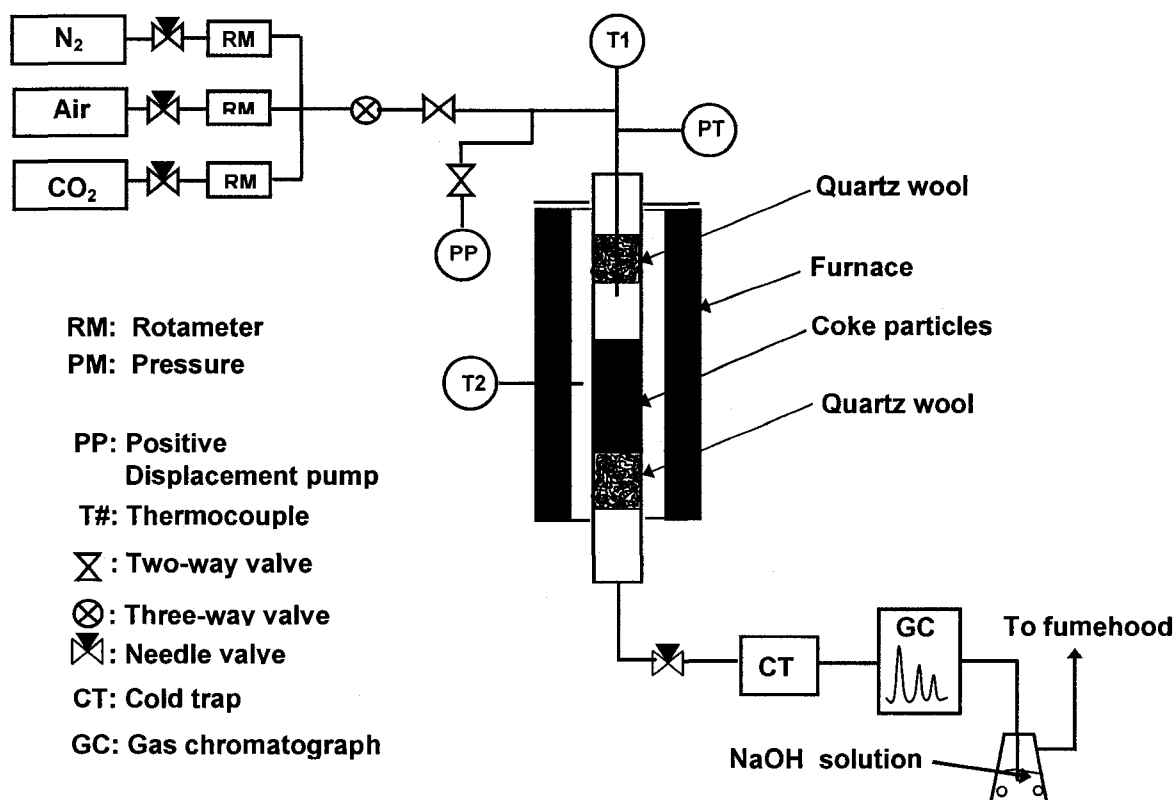


Figure 3-1. Schematic diagram of the apparatus used for thermal treatment of fluid coke.

The flow rates of treatment gases (CO<sub>2</sub>, Air, N<sub>2</sub>) were adjusted with needle valves and measured with calibrated rotameters. The flow of treatment gases in the treatment reactor was from top to bottom. Initially, a glass syringe pump KD Scientific, Model 780100 was used to inject the water at the desired rate. Because this glass syringe pump cannot operate at pressures much above atmospheric pressure, it was replaced with a positive displacement pump, (LabAlliance Series II, Model 205SFM01) for the activation runs carried out at higher pressures. Up to run MB10464, the exit gases were bubbled through a NaOH solution, and then were vented to fumehood. After Run 10464, the exit

gases from the reactor were passed through a cold trap at 0 °C and then entered an on-line gas chromatograph HP 5890 for analysis of the exit gas composition. The exit gases from the GC column were passed through a scrubber, at ambient temperature containing NaOH solution, and then vented to the fumehood.

For a typical activation run, a measured amount of coke (~10 g) was placed in the reactor between two plugs of quartz wool. A 150 mm long, 10 mm O.D. 316 stainless steel tube was placed at the bottom of the reactor tube to support the coke bed. The reactor tube was placed inside the furnace and connected to the treatment gas lines. The data acquisition program (LABVIEW) was started and the temperature controller was set to the desired temperature. Temperatures of  $\leq 800^{\circ}\text{C}$  were used for the thermal treatments. Needle valves were used to adjust the treatment gas flow rates to the desired values; the flow rate was indicated by calibrated flow meters. The treatment gases were passed over the sample at the selected final temperature, for a desired period of time. For the runs carried out at elevated pressure, the pressure in the reactor was controlled by adjusting the needle valve placed at the bottom of the reactor. The pressure was monitored by a pressure transducer and logged by the data acquisition system at 60 sec intervals. The heat-up temperature, which was typically of 30 min duration, was not included in the treatment time. After the reaction time was completed, the sample was cooled down, in an inert atmosphere ( $\text{N}_2$ ). The activated coke was measured and stored in glass vials. During the activation, the exit gases were periodically analyzed with the on-line gas chromatograph.

Typical plots of inlet pressure and top bed temperatures as a function of treatment times are shown in Figures 3-2 to 3-4. Typical variations in pressure and temperature during treatment are shown in Figure 3-2. The small pressure variations are due to flash vaporization of the water droplet in the treatment tube. More severe pressure variations, illustrated in Figure 3-3, sometimes occurred at higher water flow rate (water feed rates were 4.5 and 9.0 mL/h for IC10494 and MB10465). Occasionally very large spikes occurred in both temperature and pressure even at low water feed rates. This is illustrated in Figure 3-4; the water feed rate for IC10473 was 4.5 mL/h. Such behaviour was rare and is ascribed to large water droplets and an insufficiently thick or badly distributed quartz wool pad on the top of the coke particle bed. Subsequent analysis of the results

indicated that these variations in pressure and the brief drops in temperature, such as those shown in Figure 3-4, did not affect the coke activation. A tabulation of all the activation runs is given in Appendix A, Table A-1; variations in temperatures and pressures are indicated by the standard deviations of the measured values.

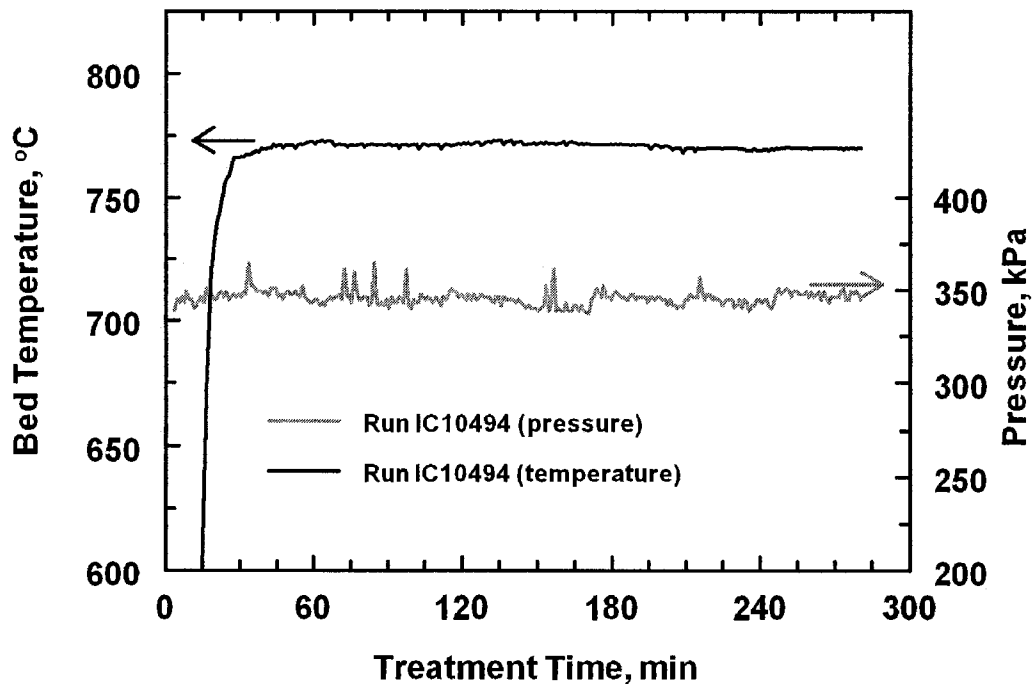


Figure 3-2. Pressure and temperature profiles for Run IC10494 showing typical variations in pressure and temperature with treatment time,

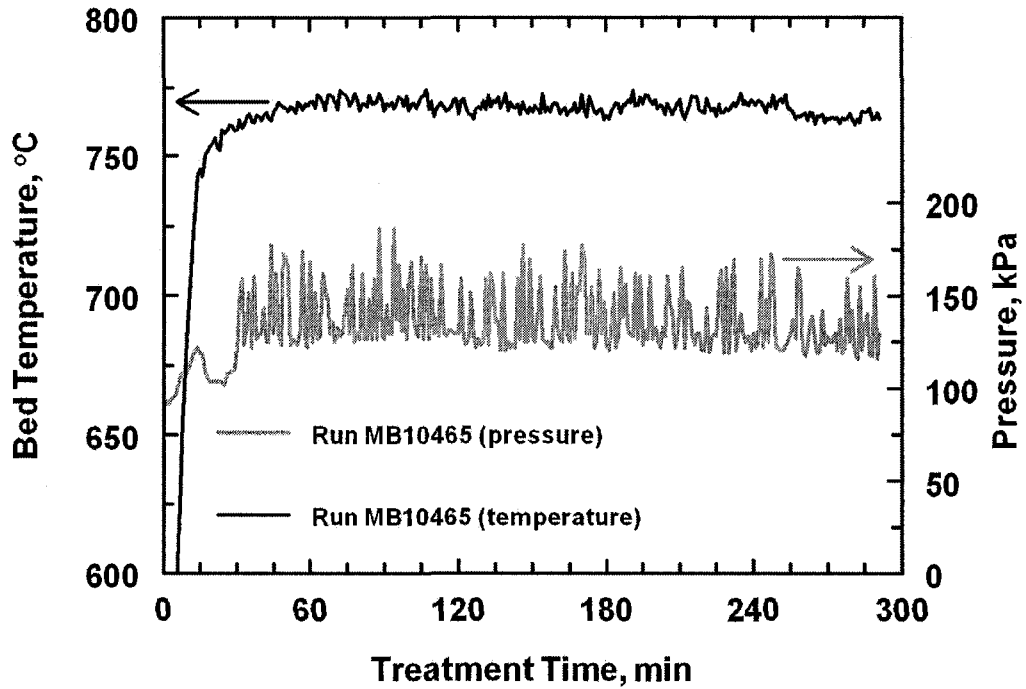


Figure 3-3. Pressure and temperature profiles for Run MB10465 showing above average variations in pressure and temperature with treatment time

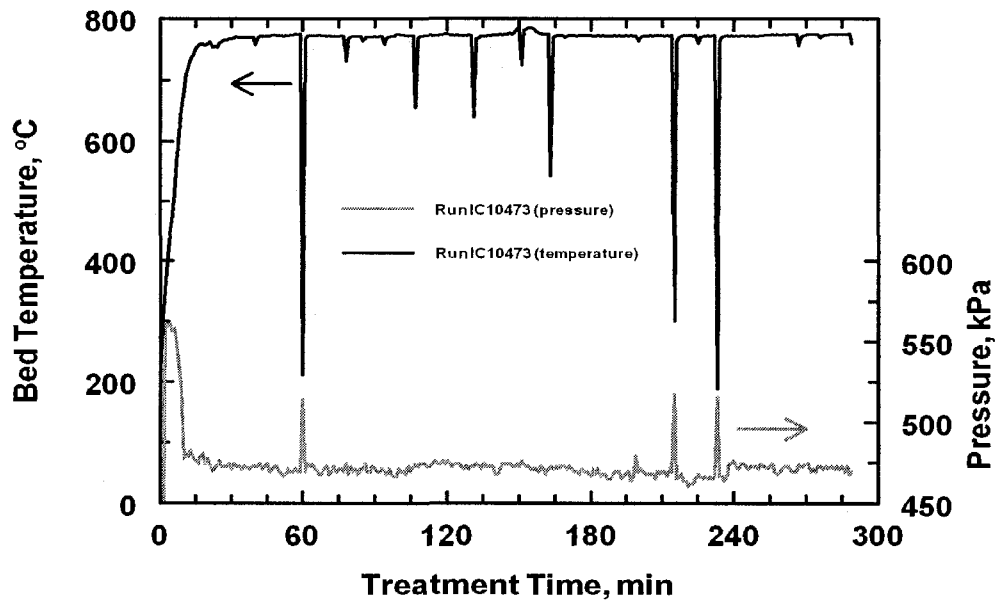


Figure 3-4, Pressure and temperature profiles for Run IC10473 showing pressure and temperature spikes during treatment.

### 3.3. Equipment and procedure used for mercury capture by fluid coke

A schematic diagram of the pulse sorption apparatus used for mercury capture on activated coke is shown in Figure 3-5. The carrier gas used in the current study was argon, ultra-high purity grade, and the flow rate was kept constant during the experiments, at 1.5 mmol/min (40 mL/min at ambient conditions). The flow rate of carrier gas was controlled by a mass flow controller. A measured amount of sample to be tested was placed in a borosilicate U-tube, between two plugs of quartz wool. The sample was heated to the desired temperature in a temperature-controlled oven. The oven temperature was maintained at the desired temperature using a PID controller.

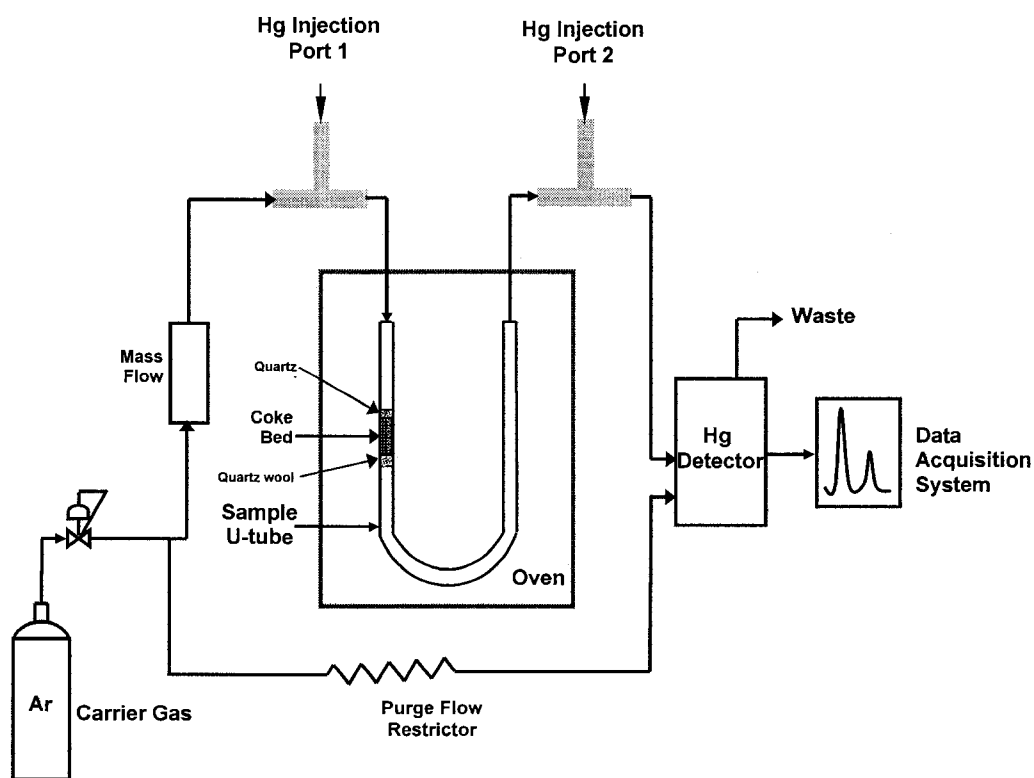


Figure 3-5. Schematic diagram of the apparatus used for mercury capture by fluid coke.

For a typical run, a measured amount of activated coke (40-50 mg) was placed into the sample holder which was then placed into the oven which had been preheated to the desired temperature, under argon flow for ~20-30 min before the first mercury injection. The argon flow was downward through the packed bed of coke. Three pulses of air saturated with mercury (50 $\mu$ L, at room temperature and atmospheric pressure) were injected into Port 2, for calibration of the detector. Several pulses of air saturated with mercury were injected into Port 1 and the mercury passed through the sample was measured by detector. A new sample of sorbent was used for every experiment.

Mercury injection into Port 1 was used to determine the mercury capturing ability of the activated fluid coke, while mercury injection into Port 2 was used to calibrate the detector. Air saturated with mercury at room temperature was injected, either into Port 1 or Port 2, using a gas-tight Hamilton syringe (50  $\mu$ L). The air saturated with mercury was stored in a 2 L glass vessel containing liquid mercury. The temperature of the air in the 2 L bulb was recorded for each injection so that the amount of mercury in each injection can be calculated from the mercury vapour pressure and the volume of injected gas.

A Cold Vapor Atomic Fluorescence Spectrophotometry (CVAFS) mercury detector (Tekran Model 2500) was used to determine the amount of mercury which was not adsorbed by the activated coke. This detector allows the measurement of elemental mercury in an argon carrier gas and can detect sub-picogram amounts of mercury in nearly any type of sample matrix. Elemental Hg atoms in an inert carrier stream are excited by a source of ultraviolet radiation. Radiation at 253.7 nm excites any Hg atoms present, which then fluoresce and re-radiate at the same wavelength (user manual). The fluorescence produced by the elemental Hg is recorded by a photomultiplier tube. The intensity of the fluorescence is directly proportional to the amount of elemental Hg present in the carrier gas. A high resolution data acquisition system (Varian Star software) was used to convert the signal registered by the photomultiplier to a chromatogram. The area under each peak is related to the amount of mercury which has passed through the detector and calibrations were done to determine the relationship between area and amount of mercury. Typical plots of the output of the detector as a function time are shown in Figures 3-6 and 3-7.



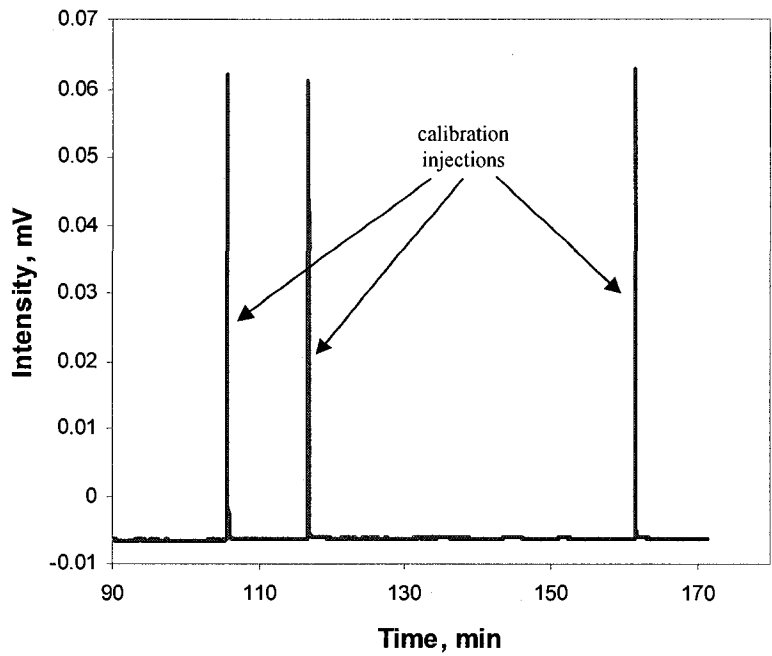


Figure 3-6a. Output of the Hg detector for activated coke IC10481 (BET SA= 489 m<sup>2</sup>/g).

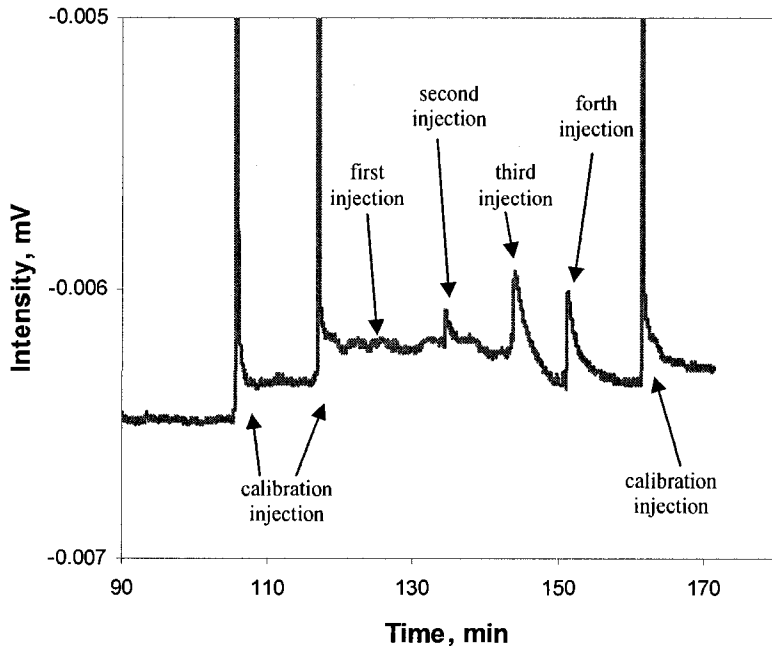


Figure 3-6b. Expanded output of the Hg detector for activated coke IC10481 (BET SA= 489 m<sup>2</sup>/g).

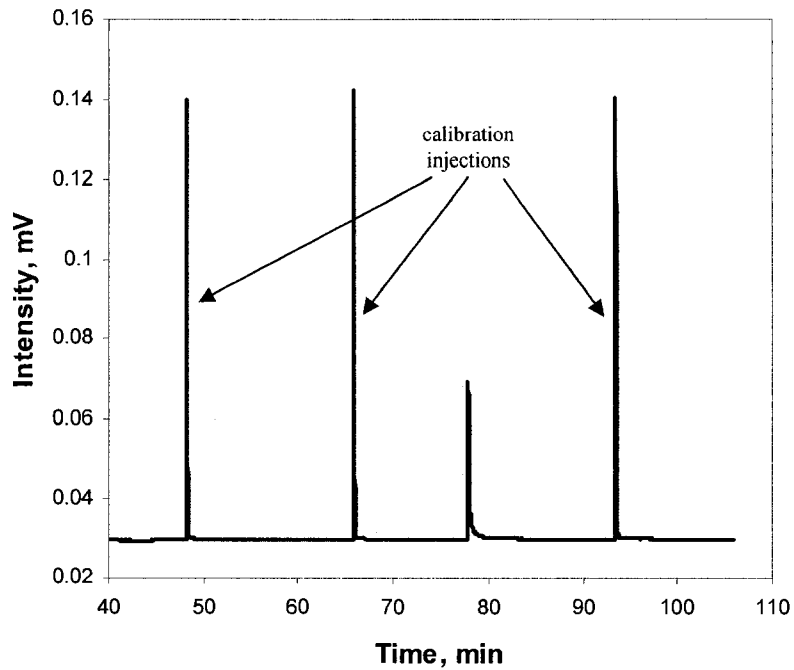


Figure 3-7a. Output of the Hg detector for activated coke IC10490 (BET SA = 22.4 m<sup>2</sup>/g).

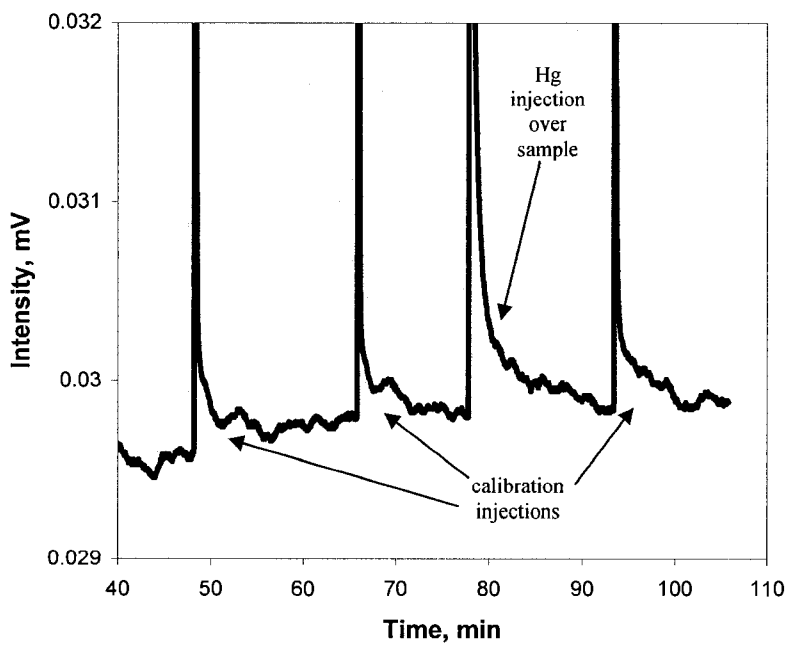


Figure 3-7b. Expanded output of the Hg detector for activated coke IC10490 (BET Surface Area = 22.4 m<sup>2</sup>/g).

Figure 3-6a shows the Hg detector output for Hg adsorption on activated coke IC10481 (BET surface area of 489 m<sup>2</sup>/g). The three large peaks represent the detector outputs for calibration injections (injections in Port 2 in Figure 3-5). Four Hg injections were performed over the sample at 140°C, but very little mercury was eluted from the sample. This can be seen in Figure 3-6b, which is an expanded representation of Figure 3-6a. Figure 3-7a shows the Hg detector output for the activated coke IC10490, with BET surface area of 22.4 m<sup>2</sup>/g. The sample was also tested at 140°C. While first, second and forth peaks illustrate the calibration injections, the third peak shows the Hg which was injected in front of the sample (Port 1, Figure 3-5): very little of this injected pulse was captured by the coke. An expanded version of this figure is shown in Figure 3-7b. The calibration peaks are much higher but much narrower. The areas under the calibration peaks are about the same as the area under the eluted injection peak.

The output of the UV lamp has a major impact on the reliability and reproducibility of the Hg adsorption measurements. The sensitivity of the Hg detector is very much influenced by the intensity of the UV lamp. The lamp intensity is adjusted by using the Lamp Intensity Adjust control on the lamp stabilizer board. Once set, the lamp stabilizer will attempt to maintain this set intensity. A lamp drive voltage of approximately 7 V for a new lamp and 8.5 Volts for an older lamp is fed to the lamp in order to keep the lamp intensity at 253.7 nm. As the lamp ages, the drive level to the lamp will increase to maintain this intensity. If the lamp has deteriorated beyond the capacity of the controller to compensate, an indicator mounted on the front panel of the detector will light up. Also, changes in baseline patterns such as a low, noisy or wandering baseline or sudden baseline shifts are signs of an aging lamp. Therefore, every time the lamp indicator went on or when changes in baseline pattern occurred the lamp intensity adjustment was performed. The baseline value was adjusted to the desired value and a calibration of the detector was done.

Calibrations were done by injecting various known volumes of air containing known amounts of mercury (from the temperature and Hg vapor pressure) into Port 2 (see Figure 3-5) and recoding the area of under the resulting detector output. Figures 3-8 to 3-10 show the calibration curves of the Hg detector, done at different times, during the Hg adsorption experiments.

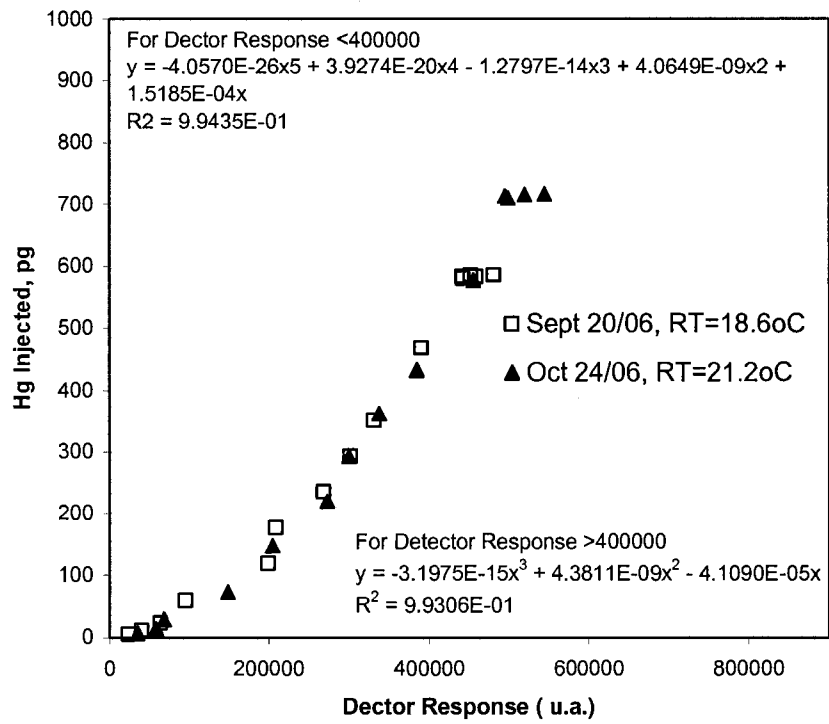


Figure 3-8. Calibration curves of Hg detector done on Sept 20/06 and Oct 24/06.

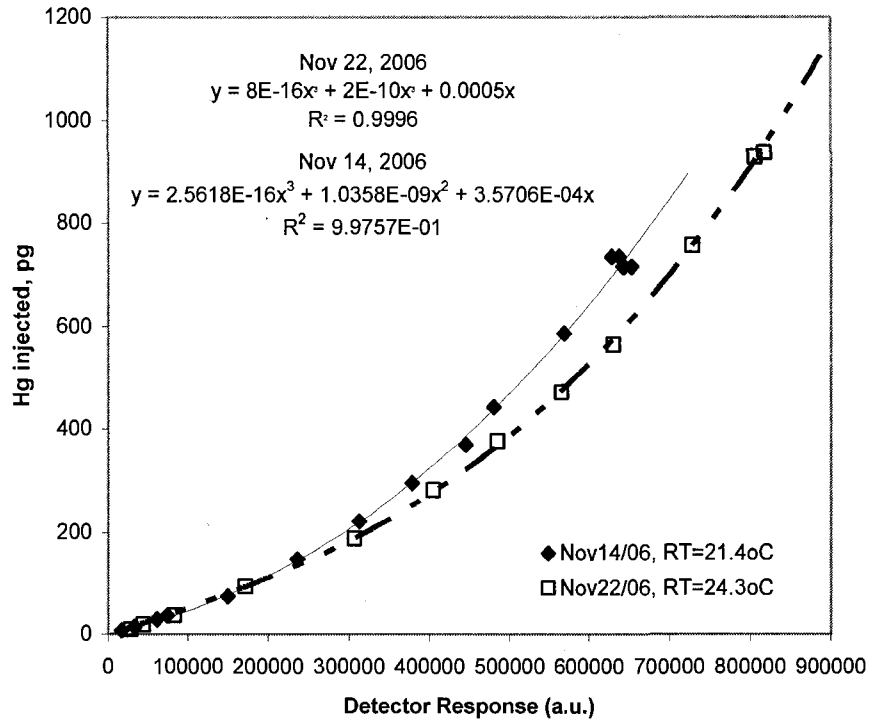


Figure 3-9. Calibration curves of Hg detector done on Nov14/06 and Nov22/06.

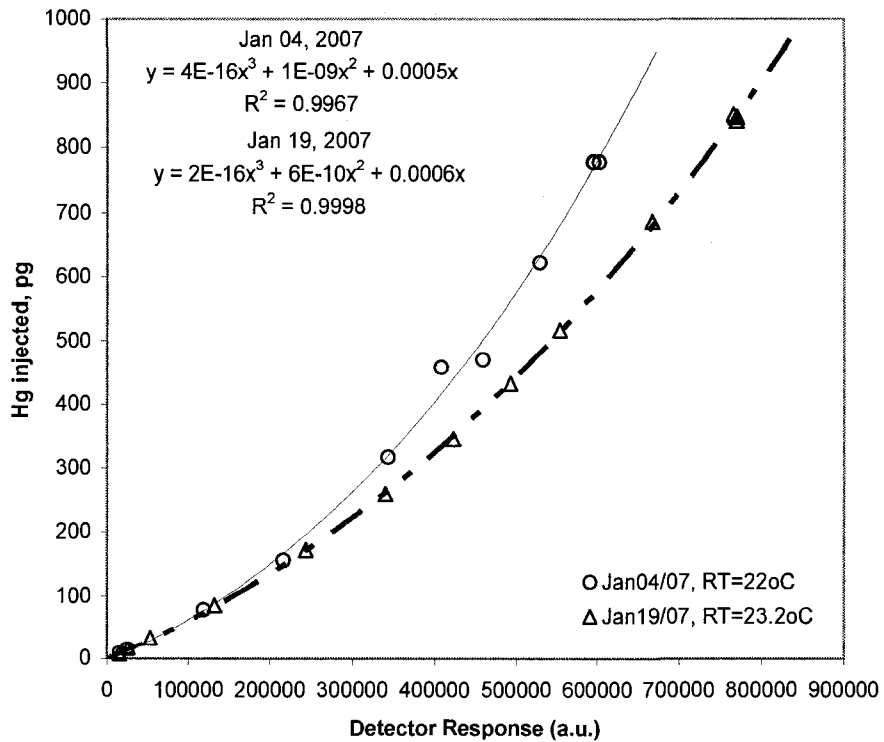


Figure 3-10. Calibration curves of Hg detector done on Jan 09/07 and Jan19/07

Figures 3-8 to 3-10 show that CVAFS mercury detector is very sensitive, i.e. capable of detecting mercury at the pictogram level (in the order of  $10^{-12}$  g). From these calibration curves, it can be concluded that the sensitivity of Hg detector decreases with the aging of UV lamp. In the small range of Hg injected (up to 200 pg), the detector output changed by about 20%, while for the larger amounts of Hg injected, the variation in measurement is as high as 40%. All the Hg adsorption capacities were calculated using the calibration curve measured close to the time of the calibration.

### 3.4. Equipment and procedure used for sulphur impregnation of activated fluid coke

A schematic diagram of the apparatus used for sulphur impregnation of activated fluid coke is presented in Figure 3-11.

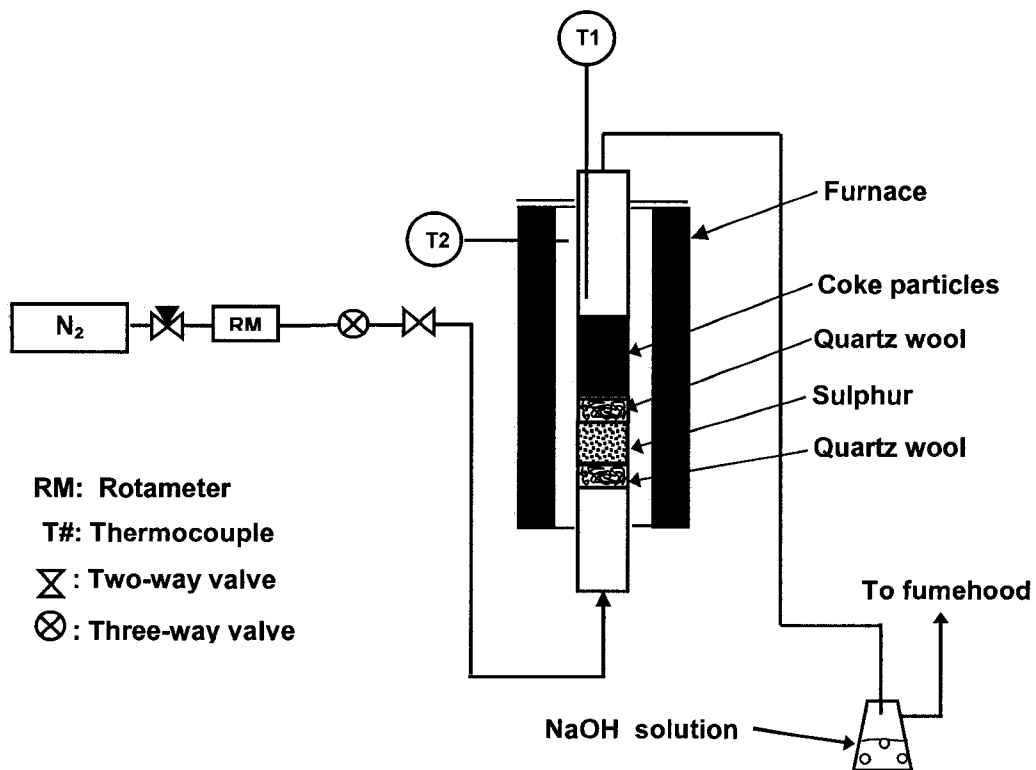


Figure 3-11. Schematic diagram of the apparatus used for sulphur impregnation of activated fluid coke.

A 235 mm long, 5 mm O.D. open-ended stainless steel tube was used to hold the fluid coke sample and the elemental sulphur. A quartz wool plug was inserted at the bottom of this tube. Typically, 0.1 grams elemental sulphur was placed in this tube over the quartz wool and covered with another quartz wool plug. About 0.5 g activated coke was placed on top of the upper layer of quartz wool, which served as separation media between activated coke and elemental sulphur. This tube was placed in another stainless steel tube, 550 inches long, 12.5 mm O.D. which was placed in a custom-made furnace. The temperature was controlled with a PID controller (Omega Series 920) using Thermocouple T2 (a 1/8" stainless steel sheathed, Type K thermocouple) as the controller input. The temperature just above the coke bed was measured using T2 (a 1/16 stainless steel sheathed, Type K thermocouple); the output from T1 was logged with a data acquisition system.

The nitrogen gas flow was from the bottom to the top, at a flow rate of 10 mL/min to maintain an O<sub>2</sub> free atmosphere in the reactor and to drive the sulphur vapours toward the coke bed. Flow rate of N<sub>2</sub> was measured with a calibrated rotameter. The exit gasses were bubbled through a NaOH solution, and the off-gases of this solution were vented to the fumehood.

The furnace temperature was adjusted at the desired value. When the required temperature was reached, the inner tube containing the reactants was placed in the exterior tube for a fixed period of 10 min. Six different temperature settings were selected for the impregnation process, namely 100, 200, 300, 400, 500 and 600°C. After the impregnation process, the inner tube containing the product was pulled out and placed in the fumehood to cool down. The impregnated coke was removed from the reactor and placed in a closed container, at room temperature for further use (i.e. sulphur analysis, mercury capture capacity).

### **3.5. Characterization methods**

#### ***3.5.1. Particle size distribution analysis***

Particle size distributions of the raw coke samples listed in Table 3-1 as well as of selected samples of activated cokes were measured with a Malvern Mastersizer 2000 particle size analyzer. The samples were dispersed to the correct concentration and then

delivered to the optical unit. In the optical unit, particles were passed through a focused laser beam. These particles scatter light at an angle that is inversely proportional to their size. Each size of particle will have its own characteristic scattering pattern. The detectors within the optical unit collect the scattered light from a particular range of angles. The map of scattering intensity versus angle is the primary source of information used to calculate the particle size distribution. Once the measurement is complete, the raw data contained in the measurement were analyzed by the Malvern software; the properties of carbon were used in the analysis. The plot  $dV/dD$  (D- particle diameter, V-particle volume) over particle diameter represents particle size distribution.

### ***3.5.2. Surface area, micropore volume and mesopore size distribution***

An Omnisorb 360 automated adsorption apparatus was used to measure the adsorption and desorption isotherms of nitrogen at liquid nitrogen temperatures for relative pressures  $P/P_0$  from 0.000 to 0.999 ( $P_0$  is the nitrogen saturation pressure). The samples were evacuated at 350°C for 4 h before nitrogen adsorption. Nitrogen was added to the sample at a rate of 0.022 mmol/min during the adsorption step and withdrawn at the same rate during the desorption step.

The specific surface areas of the raw coke and activated coke particles were calculated according to the BET method. The micropore volume was calculated using the t-plot method. The desorption isotherm and the BJH (Barrett, Joyner and Hallender) method was used to obtain the mesopore size distribution. Books by Gregg and Sing (1982) and Lowell and Shields (1991) give details of these methods for determining surface areas, micropore volume and mesopore size distribution.

### ***3.5.3. SEM and EDX analyses***

Scanning electron microscopy (SEM) was used to determine the external and internal morphology of raw and activated fluid coke particles. A Hitachi S-2700 scanning electron microscope, equipped with a Princeton Gamma Tech Prism IG detector for energy dispersive x-ray spectroscopy (EDX or EDS) analysis, was used in the studies. Whole coke particles and microtomed sections of coke particles imbedded in epoxy were



examined. Specimens were coated with gold prior to SEM and EDX examination. SEM images were obtained with accelerating voltage of 20 eV.

The sulphur distributions inside the raw and treated fluid coke samples were determined on microtomed particles by EDX line scans. The accelerating voltage for the EDX analyses also was 20 eV. EDX results were analyzed using the Princeton Gamma Tech IMIX system.

#### **3.5.4. XPS analysis**

X-ray photoelectron Spectroscopy (XPS) yields information on the elemental composition and oxidation state at the surface for all elements at the surface of the sample (Niemantsverdriet, 2000). A Kratos AXIS 165 spectrometer, located in the Alberta Centre for Surface Engineering and Science was used for the studies. Binding energies were measured for sulphur 2 p (S2p) and oxygen 1s (O1s) electrons. A binding energy of 284.6 eV for the carbons 1s electrons was used as the reference. XPS spectra were obtained for whole coke particles of different sizes and for sectioned untreated and activated particles of Coke 104.

#### **3.5.5. Gas chromatography analysis**

A HP 5890 gas chromatograph was used to determine the composition of the effluent gas from coke activation. The gas chromatograph was equipped with a 9.5 mm O.D., 90 cm long Hayesep Q packed column and a thermal conductivity detector. The effluent gas from the activation reactor was passed through a cold trap at 0°C, and then through a 6-port gas sample valve on the gas chromatograph. The volume of the sample loop was about 0.5 cm<sup>3</sup>. The carrier gas was helium, with a flow rate of 20 cm<sup>3</sup>/min. The detector temperature was set up at 140°C. Pure components CO, CO<sub>2</sub>, CH<sub>4</sub> and N<sub>2</sub> and mixtures (air, CO<sub>2</sub>/air, and H<sub>2</sub>S/H<sub>2</sub>) were used to determine retention times (R.T.) for the components at various column temperatures and He flow rates.

The gas chromatograph was operated in a temperature program mode, as follows: the column temperature was set up at 40°C for the first 3 min., followed by rapid heating (45°C/min) to 140°C and constant temperature of 140°C for the rest of the analysis. H<sub>2</sub>S

had the longest retention time of about 5.5 min. Water did not elute as a well resolved peak under these conditions.

### **3.5.6. Sulphur analysis**

Sulphur content of the raw fluid coke and activated fluid coke was determined by using a Horiba EMIA 320 Carbon/Sulphur Analyzer. Sulphur content of sulphur-impregnated activated coke was determined using an Antek 9000NS nitrogen/sulphur analyzer. The measurement principle for these sulphur analyzers is based on the combustion of sulphur in the sample in an O<sub>2</sub> stream and the spectroscopic measurement of SO<sub>2</sub> produced during combustion.

When the Horiba Carbon/sulphur analyzer was used, a measured amount of sample (10 to 50 mg) was mixed with 0.3 g tin and 1.5 g tungsten into a ceramic crucible. The sample was then introduced into a high frequency induction furnace. The sample was heated up at a programmable temperature, in the presence of O<sub>2</sub>. The gases produced during combustion were then analyzed using four infrared detectors. The concentration of sulphur in the sample was calculated based on the amount of detected SO<sub>2</sub>.

When Antek 9000NS was used, a weighed sample (~6 mg) was placed in a quartz boat and then combusted in a furnace, at 1100°C, in an O<sub>2</sub> stream. The combustion products were then analyzed by a ultraviolet (UV) detector, for quantification of SO<sub>2</sub>. The sulphur content was calculated based on the amount of SO<sub>2</sub> detected by the UV detector.

## Chapter 4. Results of Fluid Coke Characterization and Activation

The properties of fluid coke and the effects of thermal treatment at various conditions on the surface area, porosity and sulphur content are presented and discussed in this chapter.

### 4.1. Properties of Untreated Fluid Coke

Two samples of fluid coke, Coke 1 and Coke 2, were provided by Syncrude Canada Inc. These samples were obtained at different times. The samples were screened into various size fractions, following the procedure described previously. The mass fractions in each size range for the two untreated samples are given in Table 4-1.

Table 4-1. Particle size distribution from sieve analysis for Coke 1 and Coke 2.

Particle Size Range, $\mu\text{m}$	Fraction of Mass in Each Size Range	
	Coke 1	Coke 2
<53	0.010	0.034
53 – 80	0.088	0.092
80 – 100	0.052	0.044
100 – 125	0.210	0.203
125 – 180	0.344	0.349
180 – 250	0.206	0.171
>250	0.091	0.108

The results show that the two samples have similar particle size distributions. All the particles less than 250  $\mu\text{m}$  are of interest for mercury sorbents, and approximately 90% of the particles are in this size range.

The particle size distribution was also analyzed using a Malvern Mastersizer 2000 particle size analyzer. The particle size distributions for each fraction obtained by sieving of Coke 1 are shown in Figures 4-1 and 4-2, while the particle size distribution for each fraction of Coke 2 are shown in Figures 4-3 and 4-4.

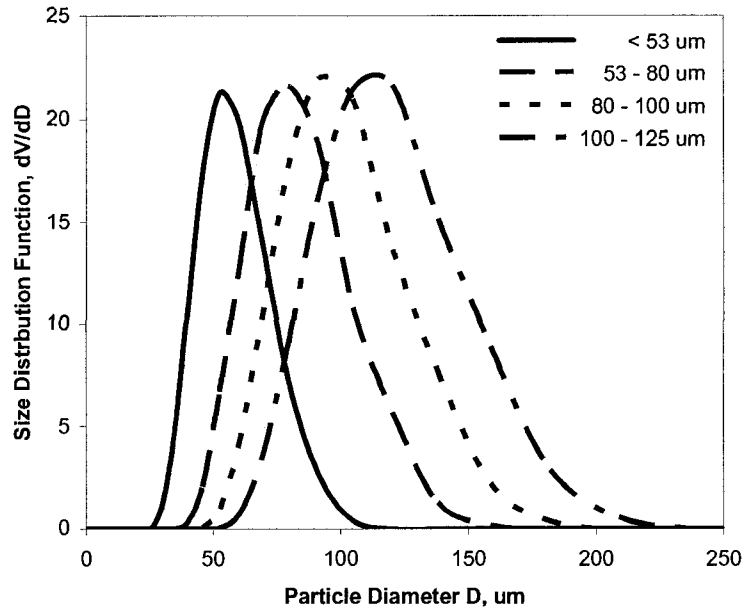


Figure 4-1. Particle size distribution for smaller size fractions of Coke 1.

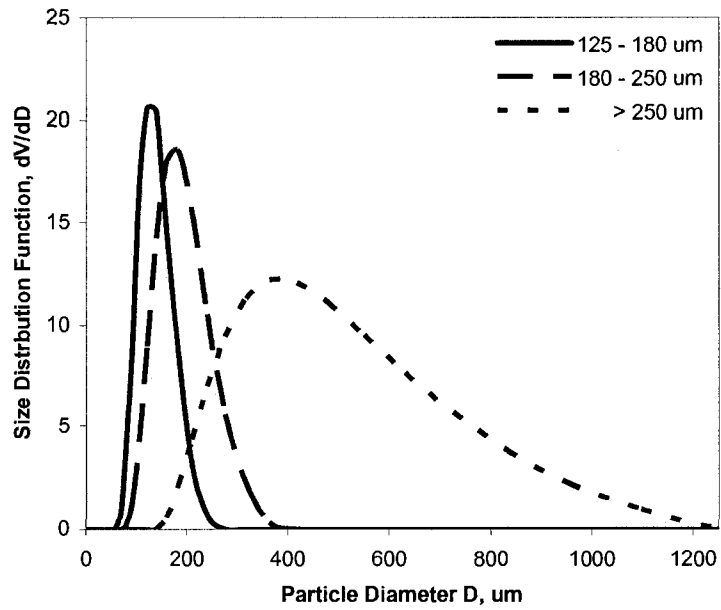


Figure 4-2. Particle size distribution for larger size fractions of Coke 1.

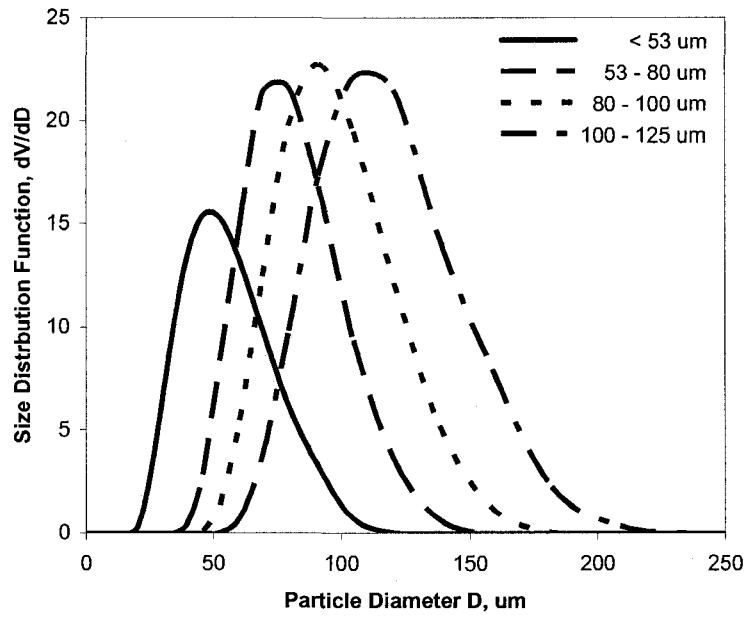


Figure 4-3. Particle size distribution for smaller size fractions of Coke 2.

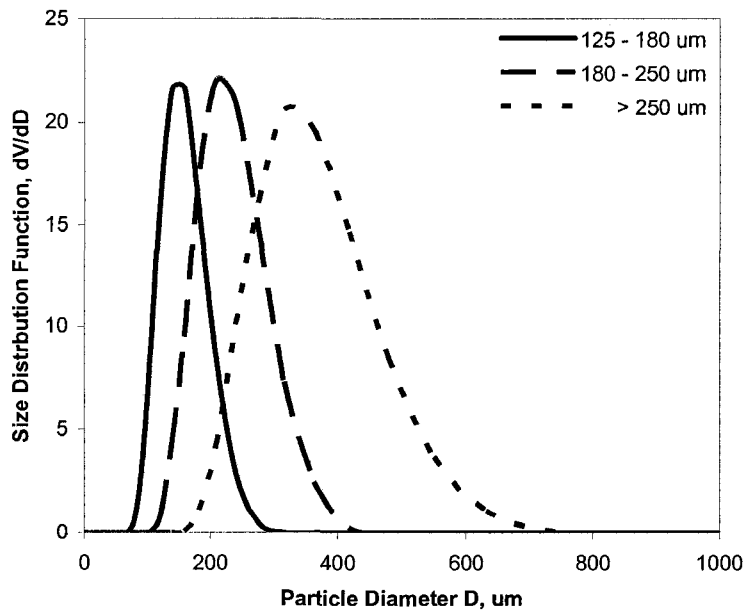


Figure 4-4. Particle size distribution for larger size fractions of Coke 2.

It is interesting to note that particle size analysis done with Malvern Mastersizer 2000 particle size analyzer of the various fractions obtained by sieving indicated that the fractions contained particles which were larger than the maximum openings in the sieves. For example, for the fraction with particle size  $< 53 \mu\text{m}$  (identified as Coke 101), about 60% of the particle volume was present in particles  $> 53 \mu\text{m}$ , according to Mastersizer 2000 analysis, based on the particle size distribution shown in Figure 4-1. The other size fractions contained also particles smaller as well as larger than the indicated sieve size range. For example, in the 100-125  $\mu\text{m}$  size fraction, identified as Coke 104, about 20% of the particle volume has sizes  $< 100 \mu\text{m}$ , and about 40% of the particle volume has sizes  $> 125 \mu\text{m}$ .

The presence of smaller particles than the indicated sieve size, for a particular size fraction, can be explained by insufficient sieving time. Particles smaller than the sieve openings did not make it through the sieves in the 15 minutes shaking time.

On the other hand, the presence of larger particles than the indicated sieve size can be explained by the shape of the particles. Many particles, especially those present in the smaller particle size fractions, have an elliptical shape rather than spherical shape and therefore will fit through the openings smaller than the corresponding spherical equivalent size recorded by the particle size analyzer. For the larger sized fraction, more particles have a spherical shape, when compared with those with elliptical shape. This variation in particle shapes is confirmed by the scanning electron micrographs, shown in Figures 4-5 to 4-8.

Three different magnifications are shown for samples of Coke 101, Coke 104, Coke 105 and Coke 107. As can be seen in these micrographs, as the particle size increases, the shape of the particles changes from oblong shape for particles sizes  $< 53 \mu\text{m}$  to roughly spherical shape for particle sizes  $> 250 \mu\text{m}$ . The morphology of the surface also changes with increasing particle size. For example, Coke 101 and Coke 104 particles have mostly a smooth surface without any cracks. Small cavities and flakes cover the surface of the particles. The surface bumps appear more pronounced for the larger particles, and cracks are present in the larger particles (see Figure 4-8).

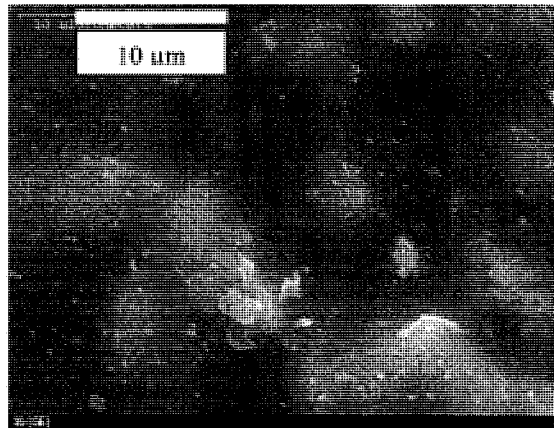
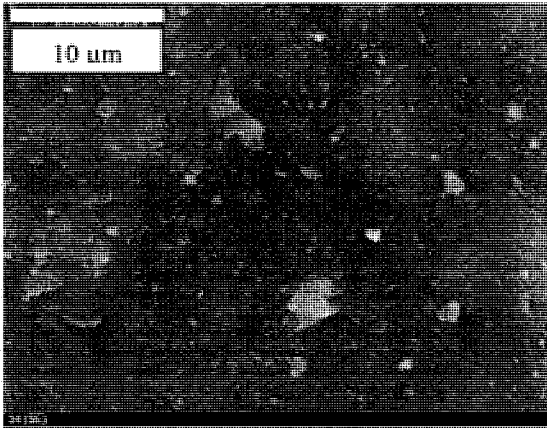
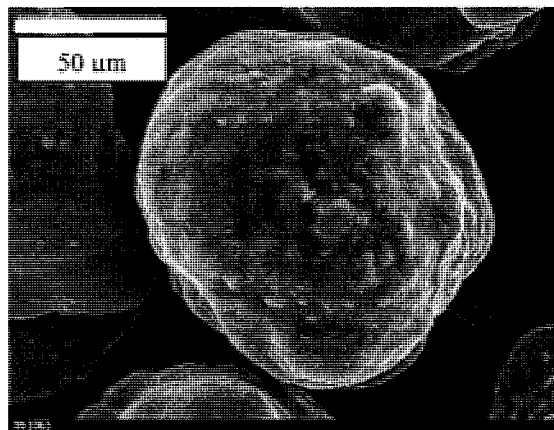
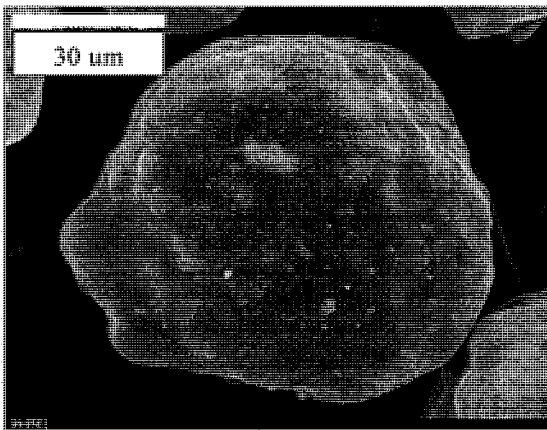
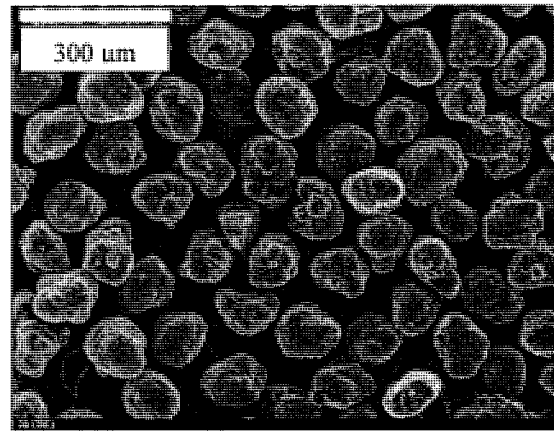
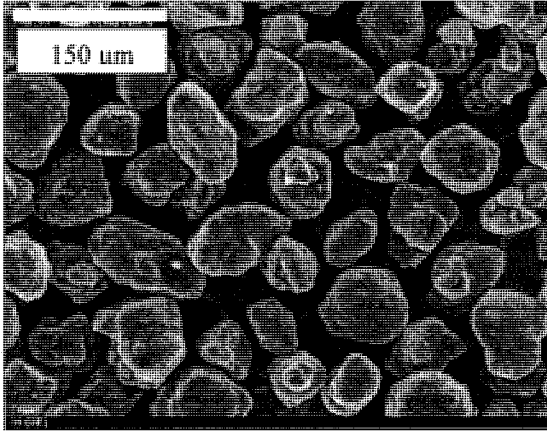


Figure 4-5. Scanning electron microscope images of Coke 101 ( $< 53\mu\text{m}$  fraction)

Figure 4-6. Scanning electron microscope images of Coke 104 (100-125  $\mu\text{m}$  fraction).

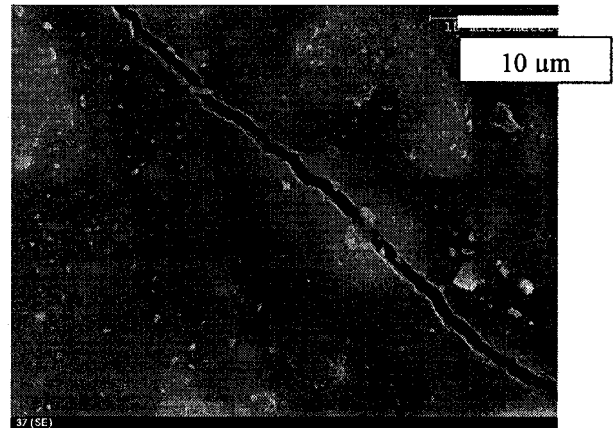
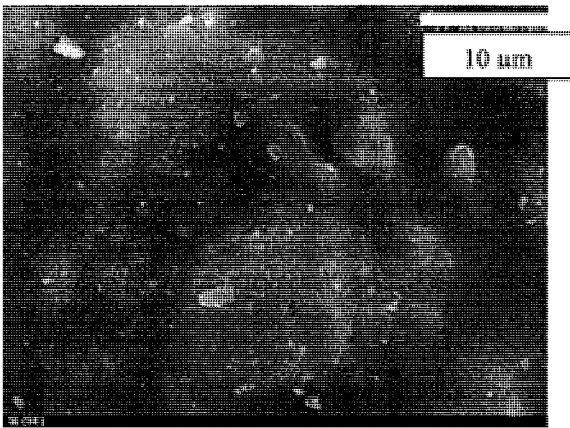
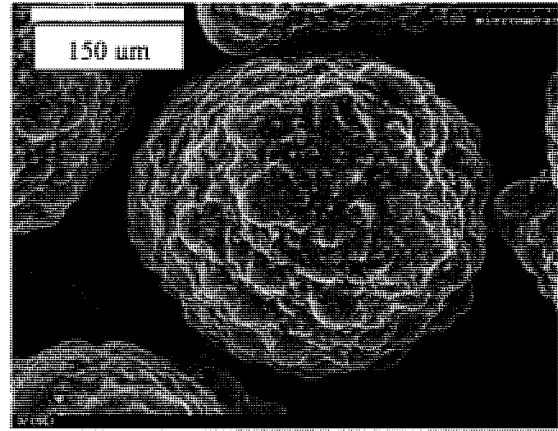
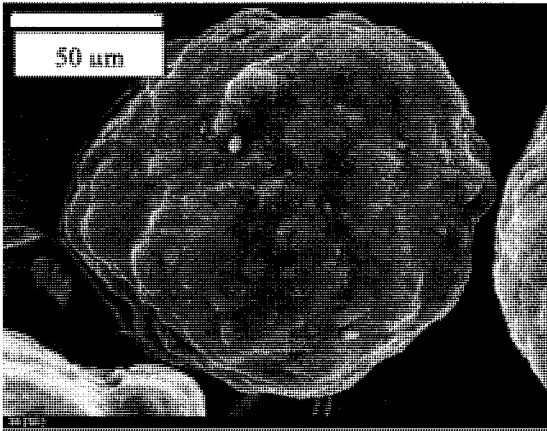
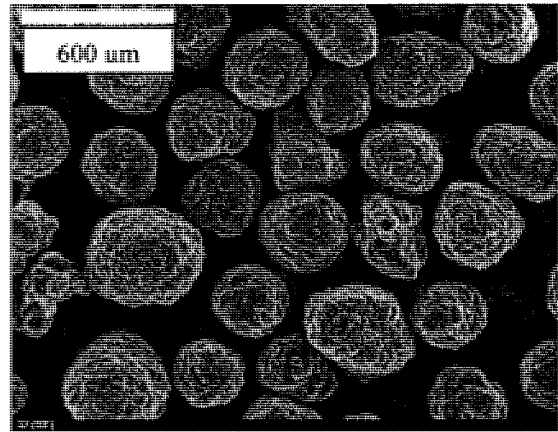
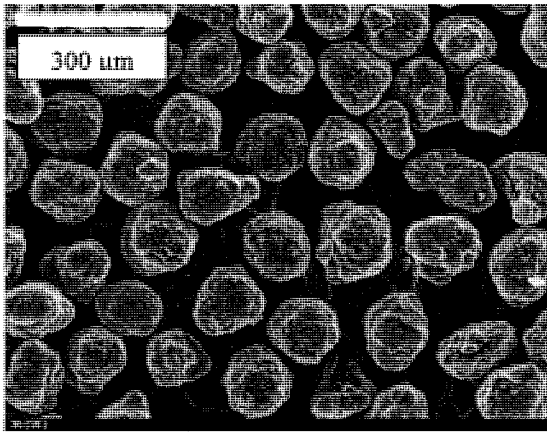


Figure 4-7. Scanning electron microscope images of Coke 105 (125-180 μm fraction).

Figure 4-8. Scanning electron microscope images of Coke 107 (>250 μm fraction).



Some particles from each size fraction were embedded in epoxy and then cut into thin layers. The cross-sectioned coke particles were examined by SEM and analyzed for sulphur by EDX. The coke particles were very brittle and many cross-sectioned pieces shattered during the cutting. The SEM and EDX results for the same four size fractions shown in Figures 4-3 to 4-6 are shown in Figures 4-9 to 4-12.

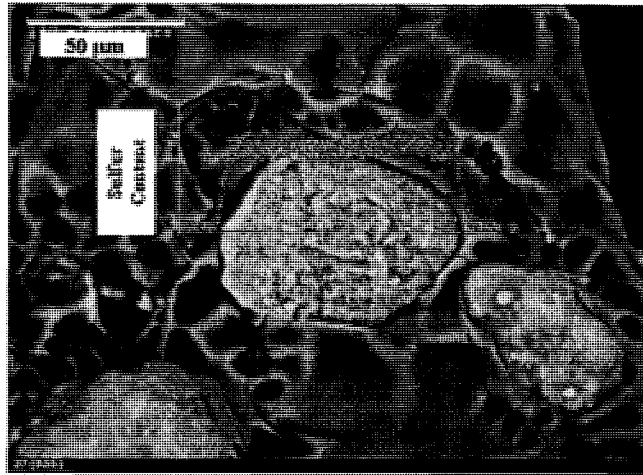


Figure 4-9. Scanning electron microscope image of Coke 101 ( $< 53\mu\text{m}$  fraction) and EDX line scan of sulphur concentration.

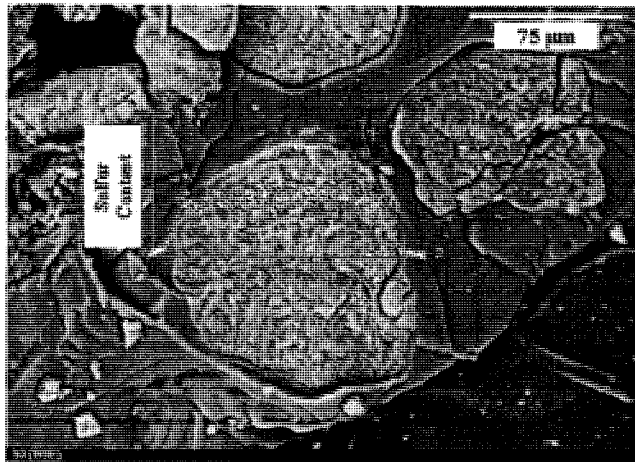


Figure 4-10. Scanning electron microscope image of Coke 104 (100-125 $\mu\text{m}$  fraction) and EDX line scan of sulphur concentration.

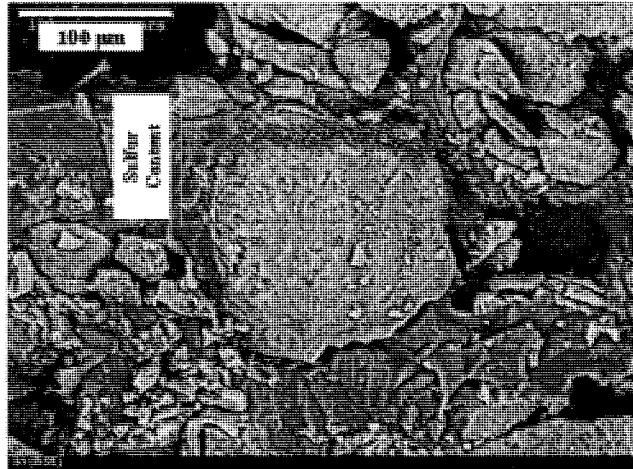


Figure 4-11. Scanning electron microscope image of Coke 105 (125-180  $\mu\text{m}$  fraction) and EDX line scan of sulphur concentration.

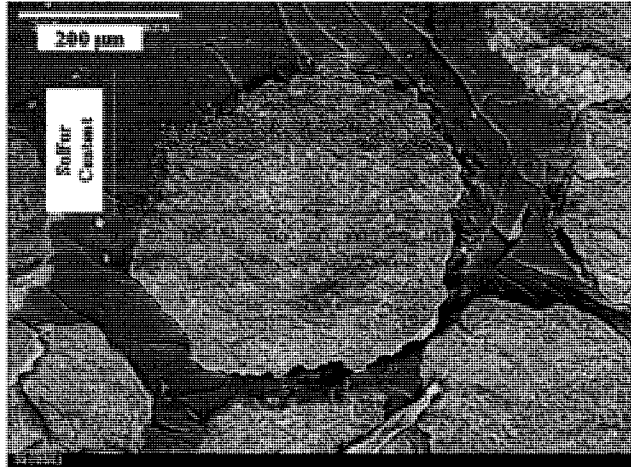


Figure 4-12. Scanning electron microscope image of Coke 107 (>250  $\mu\text{m}$  fraction) and EDX line scan of sulphur concentration.

The line scans for sulphur in the above figures show that sulphur is evenly distributed throughout the pellets, regardless of the size of the particle. The absolute concentration of sulphur cannot be easily determined by EDX because the samples were coated with a thin layer of gold prior to SEM and EDX examination. The epoxy, in which the microtomed cross-sections were imbedded, is an electric insulator and charge build-up during examination in the microscopy would result in very poor images and elemental analysis.

The total sulphur content of the coke fractions of different sizes was measured using a HoribaCarbon/Sulphur analyzer (EMIA-320 V). The sulphur and carbon contents of the different size fractions for Coke 1 and Coke 2 are shown in Figures 4-13 and 4-14.

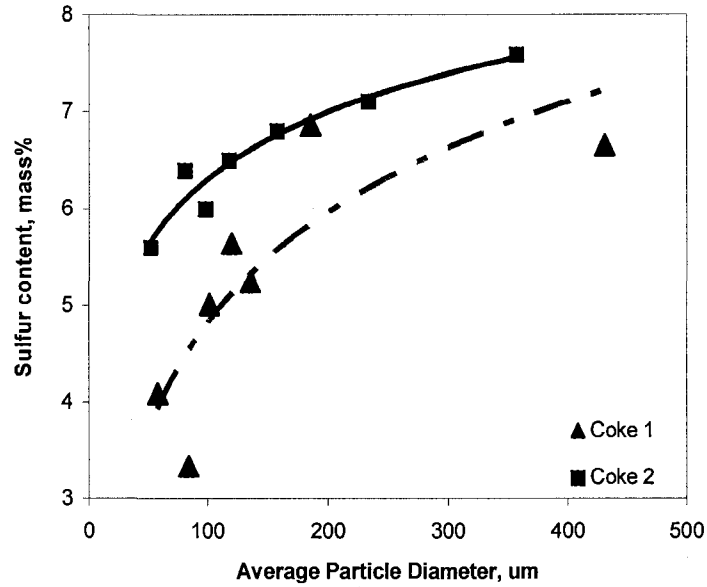


Figure 4-13. Sulphur content as a function of coke particle size for Coke 1 and Coke 2.

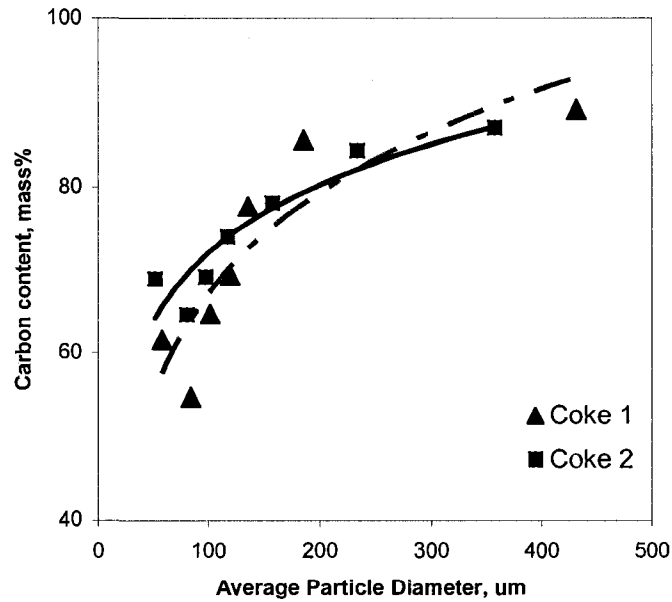


Figure 4-14. Carbon content as a function of coke particle size for Coke 1 and Coke 2.

According to the sulphur and carbon analyses, sulphur content varied from 4.1 % to 7.6 %, and the carbon content varied from 54.7 to 89.1 mass %. As is illustrated in

these figures, sulphur content appeared to increase with the increasing particle size of fluid coke, for both types of coke (Coke 1 and Coke 2). The same trend was observed for carbon content, shown in Figure 4-14. This is very unlikely, considering that the carbon/sulphur ratio was approximately constant regardless of particle size, as is illustrated in Figure 4-15.

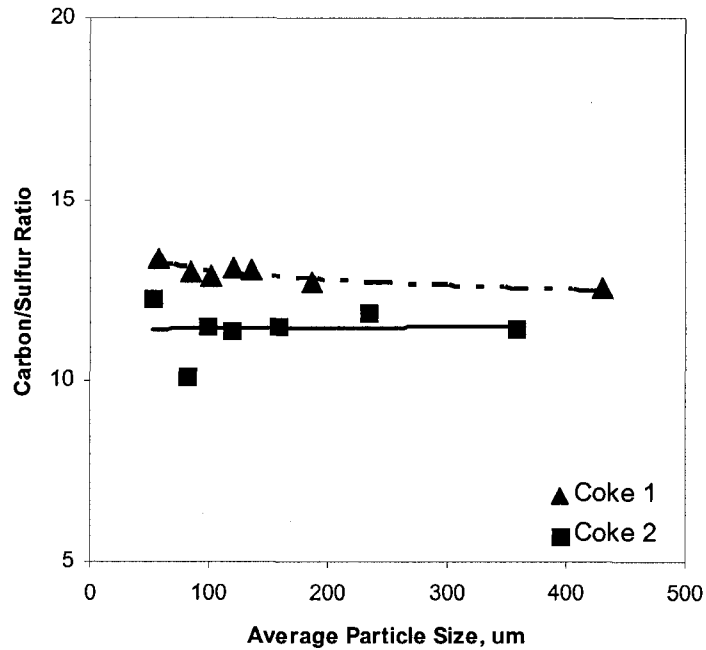


Figure 4-15. Carbon/Sulphur mass Ratio as a function of particle size for Coke 1 and Coke 2.

Repeat analyses were done several times, on different particle size fractions of Coke 1. Also, different amounts of coke were used for analysis, from 0.01g to 0.05g. The results are shown in Figure 4-16. Reducing the amount of sample used for analysis resulted in a smaller increase in the average sulphur and carbon content, especially for the smaller size fractions (Coke 101, 102, 103 104), but the sulphur content was still below the value obtained for the larger particle size fractions (Coke 105, 106, 107). When 0.01 g sample was used for analysis, the measured carbon and sulphur content is about the same, for all particle size fractions, regardless the particle size of the sample (see Figure 4-16).

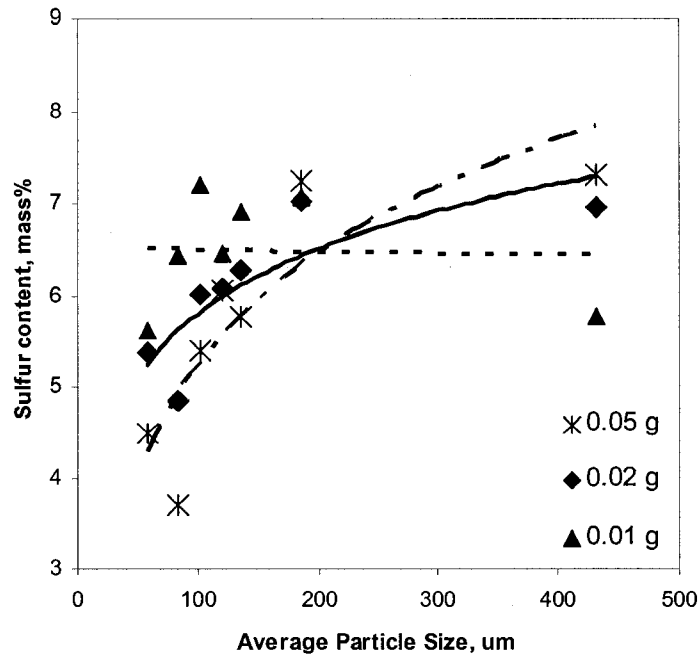


Figure 4-16. Sulphur content as a function of coke mass used for analysis, for Coke 1.

These variations of measured sulphur and carbon content of fluid coke with particle size might be related to the mass of the sample which is being analyzed. One possible cause is that for the larger samples, there may have been too small an amount of accelerator to properly combust the sample. This would result in lower amounts of  $\text{CO}_2$  and  $\text{SO}_2$  released, and therefore, the measured sulphur and carbon concentrations would be lower than the true values. Smaller samples would prevent saturating the detector and would result in more accurate results. The Horiba Carbon/Sulphur analyzer (EMIA-320 V) is most suitable for samples contained 0 to 6 mass % carbon and 0 to 1 mass % sulphur. Another reason for the low sulphur and carbon contents for the larger samples sizes is that the  $\text{CO}_2$  and  $\text{SO}_2$  concentration for the larger samples exceeded the linear region of the infrared detector.

The surface areas and the pore volumes of different particle size fractions of Coke 1 and Coke 2 were measured using an Omnisorp 360 automated adsorption apparatus. The results are presented in Table 4-2. Surface areas were obtained by the BET method, the t-plot method was used to obtain the micropore volumes and the desorption branch of

the nitrogen isotherm was used to determine the mesopore volume using the BHJ method (see Gregg and Sing (1982) for details of these methods).

Table 4-2. Comparison of surface area and pore volumes for Coke 1 and Coke 2 size fractions.

Size Range, $\mu\text{m}$	BET Surface Area, $\text{m}^2/\text{g}$		Micropore Volume, $\text{cm}^3/\text{g}$		Mesopore Volume, $\text{cm}^3/\text{g}$	
	Coke 1	Coke 2	Coke 1	Coke 2	Coke 1	Coke 2
<53	38.0	32.0	0.015	0.013	0.004	0.004
53 – 80	30.6	22.9	0.012	0.009	0.003	0.005
80 – 100	23.6	19.2	0.008	0.007	0.003	0.006
100 – 125	20.2	20.8	0.007	not meas.	0.005	0.004
125 – 180	15.8	12.6	0.006	0.004	0.003	0.004
180 – 250	7.9	7.0	0.003	0.002	0.005	0.004
>250	7.7	4.2	0.002	0.001	0.004	0.004

Specific surface area decreases with the increasing coke particle size, the same tendency was observed for both types of coke, Coke 1 and Coke 2, with surface areas of Coke 2 being slightly lower than that of Coke 1. Micropore volume decreases in the same manner, with increasing coke particle size, while the mesopore volume is approximately the same for all particle size fractions.

Two different ranges of  $P/P_0$  were used to calculate the specific surface area. First, a  $P/P_0$  range from 0.05 to 0.25 was used to calculate surface area. This range is usually used for mesoporous solids. Owing to the fact that all the samples contained a considerable amount of micropores (pores with diameter < 2 nm), a  $P/P_0$  range of 0.02 to 0.10 was used to recalculate the surface areas. The resulted data were re-examined, and it was found that significant improvement in the agreement of the data with the BET equation was obtained for a  $P/P_0$  range of 0.02 to 0.10. All surfaces area reported in this thesis are based on a  $P/P_0$  rang of 0.02 to 0.10. The Omnisorp 360 proprietary software was used for the BET, t-plot and BHJ analyses.

## 4.2. Effect of treatment time on surface area, porosity and mass loss

The influence of treatment time on surface area and porosity of the activated coke has been studied as a function of temperature and treatment gas composition. Activation was carried out at temperatures from 200 to 800 °C and treatment times up to 8 h. The starting material for all treatments was Coke 104, the 100-125 μm size fraction of Coke 1. The results for different treatment times are summarized in Table 4-3. The average pore radius,  $r_{avg}$ , was calculated from the total pore volume assuming cylindrical pores,

$$r_{avg} = 2000 V_p/S \text{ nm} \quad (4-1)$$

where  $V_p$  is the micro plus meso pore volume in  $\text{cm}^3/\text{g}$  and  $S$  is the surface area in  $\text{m}^2/\text{g}$ .

Table 4-3. Properties of activated fluid coke as a function of treatment time

Run #	Treatment Conditions				BET Surface Area, $\text{m}^2/\text{g}$	Pore Volume		Average Pore Radius, nm	Mass Loss, %
	Time, h	Temp, °C	Activation Agent mole %			Micro-pores, $\text{cm}^3/\text{g}$	Meso-pores, $\text{cm}^3/\text{g}$		
			CO <sub>2</sub>	H <sub>2</sub> O					
SS10401	4	602	100	0	25.7	0.00976	0.00304	0.996	1.6
SS10402	2	597	100	0	24.7	0.00869	0.00200	0.897	2.6
SS10403	8	611	100	0	23.9	0.00919	0.00296	0.981	0.8
SS10404	6	787	100	0	49.4	0.01846	0.00443	0.927	9.8
SS10405	4	793	100	0	37.2	0.01342	0.00424	0.950	8.1
SS10406	6	203	100	0	21.0	0.00860	0.00334	1.137	0.1
SS10407	4	417	100	0	21.9	0.00877	0.00291	1.067	0.1
SS10408	6	422	100	0	21.8	0.00808	0.00245	0.996	1.0
SS10409	6	602	100	0	24.0	0.00874	0.00397	1.059	2.6
SS10410	8	789	100	0	61.0	0.02220	0.00594	0.923	11.8
SS10411	8	426	100	0	22.0	0.00898	0.00317	1.104	0.3
SS10412	8	217	100	0	20.7	0.00766	0.00267	0.998	0.1
SS10416	6	458	64	36	20.6	0.00763	0.00427	1.154	0
SS10417	6	612	64	36	27.5	0.01028	0.00226	0.911	0.5
SS10418	4	617	31	69	26.4	0.01035	0.00367	1.062	0
SS10419	8	621	48	52	25.9	0.01009	0.00307	1.015	0
SS10423	8	624	30.4	69.6	36.4	0.01413	0.00227	0.900	1.2
LW104116	0.5	773	13	87	54.9	0.02052	0.00130	0.795	7.0
LW104118	1	774	13	87	100	0.03787	0.00225	0.802	10.4
LW104115	2	776	13	87	169	0.06546	0.00483	0.831	14.5
LW104114	4	777	13	87	275	0.1063	0.01358	0.872	22.0
LW104117	8	773	13	87	434	0.1460	0.03946	0.855	36.6

Treatment carried out at temperatures  $< 625^{\circ}\text{C}$  and treatment times up to 8 h resulted in an insignificant increase in the surface area, independent of the activation agent used (see Table 4-3); the surface area increased from  $20.2\text{ m}^2/\text{g}$  (surface area of Coke 104) to about  $25\text{ m}^2/\text{g}$  for treatment in pure carbon dioxide and to a maximum of  $36.4\text{ m}^2/\text{g}$  for treatment in  $\text{CO}_2/\text{H}_2\text{O}$  mixture. For treatment at  $790^{\circ}\text{C}$  in pure  $\text{CO}_2$ , the areas increased with increasing treatment time (see Figure 4-17), but even after 8 h the area increased to only  $61\text{ m}^2/\text{g}$ .

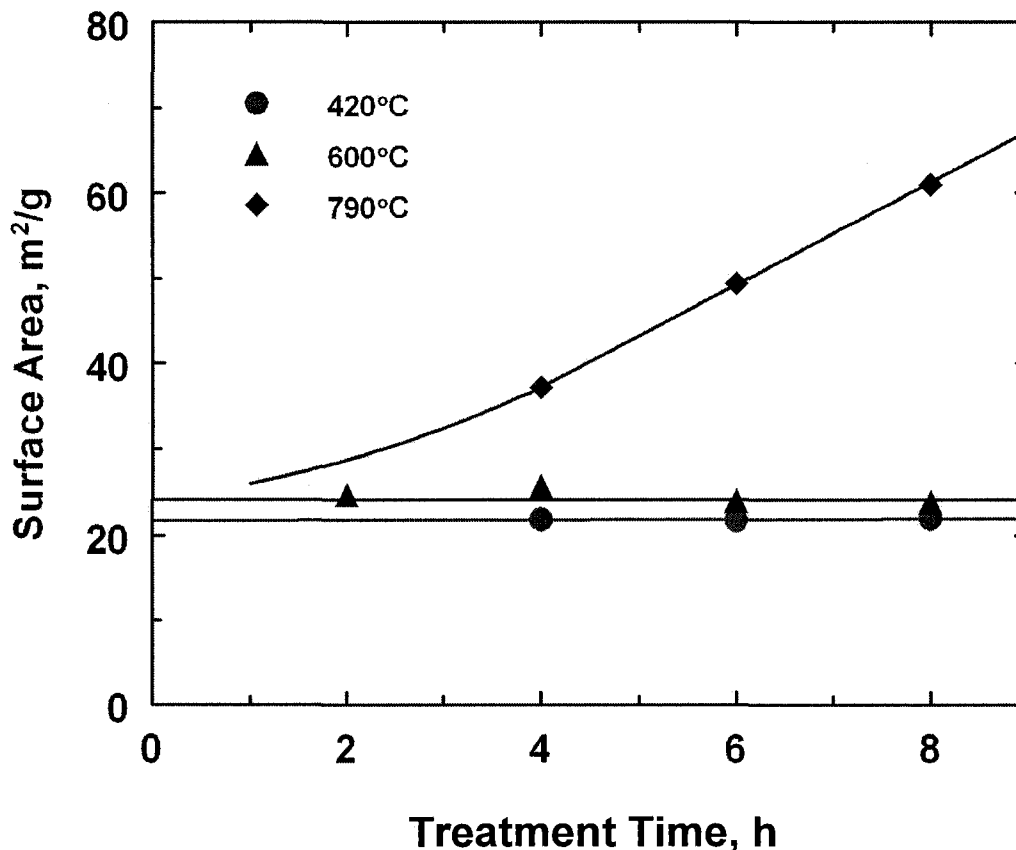


Figure 4-17. Effect of treatment time on surface area at different treatment temperatures in  $\text{CO}_2$  (flow rate:  $100\text{ mL}/\text{min}$ ).

When water was added to the  $\text{CO}_2$  treatment gas, at temperatures of about  $800^{\circ}\text{C}$ , the surface area increased markedly. At treatment times of 8 h, the surface area increased to over 20 times compared to the raw coke (see Figure 4-18). Hence, at  $800^{\circ}\text{C}$ , the reaction rate of carbon with water (Equations 2.1 and 2.2) is much faster than the reaction of carbon with carbon dioxide (Equation 2.3). For treatment in  $\text{CO}_2$ , the surface areas



increased linearly with treatment time. For treatment in CO<sub>2</sub>/H<sub>2</sub>O mixtures the surface area increased linearly with treatment time for surface areas up to about 100 m<sup>2</sup>/g. At higher surface areas the increase with treatment time was slower. This is probably due to mass transfer limitations: as the surface area increases, the pores penetrate further and further into the particles. Diffusional limitation can affect the rate of carbon gasification as the distance which the activating water and the gaseous reaction products have to diffuse increases.

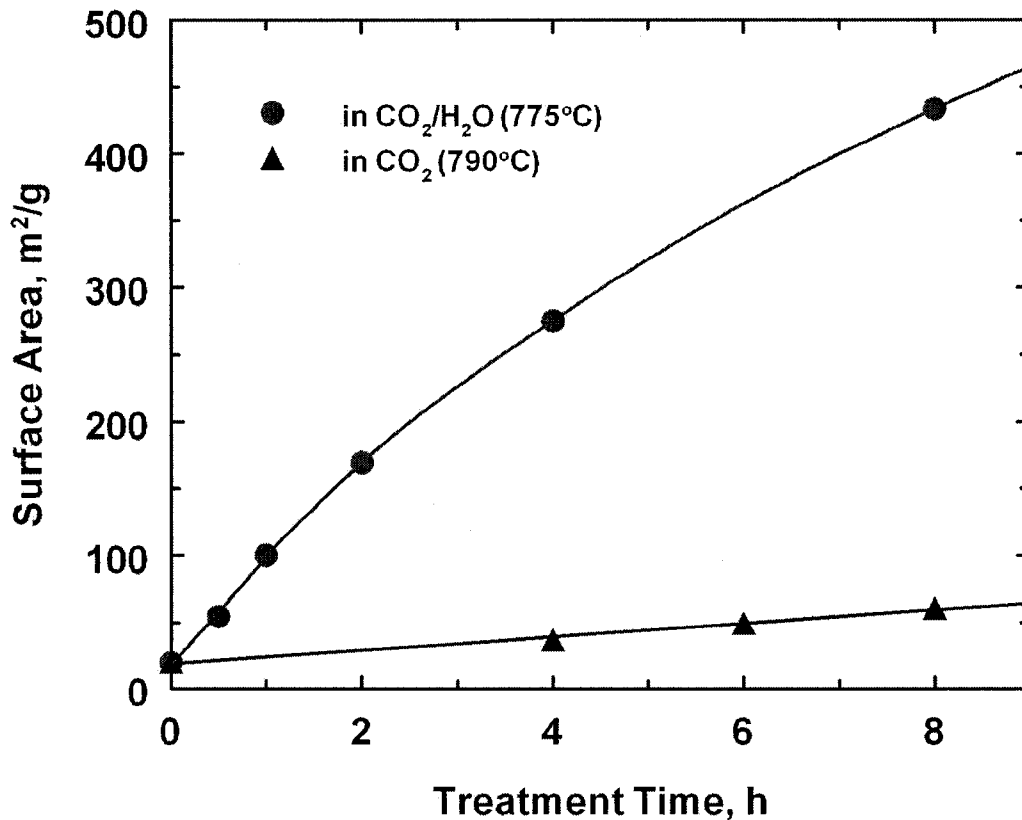


Figure 4-18. Effect of treatment time on surface area using different activating agents.

The pore volume increased with increasing treatment time, in the same manner as surface area. As can be seen in Figure 4-19, the increase depended on the treatment temperature and the composition of activation agent. No significant changes were observed in the pore radius; the average pore radii were practically constant at about 1 nm, regardless of the treatment time, treatment temperature or the nature of activating agent. This means that the increase in pore volume is due not to the widening of the existing pores, but due to the growth in length and/or number of the pores.

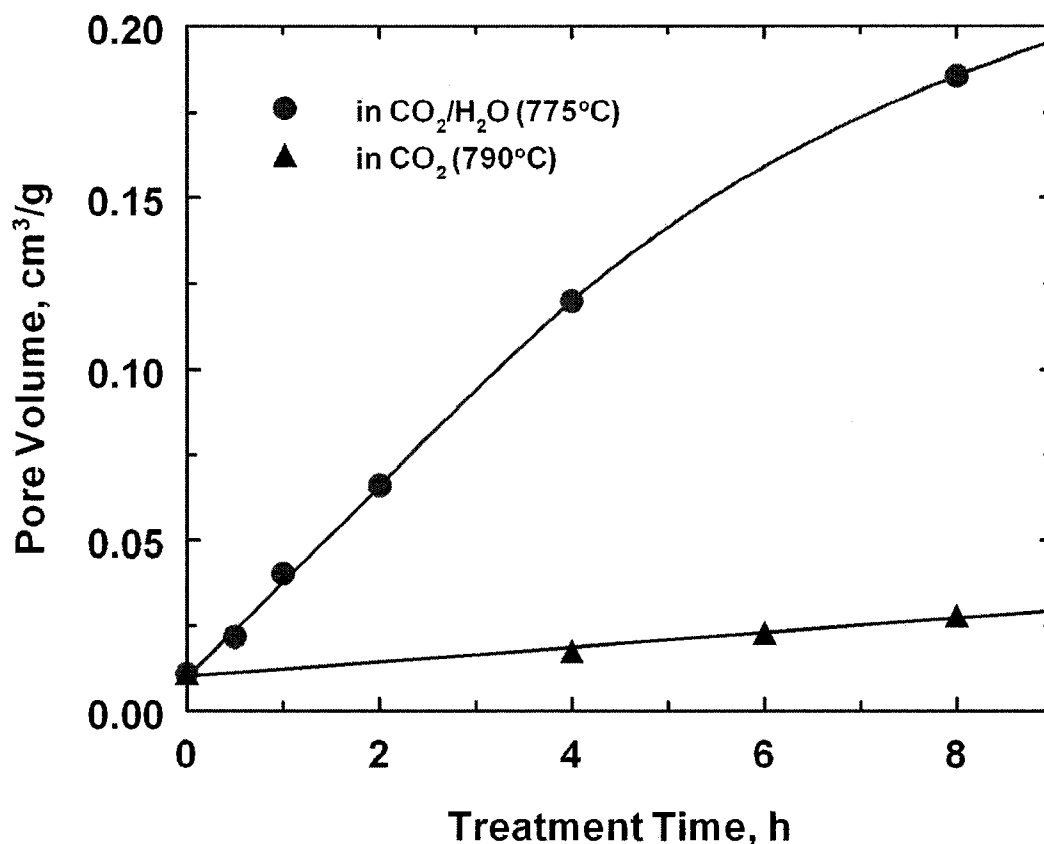


Figure 4-19. Effect of treatment time on pore volume.

If the average pore radius remains relatively constant, then a plot of pore volume as a function of surface area should be linear because the pore volume is proportional to the average pore radius squared and the pore wall area (i.e. the surface area) is directly proportional to average pore radius. For cylindrical pores this relationship is

$$V_p = (r_{avg}/2000)S \text{ cm}^3/\text{g} \quad (4-2)$$

with the average pore radius,  $r_{avg}$ , in nm, and the surface area,  $S$ , in  $\text{m}^2/\text{g}$ . A plot of all the total pore volume (micro- plus meso-pore volume) data as a function of surface area listed in Table 4-3 is shown in Figure 4-20. The linearity of this plot means that the average pore size of the activated coke samples is neither a function of treatment time nor treatment atmospheres for the conditions studied. The slope of  $4.3 \times 10^{-4} \text{ cm}^3/\text{m}^2$  corresponds to an average pore radius of 0.86 nm.

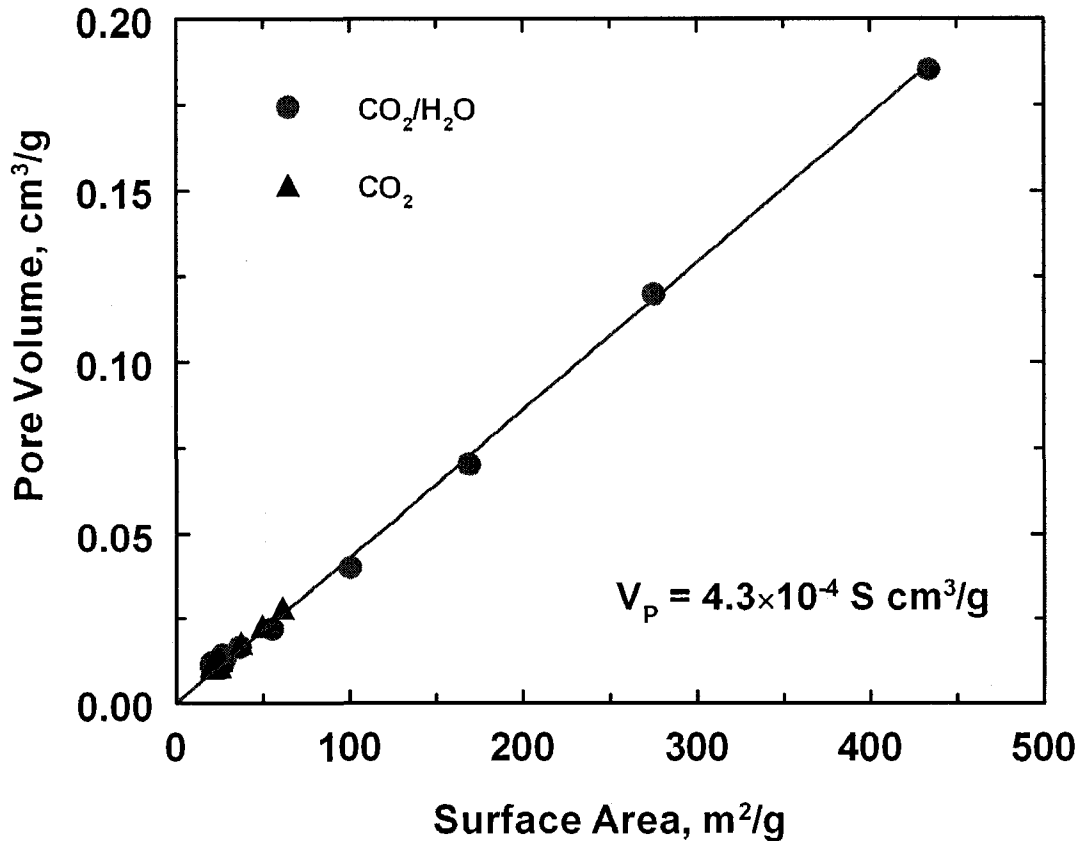


Figure 4-20. Relationship between total pore volume and surface area for Coke 104 activated for various times.

The relationship between the mass loss and surface area is shown in Figure 4-21. The relationship between mass loss and surface area is more complex than the relationship between pore volume and surface area. The results indicate that higher mass losses are required for treatment with CO<sub>2</sub> than with CO<sub>2</sub>/H<sub>2</sub>O mixtures to obtain the same surface area. For treatments in the CO<sub>2</sub>/H<sub>2</sub>O mixture, the mass loss varies approximately linearly with surface area at surface areas above 100 m<sup>2</sup>/g. The initial mass losses do not result in large surface area gain because some of the mass loss is due to desorption of volatiles which does not generate significant amounts of surface area.

The following conclusions and observations are made from the effects of treatment time on properties of the treated fluid coke:

1. CO<sub>2</sub>/H<sub>2</sub>O mixtures are much more effective in increasing the surface area of fluid coke than pure CO<sub>2</sub>.

2. Surface area of fluid coke increases linearly with treatment times during treatment in  $\text{CO}_2/\text{H}_2\text{O}$  or  $\text{CO}_2$  at  $\approx 800^\circ\text{C}$  for surface areas up to about  $100\text{ m}^2/\text{g}$ ; the increases in surface area is slower at higher surface areas.
3. The dependence of pore volume on treatment time at  $\approx 800^\circ\text{C}$  is very similar to the dependence of surface area on treatment time.
4. The average pore size (e.g. radius) is independent of treatment time and surface area. This leads to the conclusion that increases in surface areas occur by the lengthening and/or formation of new pores with similar sizes with increasing treatment times.
5. The relation between mass loss and surface area depends on the composition of the activation gases.

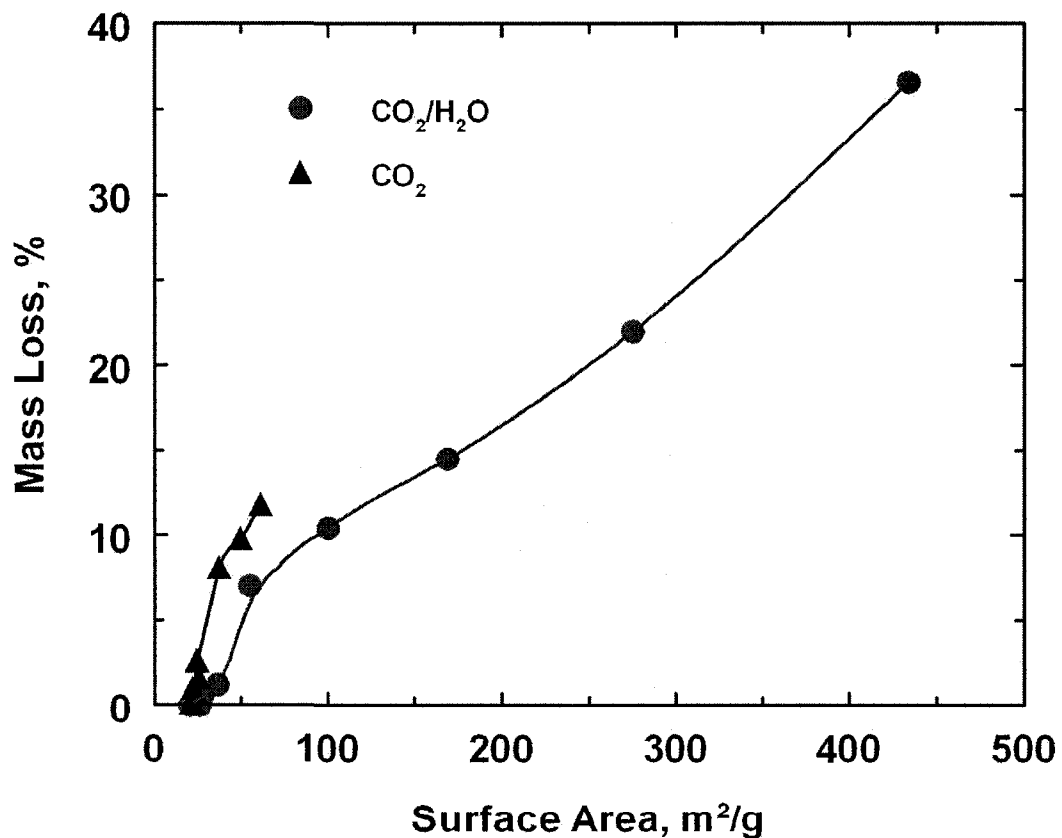


Figure 4-21. Relationship between mass loss and surface area at different treatment times.

### 4.3. Effect of treatment temperature on surface area, porosity and mass loss

In this section, the effects of treatment of fluid coke at various temperatures on surface area and porosity are described. Activation was carried out at temperatures in the range of 200 to 800°C. The starting material for all treatments was Coke 104, the 100-125 µm size fraction of Coke 1. The results of treatments at different temperatures are summarized in Table 4-4 and the effects of treatment time on surface area, pore volume and mass loss are shown.

Table 4-4. Influence of treatment temperature on surface area, pore volume, and mass loss.

Run	Treatment Conditions					Surface Area, m <sup>2</sup> /g	Pore Volumes		Mass Loss, %				
	Treatment Gas Rates		P, kPa	Time, h	Temp. °C		Micro, cm <sup>3</sup> /g	Meso, cm <sup>3</sup> /g					
	CO <sub>2</sub> , mL/min	H <sub>2</sub> O, g/h											
SS10412	100	0	103	8	217	20.7	0.0077	0.0027	0.0				
SS10411					426	22.0	0.0090	0.0032	0.3				
SS10403					611	24.8	0.0092	0.0030	0.8				
SS10410					789	60.4	0.0224	0.0059	11.8				
MB01462	67	1.5	103	4	542	26.8	0.0107	0.0020	2.4				
MB10461					702	44.0	0.0161	0.0007	7.9				
MB10463					754	104	0.0394	0.0026	12.7				
MB10460					792	165	0.0632	0.0092	17.8				
IC10478	188	4.5	345	4	509	26.8	0.0104	0.0026	2.4				
IC10490					600	33.4	0.0122	0.0015	3.0				
IC10476					608	36.7	0.0137	0.0012	4.7				
IC10472					685	150	0.0564	0.0024	12.5				
IC10477					725	257	0.0998	0.0086	17.9				
IC104103					734	285	0.1109	0.0124	17.0				
IC104104					762	365	0.1415	0.0114	25.0				
IC10469					766	381	0.1480	0.0212	24.6				
IC10489					770	346	0.1339	0.0114	25.2				
IC10485					231	8.1	627	4	475	25.4	0.0025	0.0025	0.6
IC10487									578	39.4	0.0143	0.0011	2.6
IC10484	667	241	0.0928	0.0058					28.3				
IC10488	715	377	0.1476	0.0198					22.2				
IC104101	738	370	0.1448	0.0186					22.3				
IC10486	752	452	0.1744	0.0408					32.7				
IC104100	767	429	0.1636	0.0435					34.7				

Figure 4-22 shows the effect of temperature on surface area. Activation carried out at temperatures below 600°C did not have a significant effect on the development of surface area, regardless of the treatment gas composition. This observation was expected, since the raw coke was produced at about 550°C. It is most probable that this slight increase in surface area is due to the evolution of volatile matter present in the raw coke matrix.

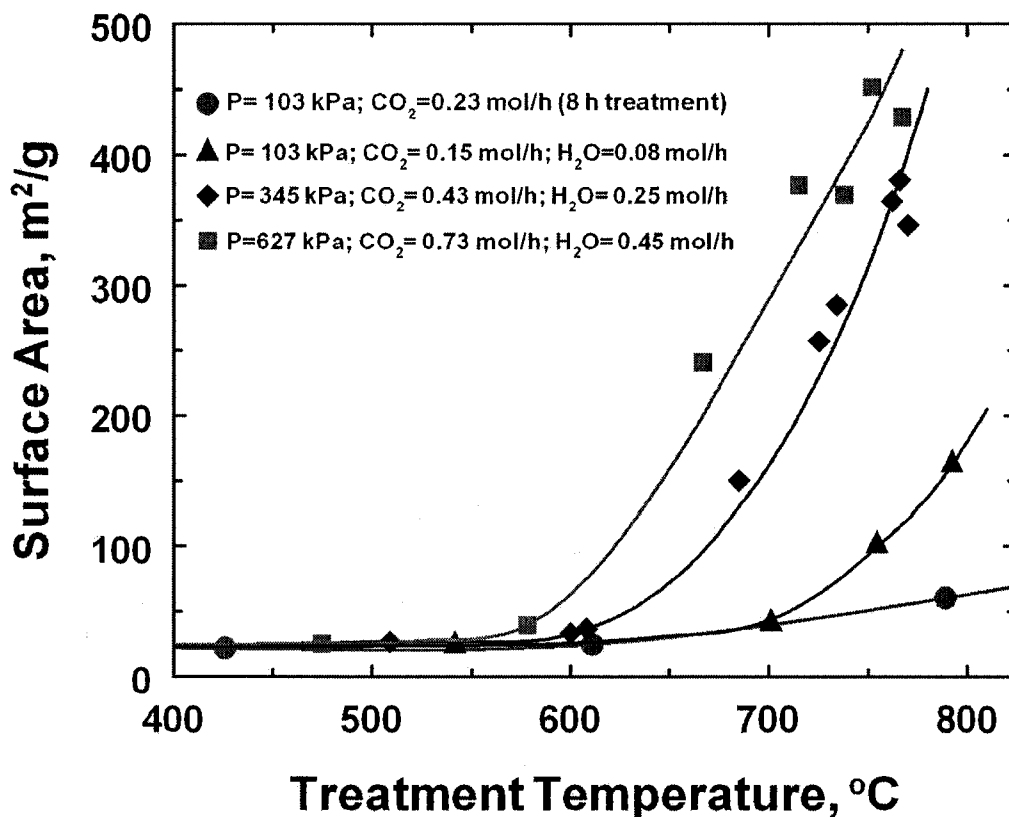


Figure 4-22. Effect of treatment temperature on the surface area (treatment time was 4 h unless indicated otherwise).

At higher treatment temperatures above 600°C, surface areas increases, but the magnitude of the increase was very much dependent on the treatment gas composition. When activations were performed with pure carbon dioxide as the treatment gas, surface areas increased moderately with increases in temperature. As shown in Figure 4-22, a maximum surface area of 60.4 m<sup>2</sup>/g was achieved at a treatment temperature of 789°C and a treatment time of 8 hours. When steam was added to the carbon dioxide, during activation process the surface area increased sharply. Surfaces areas higher than

400 m<sup>2</sup>/g were obtained at treatment temperature of 800°C for 4 h. The effect of water depended on the amount of water added; increasing amounts of water and increasing water partial pressure resulted in increasing surface areas.

This effect of water amount and concentration is expected because the coke activation reactions consume water (see Equations 2-1). Every gram of coke converted to CO by reaction with water consumes 1.5 g of H<sub>2</sub>O, and an additional 1.5 g of H<sub>2</sub>O is consumed per gram of carbon if the CO formed is converted to CO<sub>2</sub> by reaction with H<sub>2</sub>O (Equation 2-2). If 3.0 g of water are consumed per g of carbon reacted, then the maximum mass loss for Runs MB10460 to MB10463 (see Table 4-4 and solid triangles in Figure 4-22) would be 20 mass %. For such low amounts of water, the increase in surface area is limited by the amount of water.

The difference in the effect of CO<sub>2</sub> and H<sub>2</sub>O on the activation is due to both kinetic and thermodynamic factors. The equilibrium constants, K<sub>P</sub>, for the main reactions in coke activation (Equation 2-1 to 2-5) for the temperature range of 500 to 900°C can be approximated by

$$\log_{10} K_{P,i} = a_i + b_i/T \quad (4-3)$$

Values of a<sub>i</sub> and b<sub>i</sub> for the five main overall reactions in coke activation, along with K<sub>P,i</sub> values at 600 and 800°C, are listed in Table 4-5. All reactions of carbon with H<sub>2</sub>O and CO<sub>2</sub> are endothermic; hence values of K<sub>P,i</sub> for these reactions increase with increasing temperature. At 800°C, the equilibrium constants for the first three reactions are of similar magnitude, but experimental results showed that the rate of reaction of carbon with CO<sub>2</sub> was much lower than the rate of reaction with H<sub>2</sub>O. The lower rates of reaction of carbon with CO<sub>2</sub> compared to H<sub>2</sub>O are probably due to a higher activation energy for the CO<sub>2</sub> carbon reaction. The carbon-hydrogen reaction (Equation 2-4) is exothermic; hence, the equilibrium constant of the gasification of carbon by hydrogen decreases with increasing temperature. However, kinetics limit methane formation at low temperature where the equilibrium constant is high. No quantitative kinetic experiments, which would allow estimation of activation energies and concentration dependencies of the activating gases of the coke gasification rates, were done.

Table 4-5. Equilibrium constants for main overall reactions during activation of coke (values estimated from Fig. 11-1 in Modell and Reid, 1983).

Reaction	Equation Number	Constants in Eq. 3.1		K <sub>p</sub> at 600 and 800°C	
		a <sub>i</sub>	b <sub>i</sub>	600°C	800°C
$C + H_2O \rightleftharpoons CO + H_2$	(2-1)	7.5	-7000	0.30	9.5
$C + 2 H_2O \rightleftharpoons CO_2 + 2 H_2$	(2-2)	5.8	-5200	0.70	9.0
$C + CO_2 \rightleftharpoons 2 CO$	(2-3)	9.1	-8800	0.11	7.9
$C + 2 H_2 \rightleftharpoons CH_4$	(2-4)	-5.8	4700	0.38	0.04
$CO + H_2O \rightleftharpoons CO_2 + H_2$	(2.5)	-1.7	1800	2.3	0.95

High surface areas are generated during the activation of fluid coke by producing pores in the coke particles. The pore volume is related to the surface area and the mass loss during activation. The effects of treatment temperature on the pore volume and mass loss of activated coke for the runs listed in Table 4-4 are shown in Figures 4-23 and 4-24.

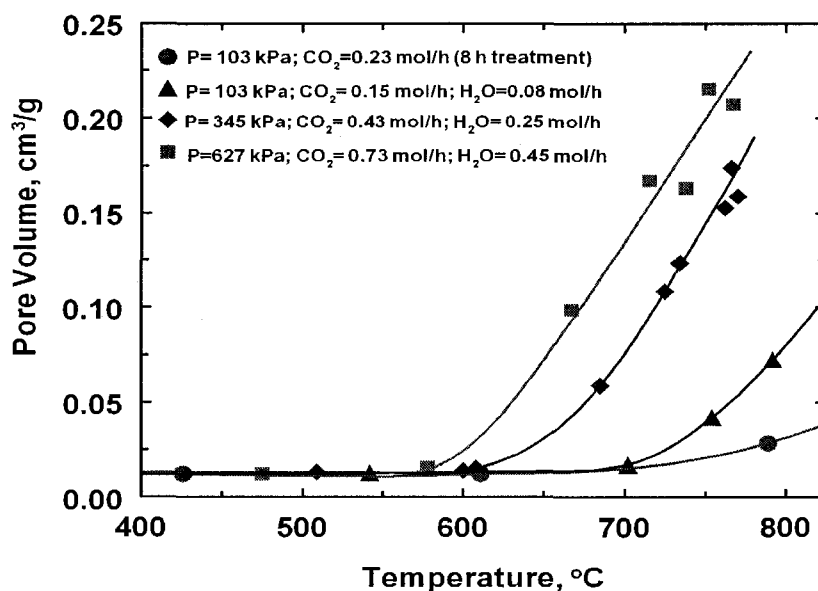


Figure 4-23. Effect of treatment temperature on the pore volume (meso plus micro) (treatment time was 4 h unless indicated otherwise).



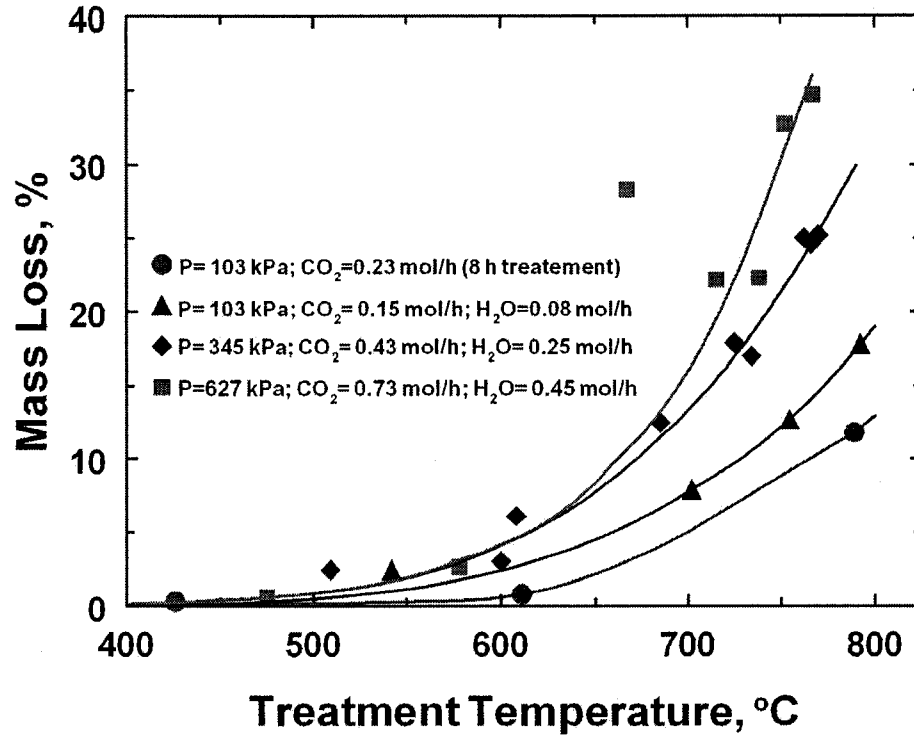


Figure 4-24. Effect of treatment temperature on the mass loss (treatment time was 4 h unless indicated otherwise).

The mass loss is defined as

$$\% \text{ mass} = \frac{(\text{initial mass}) - (\text{final mass})}{(\text{initial mass})} \quad (4-4)$$

The pore volume and mass loss results follow similar patterns to that described for surface area, i.e. very little increase in pore volume or mass loss at temperatures below 600°C. The small, and variable, mass losses at temperatures below 600°C were due to loss of volatiles, mostly moisture, and are not accompanied by increases in pore volumes or surface area. This is not surprising because the fluid coke is exposed to temperatures of about 550°C during its production in the fluid coking process.

The similarity in the shapes of the surface area, pore volume and mass loss curves indicates that correlations should exist between these three variables; Figures 4-25 and 4-26 illustrate these relationships for the results listed in Table 4-4. The linear correlation between total pore volume,  $V_p$ , and BET surface area,  $S$ , is excellent (see Figure 4-25). The linear relation implies that the pore size is independent of the pore volume. The

average pore radius, according to the correlation in Figure 4-25, is 0.90 nm; this value is essentially the same as the value of 0.86 nm in Section 4.2.

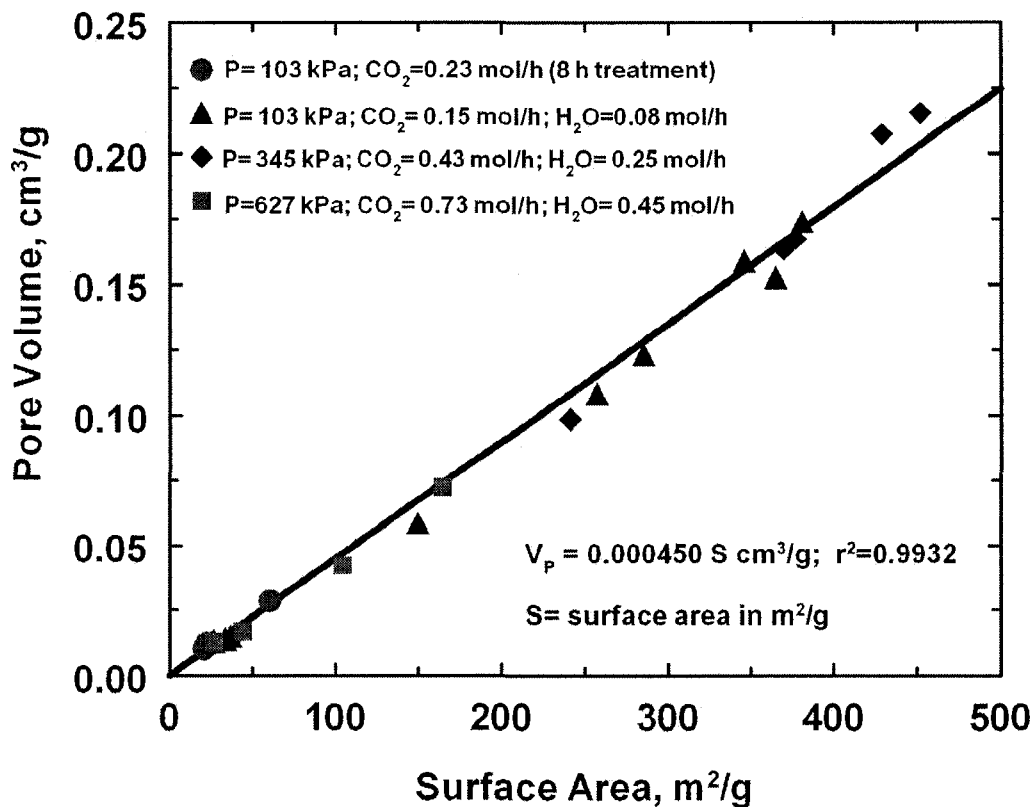


Figure 4-25. Relationship between pore volume (micro+meso) and surface area. (treatment time was 4 h unless indicated otherwise).

The correlation between mass loss and surface area (Figure 4-26) was not as good as the pore volume – surface area correlation (Figure 4-25). Mass loss does not necessarily result in increases in surface area because mass loss can be due to gasification of carbon on the external surface of the particles which would not result in the generation of surface area. Loss of some volatile components and conversion of sulphur in organic sulphur compounds to hydrogen sulphide also result in mass loss without significant increases in surface area. The excellent correlation between pore volume and surface area shows that the pore size distribution does not change much with changes in surface area, and the poorer correlation of mass loss with surface area shows that not all mass loss results in increases in surface area.

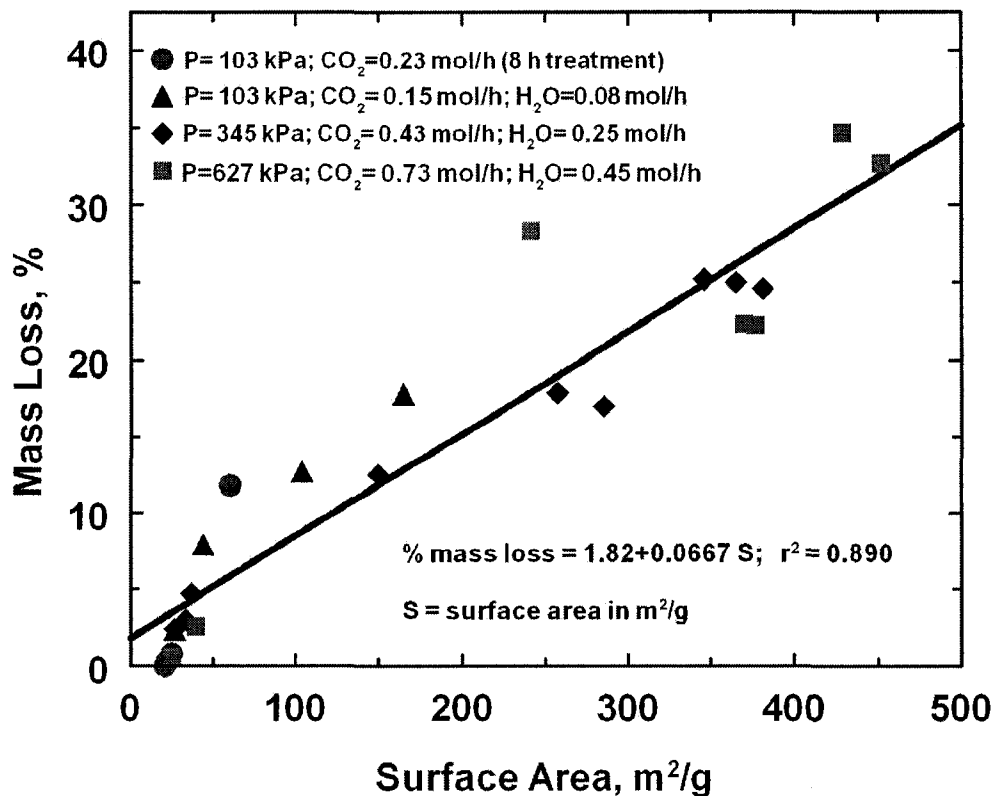


Figure 4-26. Relationship between mass loss and surface area (treatment time was 4 h unless indicated otherwise).

The following conclusions and observations are made from the effects of treatment temperature on properties of the treated fluid coke:

1. Treatments in CO<sub>2</sub>/H<sub>2</sub>O or CO<sub>2</sub> at temperatures ≤600°C for ≤8 h do not result in significant increases in the surface area of fluid coke.
2. Surface areas increase significantly with increases in treatment temperatures from 600 to 800°C and the effect of increasing temperatures is more pronounced for H<sub>2</sub>O containing treatment gases than for treatment with pure CO<sub>2</sub>.
3. The dependence of pore volume on treatment temperature at treatment temperatures of 600 to 800°C is very similar to the dependence of surface area on treatment temperature.
4. The average pore size (e.g. radius) is independent of treatment temperature and surface area. This leads to the conclusion that increases in surface areas occur by

the lengthening of pores and/or the formation of pores with similar sizes with increasing treatment temperatures.

5. The correlation between mass loss and surface area is not as good as the correlation between pore volume and surface area.

#### **4.4. Effect of treatment gas composition on surface area, porosity and mass loss**

The effect of treatment gas composition on the surface area and porosity of the activated coke was studied. Activation was carried out at temperature of 800°C, 4 h treatment time and different treatment gas compositions. The starting material for all treatments was Coke 104, the 100-125 µm size fraction of Coke 1. Results of treatment in pure CO<sub>2</sub> were ineffective in increasing surface area (see Sections 4.2 and 4.3); hence, discussion for treatment in pure CO<sub>2</sub> will not be included in this section. The effects of different CO<sub>2</sub>/H<sub>2</sub>O ratios, N<sub>2</sub>/H<sub>2</sub>O treatment gas and treatment in O<sub>2</sub> containing streams will be discussed.

##### ***4.4.1 Activation of fluid coke with CO<sub>2</sub>/H<sub>2</sub>O mixture***

Activation of fluid coke in H<sub>2</sub>O/CO<sub>2</sub> mixture was done at temperature of 800°C, 4 h treatment time and pressure of 345 kPa. The CO<sub>2</sub> flow rate was maintained constant at 188 ml/min while H<sub>2</sub>O flow rate was varied from 2.3 to 18 mL/h. The effect of H<sub>2</sub>O flow rate on the surface area and mass loss is shown in Figure 4-27, and the effect of H<sub>2</sub>O flow rate on the porosity of activated coke is shown in Figure 4-28. Figure 4-29 shows the relationship between the pore volume and surface area of the activated coke, at the treatment conditions mentioned above.

The surface area and mass loss increased linearly with increasing water concentration, and the same trend is observed for the pore volume (Figures 4-27 and 4-28). This results in a linear relationship between pore volume of activated coke and BET surface area when pore volume is plotted versus BET surface area (Figure 4-29). These relationships again show, even at higher treatment pressures, that surface area development occurs by the gasification of the carbon with water which creates new and/or longer pores with an average radius which is constant. The average radius of these pores from the slope of V<sub>p</sub>, total pore volume versus area line in Figure 4-29 is 0.96 nm.

This average radius is about the same as the average radii of about 0.86 and 0.90 nm obtained with treatments at lower concentrations of water, i.e. treatment at atmospheric pressure (Sections 4.2. and 4.3).

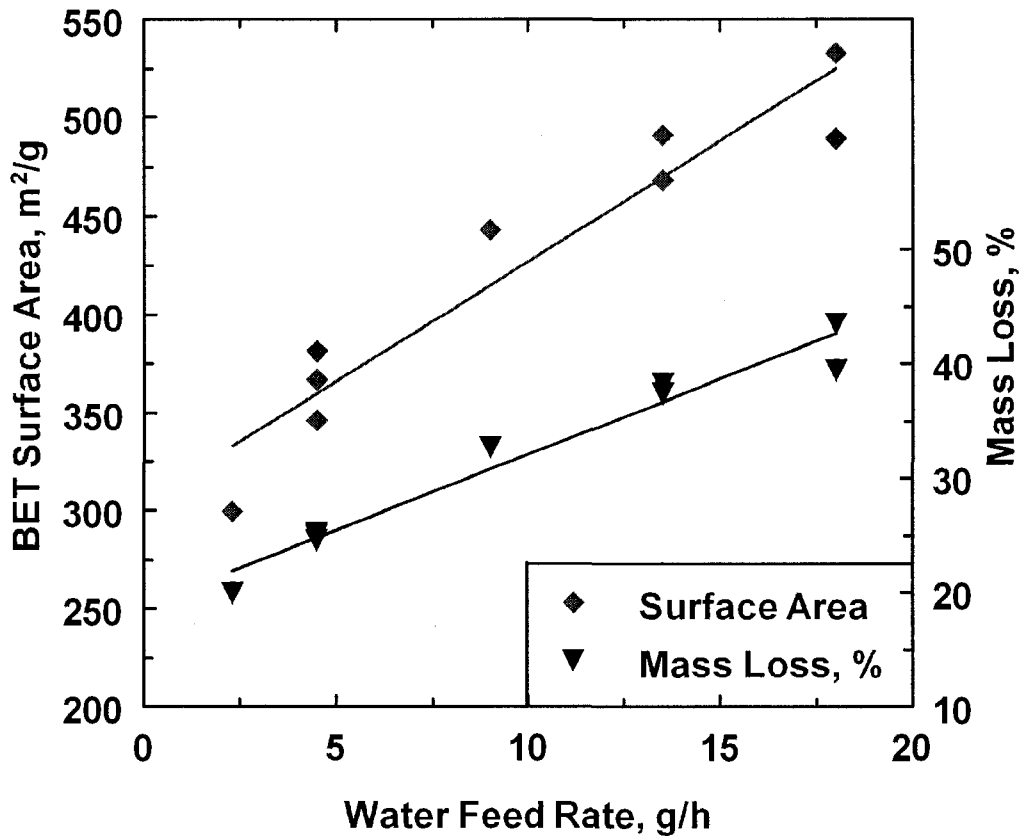


Figure 4-27. Effect of H<sub>2</sub>O flow rate on the BET surface area and mass loss (treatment conditions: 800 °C, 345 kPa).

The main gasification reaction of carbon in the H<sub>2</sub>O/CO<sub>2</sub> mixture is the reaction of H<sub>2</sub>O with carbon to form CO and CO<sub>2</sub> (Reactions 2-1 and 2-2). Secondary reactions of H<sub>2</sub>, formed during the above reactions, with carbon to form CH<sub>4</sub> (Reaction 2-4), and with sulphur, to form H<sub>2</sub>S also contribute to the mass loss and area generation. Gas chromatographic (GC) analyses show the presence of CH<sub>4</sub> and H<sub>2</sub>S in the effluent gases from the activation reactor.

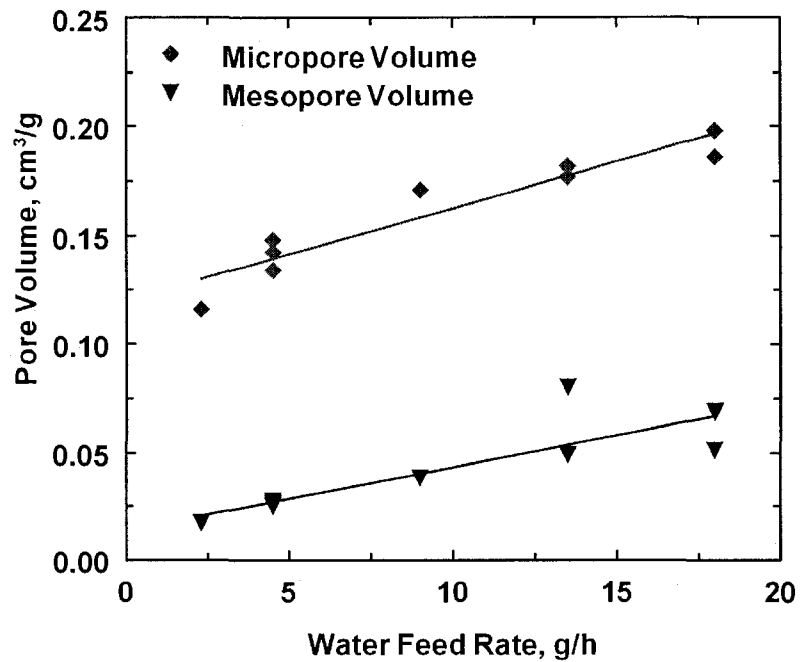


Figure 4-28. Effect of H<sub>2</sub>O flow rate on the pore volumes (treatment conditions: 800 °C, pressure: 345 kPa).

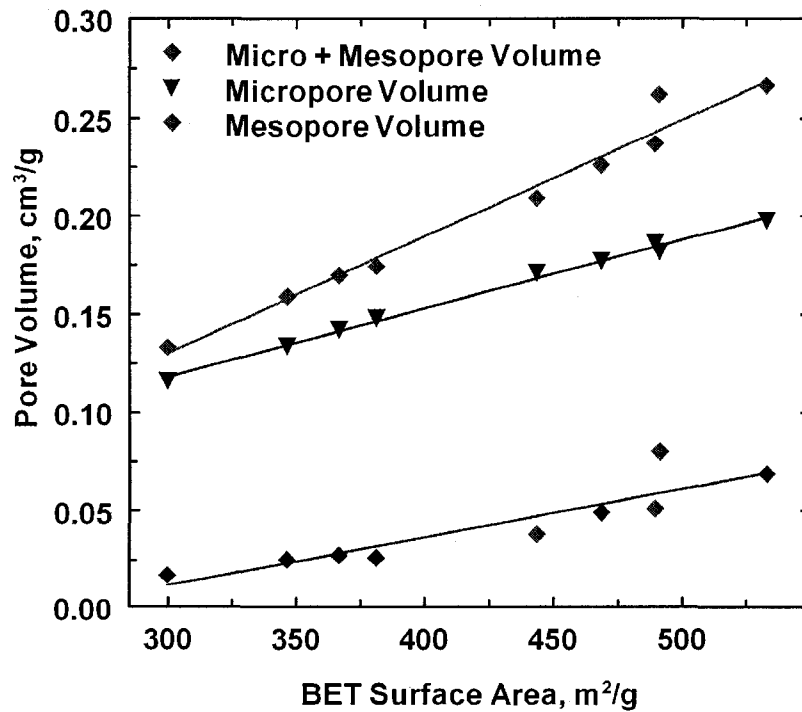


Figure 4-29. Relationship between the pore volume and BET surface area (treatment conditions: 800 °C, pressure: 345 kPa, H<sub>2</sub>O flow rate from 2.3 to 18 mL/h)

The effect of water feed rate, for the 4 h treatments at 800°C and 345 kPa, on the relative amounts of CH<sub>4</sub>, CO and H<sub>2</sub>S are shown in Figures 4-30 and 4-31. The GC areas for CH<sub>4</sub>, CO and H<sub>2</sub>S are directly related to the amount of these components in the effluent mixtures because the response factors for these three compounds do not differ greatly. The average ratios of CO:CH<sub>4</sub>:H<sub>2</sub>S for the results shown in Figures 4-30 and 4-31 are about 1:0.1:0.04. The trend in the concentrations of CO, CH<sub>4</sub> and H<sub>2</sub>S, with increasing H<sub>2</sub>O concentrations, shown in these figures is as expected, i.e. increasing H<sub>2</sub>O concentrations would result in increased conversion of CO to CO<sub>2</sub> and H<sub>2</sub> according to the water gas shift reaction (Reaction 2-5) and increased H<sub>2</sub> concentrations would result in increased formation of CH<sub>4</sub> (Reaction 2-4) and H<sub>2</sub>S. More detailed effluent composition results are presented in Section 4.6.

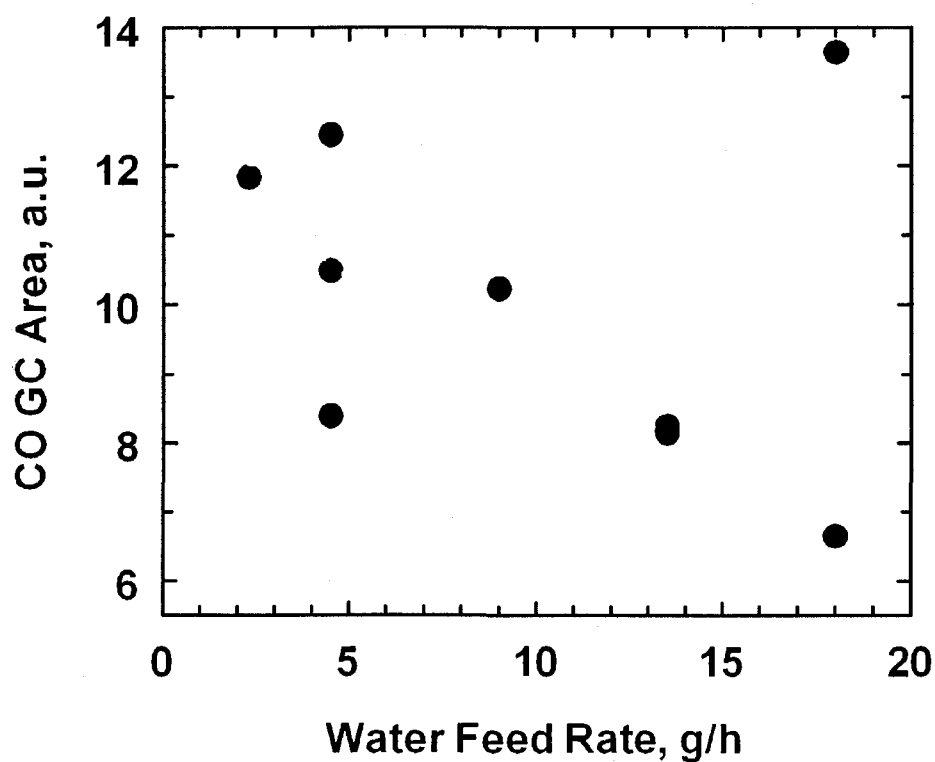


Figure 4-30. Effect of H<sub>2</sub>O flow rate on the CO concentration (treatment conditions: 800°C, 345 kPa).

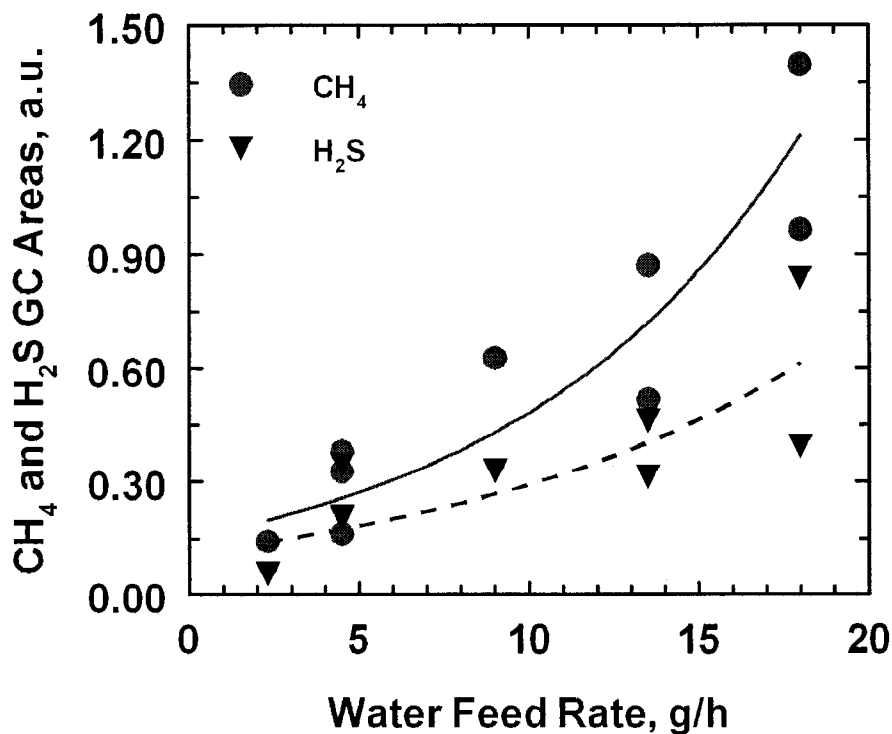


Figure 4-31. Effect of H<sub>2</sub>O flow rate on the CH<sub>4</sub> and H<sub>2</sub>S concentration (treatment conditions: 800°C, pressure:345 kPa).

#### 4.4.2 Activation of fluid coke with N<sub>2</sub>/H<sub>2</sub>O mixture

Activation of fluid coke with N<sub>2</sub>/H<sub>2</sub>O mixture was done at temperature of about 800°C and close to atmospheric pressure with 4 h treatment time, and different H<sub>2</sub>O concentrations. The results of these treatments are summarized in Table 4-6 and plotted in Figures 4-32 and 4-33.

Table 4-6. Results of activation with N<sub>2</sub>/H<sub>2</sub>O mixture

Run #	Treatment conditions				BET Surface Area, m <sup>2</sup> /g	Pore Volume		Mass Loss, %
	Temp, °C	Feed Composition, mol %		H <sub>2</sub> O Rate, mL/h		Micro-pores, cm <sup>3</sup> /g	Meso-pores, cm <sup>3</sup> /g	
		N <sub>2</sub>	H <sub>2</sub> O					
IC10466	788	48	52	2.3	161.9	0.06186	0.00744	18
SS10427	803	47	53	2.3	203.4	0.07790	0.01376	19.2
IC10464	782	32	68	4.5	211	0.08029	0.00983	19.3
MB10465	767	19	81	9.0	342.7	0.13170	0.02844	28.3
SS10425	787	18	82	9.0	425.5	0.16470	0.03342	27
MB10458	825	29	71	9.0	385.9	0.14290	0.04504	38.6



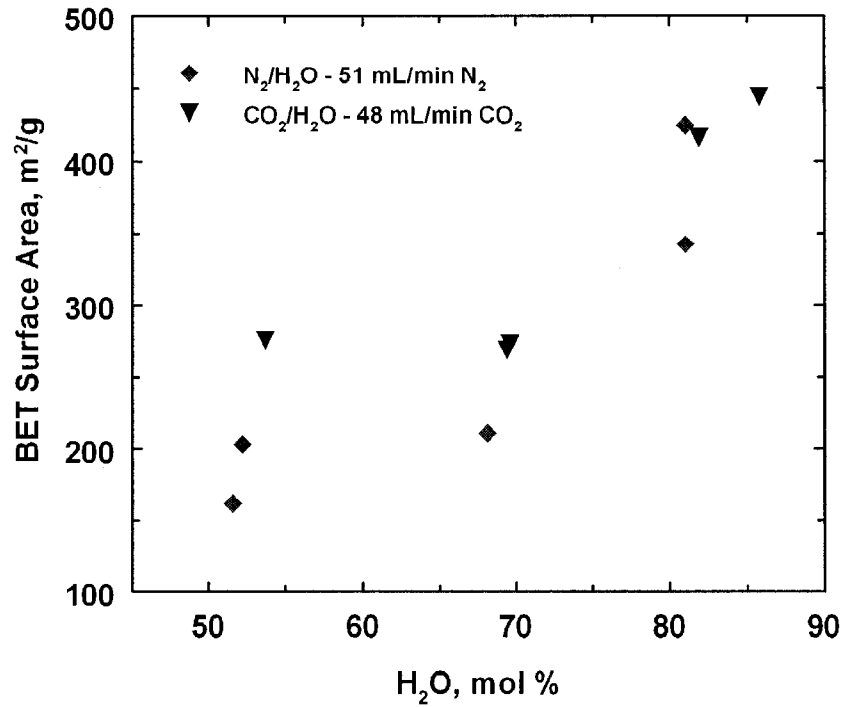


Figure 4-32. Comparison of the effects of N<sub>2</sub>/H<sub>2</sub>O and CO<sub>2</sub>/H<sub>2</sub>O mixtures on the surface area of activated fluid coke.

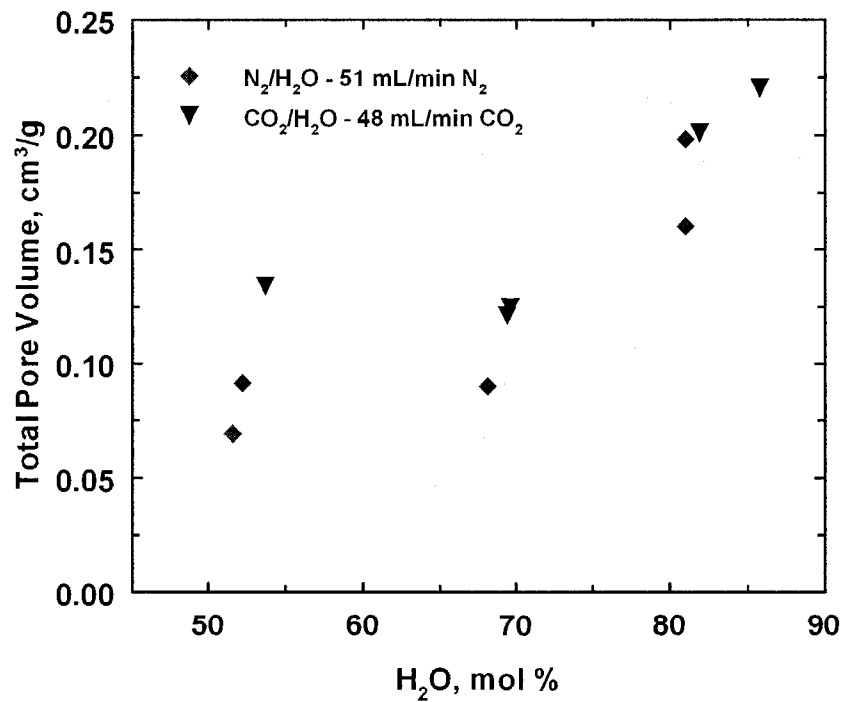


Figure 4-33. Comparison of the effects of N<sub>2</sub>/H<sub>2</sub>O and CO<sub>2</sub>/H<sub>2</sub>O mixtures on the pore volumes of activated fluid coke.

The surface areas and pore volumes shown in Figures 4-32 and 4-33 are higher for the CO<sub>2</sub>/H<sub>2</sub>O mixtures compared to the N<sub>2</sub>/H<sub>2</sub>O at low H<sub>2</sub>O concentrations, but at high H<sub>2</sub>O concentrations the difference between the two gas mixtures is small. The feed rate of water at the low H<sub>2</sub>O concentration was only 2.3 mL and the gasification reactions may have been limited due to water availability. Under these conditions, the presence of additional CO<sub>2</sub> may have resulted in the generation of additional surface area, either by direct participations in the gasification (Reaction 2-3) or the production of additional water by the water gas shift reaction (Reaction 2-5). However, in the case when excess water was available, the substitution of CO<sub>2</sub> with N<sub>2</sub> did not significantly affect surface areas and pore volumes.

#### ***4.4.3 Activation of fluid coke with mixtures containing O<sub>2</sub>***

Activation of fluid coke in nitrogen/air mixture was carried out at 800°C, 4 h treatment time, and different air flow rate, from 3 to 99 mL/min. The purpose of O<sub>2</sub> activation was to see if it would result in increased pore sizes. Unfortunately, this did not occur. Treatment in O<sub>2</sub>/N<sub>2</sub> did not result in any activation, i.e. the specific surface area did not increase (see Table 4-7) even though significant mass losses occurred. The loss of mass without any change in the specific surface area means the oxygen was burning the carbon on the external surface of the coke particles. The presence of ash in the final product confirmed this.

When water was added to the nitrogen/air mixture, a considerable increase in surface area and porosity was achieved, as illustrated in Table 4-7. The increases in areas were similar to those obtained with H<sub>2</sub>O/N<sub>2</sub> and H<sub>2</sub>O/CO<sub>2</sub> mixtures. However, the mass losses were higher for the cases where oxygen was present, but the pore size were not different from those obtained without the presence of oxygen. It can be concluded that the addition of oxygen only burned carbon off the exterior surface of the fluid coke particles since the addition of O<sub>2</sub> to H<sub>2</sub>O/CO<sub>2</sub> mixtures increased neither the surface areas nor the average pore sizes. Hence, the presence of oxygen in the flue gas should be minimized unless the combustion of the coke is used to provide some of the energy required for the gasification if direct fired activation is being used. However, careful

control of the oxygen concentration would be required to avoid the total combustion of especially the small fluid coke particles.

Table 4-7. Results of activation with N<sub>2</sub>/O<sub>2</sub>/H<sub>2</sub>O mixture

Run #	Treatment Conditions						BET Surface Area, m <sup>2</sup> /g	Pore Volume		Pore Radius, nm	Mass Loss, %
	Temp, °C	Feed Composition, mol %				H <sub>2</sub> O Feed Rate, mL/min		Micro-pores, cm <sup>3</sup> /g	Meso-pores, cm <sup>3</sup> /g		
		N <sub>2</sub>	O <sub>2</sub>	CO <sub>2</sub>	H <sub>2</sub> O						
MB10438	797	79	21				22	0.0077	0.0030	0.98	16.1
MB10439	799	88	12				20	0.00733	0.0032	1.03	23.3
MB10444	799	87	13				22	0.00775	0.0029	0.97	24.3
MB10445	798	29	1.4		70	4.5	236	0.0900	0.0273	0.99	24.2
MB10446	792	44	4.0		52	4.5	242	0.0925	0.0273	0.99	33.0
IC10470	738	29	2.6		69	9.0	285	0.1099	0.0209	0.92	45.3
MB10447	784	29	2.6		69	9.0	321	0.1232	0.0356	0.99	41.5
MB10449	795	25	6.6		69	9.0	286	0.1085	0.0358	1.01	65.2
MB10448	794	15	3.9		82	9.0	349	0.1318	0.0412	0.99	42.5
IC10471	710*	10	2.6	19	69	9.0	306	0.1183	0.0202	0.91	46.6

\* Median temperature was 765°C

#### 4.5 Effect of particle size on surface area, porosity and mass loss

Activation of different particle size fractions of Coke 2 was carried out at a treatment temperature of about 800°C and treatment time of 4 h. The total feed rate of treatment gas was 12.1 mmol/min and the composition of treatment gas was: 69 mol % H<sub>2</sub>O, 28 mol % N<sub>2</sub> and 3 mol % O<sub>2</sub>. The results are summarized in Table 4-8. Surface areas were larger and mass losses were more pronounced for small fluid coke particles compared to larger fluid coke particles. There are two probable causes for this observed behaviour. One, the initial surface area and porosity of the large fluid coke particles were lower than those of the smaller particles. The initial porosity has an effect on the creation of surface area during the activation (see Section 2.1.2 on the importance pore structure after carbonization), and two, the effect of particle size on mass transfer rates. It is more

difficult for the activating gases to penetrate into the interior of large particles compared to small particles. It is also more difficult for the products of the coke gasification to leave the interior of large particles. Hence, small fluid coke particles are better candidates for producing high-surface area fluid coke particles.

Table 4-8. Surface Area and Pore Volume of different size fractions of Coke 2 before and after activation.

Size Fraction, $\mu\text{m}$	Sample ID	Before Activation			After Activation			Mass Loss, %
		BET Surface Area, $\text{m}^2/\text{g}$	Micro-pore Volume, $\text{cm}^3/\text{g}$	Meso-pore Volume, $\text{cm}^3/\text{g}$	BET Surface Area, $\text{m}^2/\text{g}$	Micro-pore Volume, $\text{cm}^3/\text{g}$	Meso-pore Volume, $\text{cm}^3/\text{g}$	
80-100	203	19.1	0.007	0.006	292.5	0.1086	0.0290	55.4
100-125	204	20.8	--	0.003	274.1	0.1017	0.0261	41.3
125-180	205	12.6	0.004	0.004	251.7	0.0932	0.0253	36.5
180-250	206	7	0.002	0.004	179.1	0.0662	0.0179	33.9
> 250	207	4.2	0.001	0.004	159.8	0.0577	0.0169	31.4

#### 4.6. Effluent gas composition

The effluent gases from the activation reactor were analyzed by gas chromatography. The procedure is described in Section 3.5.5. The column and conditions used allowed for the detection of  $\text{H}_2$ ,  $\text{O}_2/\text{N}_2$ ,  $\text{CO}$ ,  $\text{CH}_4$ ,  $\text{CO}_2$  and  $\text{H}_2\text{S}$ . Hydrogen was separated and could be detected, but could not be quantified because the hydrogen concentrations were such that both positive and negative peaks occurred. This is due to the odd behaviour of the thermal conductivity of  $\text{H}_2/\text{He}$  mixtures, i.e. the thermal conductivity of  $\text{H}_2/\text{He}$  mixtures decreases with increasing  $\text{H}_2$  concentrations at low  $\text{H}_2$  concentration and then increases (Shahkov et al., 1973). This makes it impossible to use a thermal conductivity detector for quantitative detection of hydrogen over a wide range of hydrogen concentrations when helium is used as the carrier gas. This problem does not occur if argon is used as the carrier gas, but the sensitivity for all compounds other than hydrogen is low if argon is used as the carrier gas. The  $\text{O}_2/\text{N}_2$  eluted as a single peak,

neither nitrogen nor oxygen is a reaction product; hence this is not a serious deficiency in the analysis.

Unfortunately, water could not be analyzed; it is usually difficult to obtain well-resolved peaks for water if several compounds which are chemically very different from water, e.g. non-polar, are to be separated by the column. Most of the water in the effluent stream was condensed in the cold trap which was kept at 0°C. Hence, the GC analyses in the current work focused on CO, CH<sub>4</sub>, CO<sub>2</sub> and H<sub>2</sub>S, and the results will be reported as mol % on a H<sub>2</sub>, O<sub>2</sub>/N<sub>2</sub> and H<sub>2</sub>O-free basis. The GC areas were converted to mol % using the relative response factors reported in the literature, i.e. the response factors for CO, CH<sub>4</sub>, CO<sub>2</sub>, and H<sub>2</sub>S are 42, 35.7, 48 and 38, respectively (Dietz, 1967), and Equation 4.5.

$$y_i = \frac{A_i / R_i}{\sum_{j=1}^{j=4} A_j / R_j} \times 100 \quad (4.5)$$

Where  $A_i$  is the area under the GC peak for component  $i$  and  $R_i$  is the response factor for component  $i$ ;  $j$  is summed from 1 to 4 for the four components under consideration, i.e. CO, CH<sub>4</sub>, CO<sub>2</sub>, and H<sub>2</sub>S.

#### ***4.6.1 Effluent gas composition as a function of treatment temperature***

Typical results of effluent compositions as a function of activation temperature are shown in Figures 4-34 to 4-37; these figures show the variation in CO, CO<sub>2</sub>, CH<sub>4</sub> and H<sub>2</sub>S content in the effluent stream as a function of activation time and temperature. These results are for 4 runs with activation temperatures of 509 to 770°C, all at a pressure of about 345 kPa, a water feed rate of 4.5 mL/h and a CO<sub>2</sub> feed rate of 188 mL/min (i.e. a feed composition of 63 mol% CO<sub>2</sub> and 37 mol% H<sub>2</sub>O). The trends in the composition variations with treatment time obtained for these 4 runs are similar to those obtained in other runs.

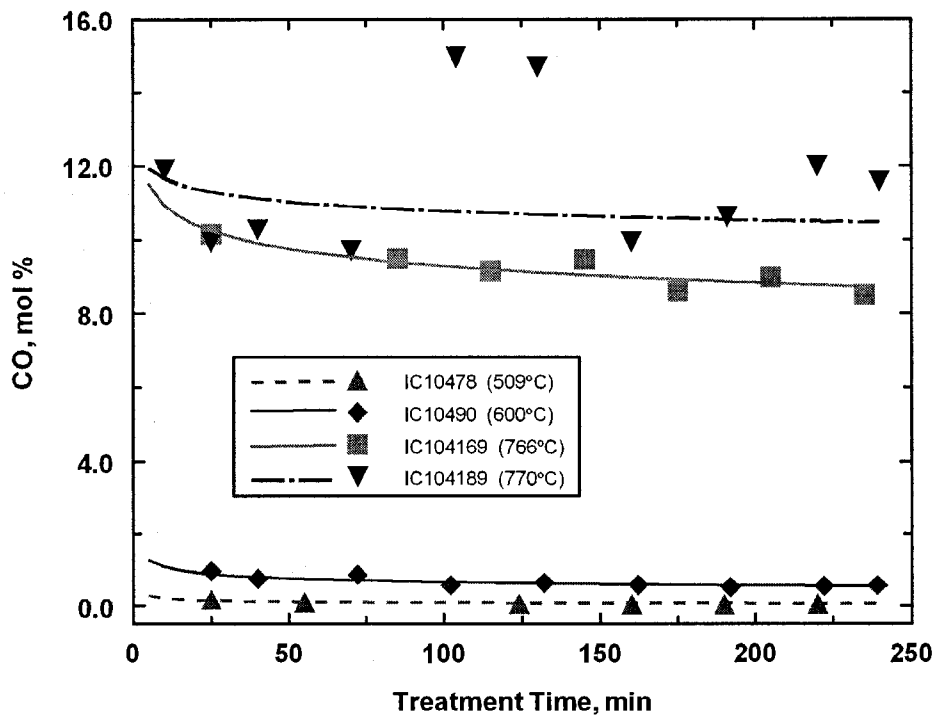


Figure 4-34. Variations in CO concentration in effluent gas as a function of treatment temperature (composition on a H<sub>2</sub> and H<sub>2</sub>O-free basis).

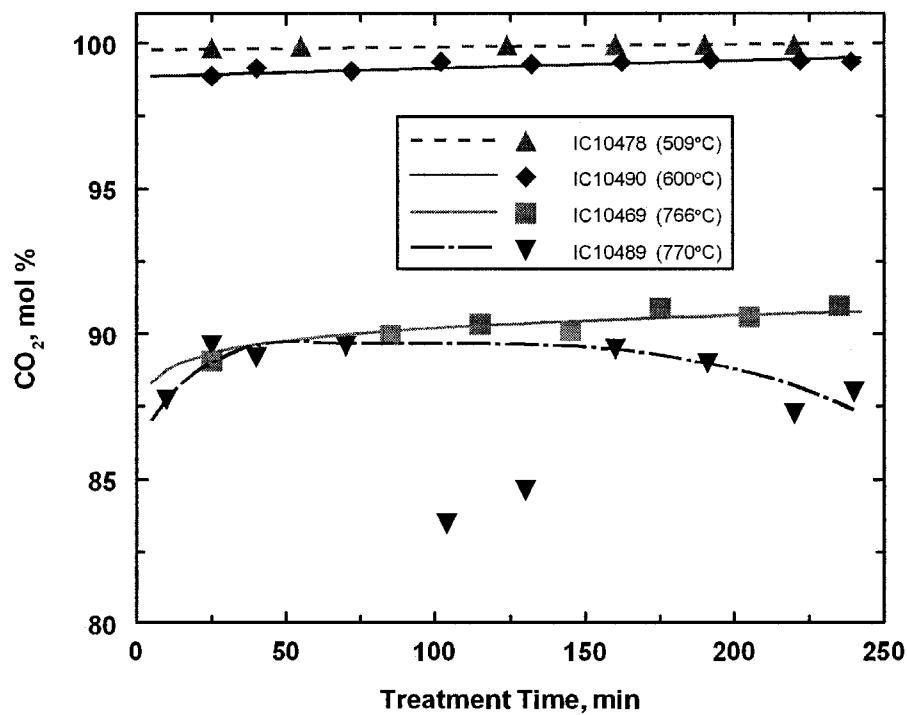


Figure 4-35. Variations in CO<sub>2</sub> concentration in effluent gas as a function of treatment temperature (composition on a H<sub>2</sub> and H<sub>2</sub>O-free basis).

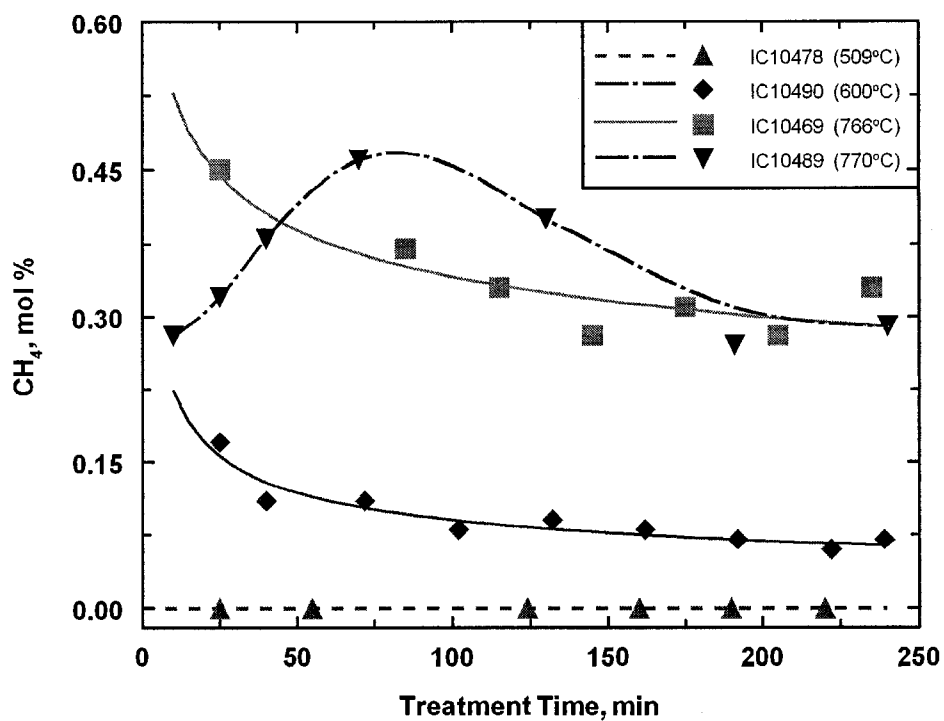


Figure 4-36. Variations in CH<sub>4</sub> concentration in effluent gas as a function of treatment temperature (composition on a H<sub>2</sub> and H<sub>2</sub>O-free basis).

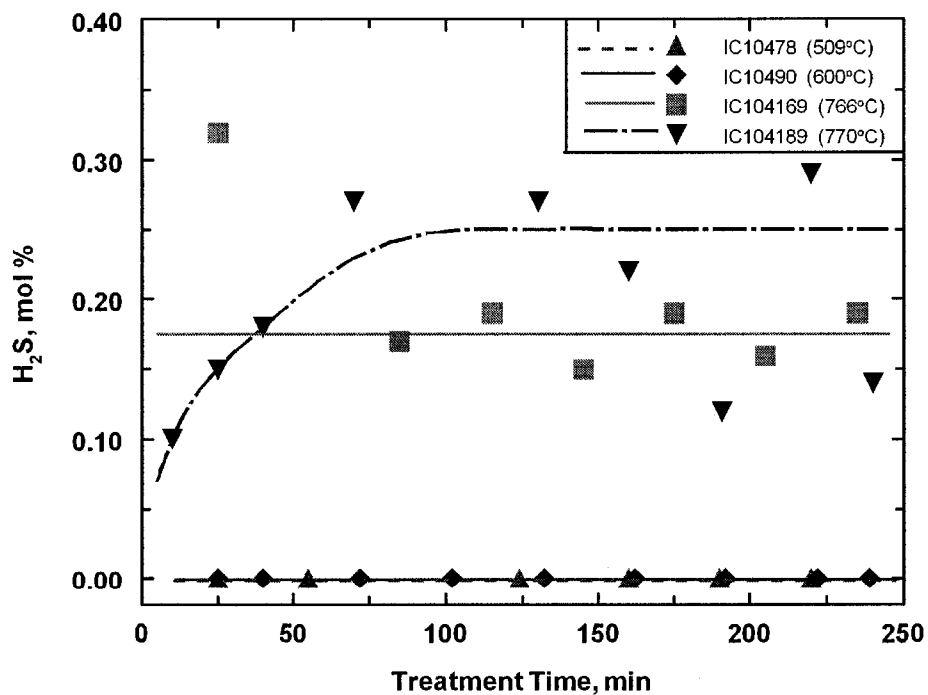


Figure 4-37. Variations in H<sub>2</sub>S concentration in effluent gas as a function of treatment temperature (composition on a H<sub>2</sub> and H<sub>2</sub>O-free basis).

The treatment conditions for Runs IC10469 and IC10489 were very similar, the average treatment temperature was only 4°C different for the two runs and the treatment feed gas had the same composition. However, the results for Run IC10489 were rather scattered and the trend at low activation times was different from that of most other runs. The results for Run IC10489 were included to illustrate that for some of the runs large fluctuation occurred in the effluent gas composition. Although there was scatter in the compositional data for some of the runs, some general trends in the composition of the effluent were easily discernible. The general observations include:

1. CO concentration increased with increasing temperature and decreased with increasing treatment time.
2. CO<sub>2</sub> concentration decreased slightly with increasing treatment temperature and increasing treatment time.
3. CH<sub>4</sub> concentration increased with increasing treatment temperature and decreased with decreasing treatment time.
4. No significant H<sub>2</sub>S was formed at treatment temperatures <700°C and at higher temperatures the concentration of H<sub>2</sub>S increased with increasing temperatures and remained relatively constant or decreased slightly with treatment time.

The above trends are mainly due to kinetic and mass transfer effects rather than thermodynamic factors. The concentration of CH<sub>4</sub> should be highest at low temperatures according to the thermodynamics (see Equation 2-4 and Table 4-5); similarly, CO formation over CO<sub>2</sub> formation is favoured at high temperature. The H<sub>2</sub>S formation is also limited by chemical kinetics because it only forms at the higher temperatures. The decreases in CO and CH<sub>4</sub> amounts with time on stream are probably due to the increasing mass transfer limitations with increasing treatment time because with increasing treatment time the H<sub>2</sub>O has to diffuse further and further into the porous fluid coke particles.



#### ***4.6.2 Effluent gas composition as a function of treatment gas composition***

The effluent gas composition changed with activation time, but variations were not large and at temperatures of 750 to 800°C, especially for CO, CO<sub>2</sub> and H<sub>2</sub>S (see Figures 4-34 to 4-37). Hence, the effect of treatment gas composition on effluent gas composition for treatment temperatures of about 760°C is examined in terms of the average effluent gas composition for 4 h treatment times at CO<sub>2</sub> feed rates of 188 mL/min, pressure of 345 kPa and water feed rates of 2.3 to 18 mL/h. The feed treatment gas consisted only of CO<sub>2</sub> and H<sub>2</sub>O, and the variations in water feed rates results in variations in water content of the feed gas from 23 to 70 mol%. The runs for these conditions are IC10469, IC10479, IC10480, IC10481, IC10482, IC10483, IC10489 and IC104102. The average composition of the exit flue gases for these runs, on a H<sub>2</sub>O and H<sub>2</sub> free basis, are shown in Figure 4-38.

The logarithmic scale smoothes some of the scatter, but the trends in relative concentrations of the four components are evident. The CO<sub>2</sub> concentration decreased with increasing water feed rate due to production of CO and to a lesser degree CH<sub>4</sub> and H<sub>2</sub>S. The amount of CO increased from about 10 to 15 mol% with increasing water flow rate; however, the CH<sub>4</sub> and H<sub>2</sub>S concentrations increased by about a factor of 10 when the water feed rate was increased from 2.3 to 18 mL/h. This significant increase in the concentration of these two components must be related to an increase in the hydrogen concentration with increasing water feed rate. The GC hydrogen signals did indicate significantly higher H<sub>2</sub> concentrations at the higher water feed rates, but the increase cannot be quantified for previously stated reasons.

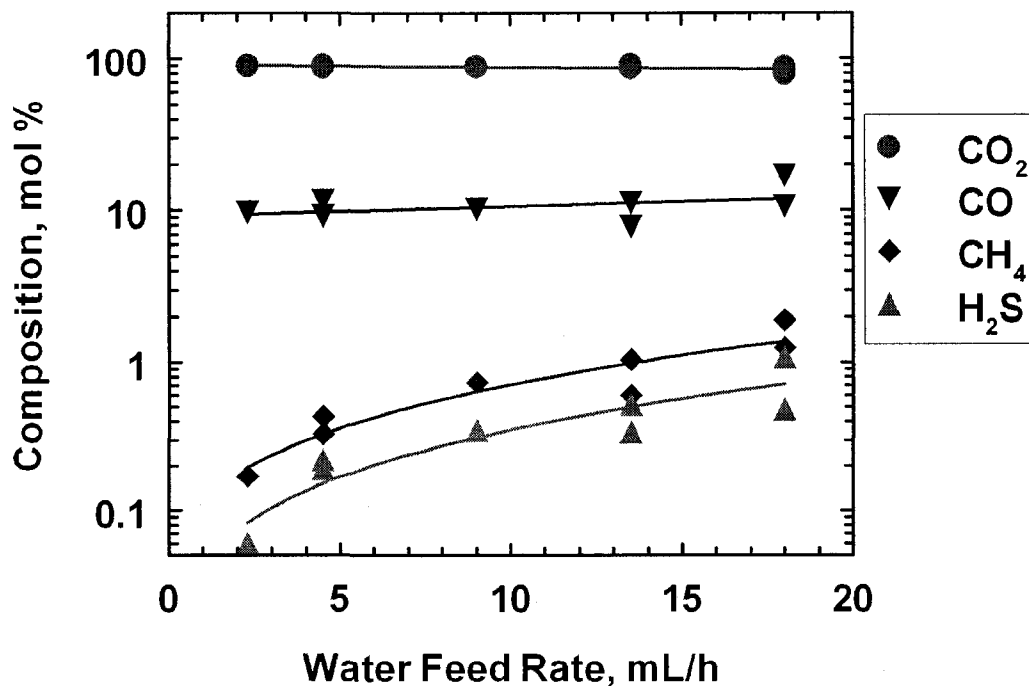


Figure 4-38. Average effluent gas composition (on H<sub>2</sub>O and H<sub>2</sub> free basis) as a function of water feed rate (T=760°C, P=345 kPa and CO<sub>2</sub> feed rate = 188 mL/min).

A few experiments were done without CO<sub>2</sub> in the feed. In these runs, the treatment feed gas consisted of N<sub>2</sub> and H<sub>2</sub>O. The average effluent gas compositions as a function of water feed rate at a constant N<sub>2</sub> feed rate of 42.5 mL/min, an average temperature of about 780°C and a pressure of about 120 kPa, are shown in Figure 4-39. The runs on which this figure is based are IC10464, MB10465, IC10466 and IC10467. As expected, all the products of coke gasification increased with increasing water feed rate. The unexpected observation was that no carbon monoxide was detected in any of these runs. It appears that for low CO<sub>2</sub> concentration CO production does not occur. This is surprising because the water gas shift reaction (Equation 2-5) should produce CO at high temperatures and high H<sub>2</sub>O concentrations. The H<sub>2</sub>O content of the feed treatment gas varied from 52 to 81 mol %. Additional experiments are needed to determine whether the lack of CO production at these conditions is real or whether analysis or other problems are the cause of this unusual observation. It is also worth noting that the H<sub>2</sub>S concentrations for all the results in Figure 4-39 are higher than the CH<sub>4</sub> concentrations. This was not the case when CO<sub>2</sub> was present in the feed gas (see Figure 4-38). It is not

known whether the presence of high concentration of  $\text{CO}_2$  affects  $\text{H}_2\text{S}$  and  $\text{CH}_4$  formation. This is another area which requires further study.

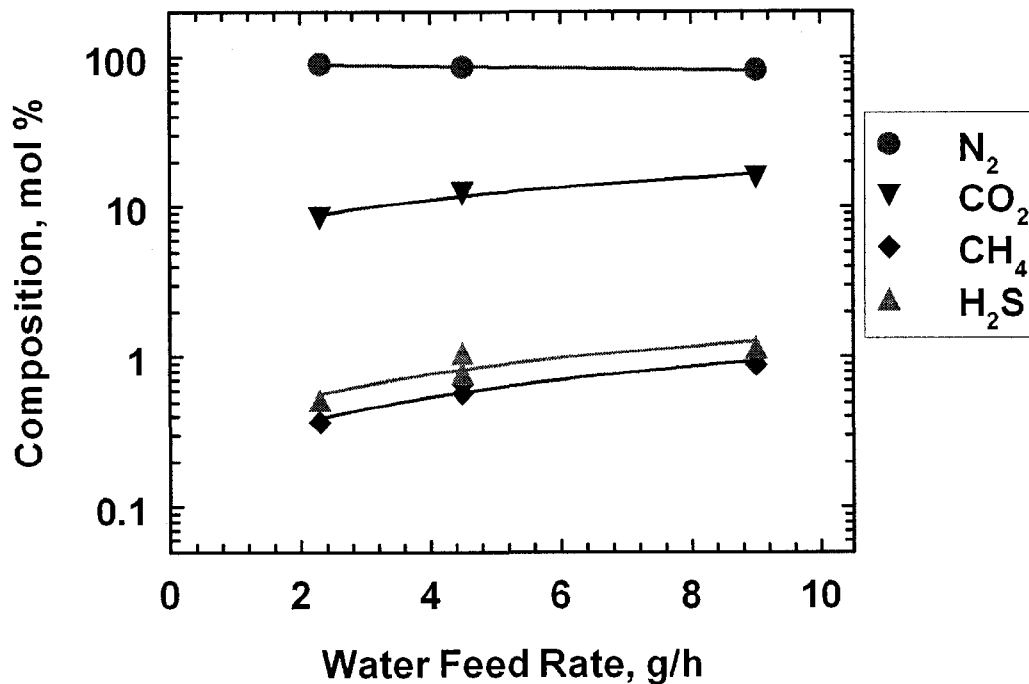


Figure 4-39. Average effluent gas composition (on  $\text{H}_2\text{O}$  and  $\text{H}_2$  free basis) as a function of water feed rate without any  $\text{CO}_2$  in the feed ( $T=760^\circ\text{C}$ ,  $P=345$  kPa and  $\text{N}_2$  feed rate = 42.5 mL/min).

## Chapter 5. Mercury adsorption by activated fluid coke

Selected fluid coke samples, which had been activated by steam treatment, were tested for their ability to capture mercury from gas streams at various temperatures. The equipment described in Chapter 3 (see Figure 3-5) was used for these measurements. The ability of a fluid coke sample to capture mercury was determined by the removal of mercury from mercury-saturated air pulses injected into the argon stream. The amount of mercury in each injected pulse which was not removed was measured by the mercury detector. Similar mercury-containing air pulses were injected into the argon stream after the fluid coke bed as calibration pulses before each mercury sorption measurement.

It should be pointed out that incomplete capture of an injected pulse does not necessarily mean that the coke sample was saturated with mercury because by-passing or channelling could occur with the small quantities of coke (40 to 50 mg) and the relatively high flow rates of argon (1.5 mmol/min). All the mercury capture experiments were done at pressure of about 0.1 MPa and most of the capture experiments were done at 140°C. At these conditions, the average residence time of the mercury pulse in the fluid coke bed is <0.1 s. Repeat experiments showed that for some of the experiments early mercury breakthrough occurred, e.g. breakthrough in the first injected pulse; this, in some cases, was probably due to by-passing because repeat experiments, with new loadings of fluid coke in the sample tube, showed complete capture of the first pulse. For other experiments, especially those with activated fluid coke having low surface areas, breakthrough always occurred during the first pulse.

Breakthrough is defined as the detection of mercury by the detector after mercury has been injected into the argon in front of the fluid coke bed, i.e. breakthrough after Injection 1 indicates that not all the mercury in the first pulse was adsorbed by the fluid coke bed. Breakthrough after Injection **n** means that all the mercury injected in Pulses 1 to (**n**-1) was captured, but not all the mercury in Pulse **n** was captured.

The effects of activated fluid coke surface area, sorption temperature, hydrogen treatment of fluid coke, and elemental sulphur addition to fluid coke on mercury sorption are presented in the following sections.

### 5.1. Mercury adsorption as a function of surface area

The effect of surface area of activated fluid coke on Hg adsorption was measured. The experimental procedure for Hg adsorption experiments was described previously in Section 3.3. Samples of 40 to 50 mg activated coke were used in the experiments. All the samples were tested at 140°C by injecting 50  $\mu\text{L}$  pulses of air saturated with Hg at room temperature. The amount of Hg injected was calculated from the mercury vapour pressure at the temperature of the gas and the size of the injected gas pulses. The amount of Hg adsorbed was calculated by subtracting the amount of Hg eluted from the amount of Hg injected. The results of Hg adsorption experiments for 75 different samples having surface area between 20 and 533  $\text{m}^2/\text{g}$ , are shown in Figure 5-1. Two successive pulses, 5-10 min apart, were injected for all of the samples. The percentage of the injected mercury which was adsorbed by the fluid coke for each pulse is shown in Figure 5-1.

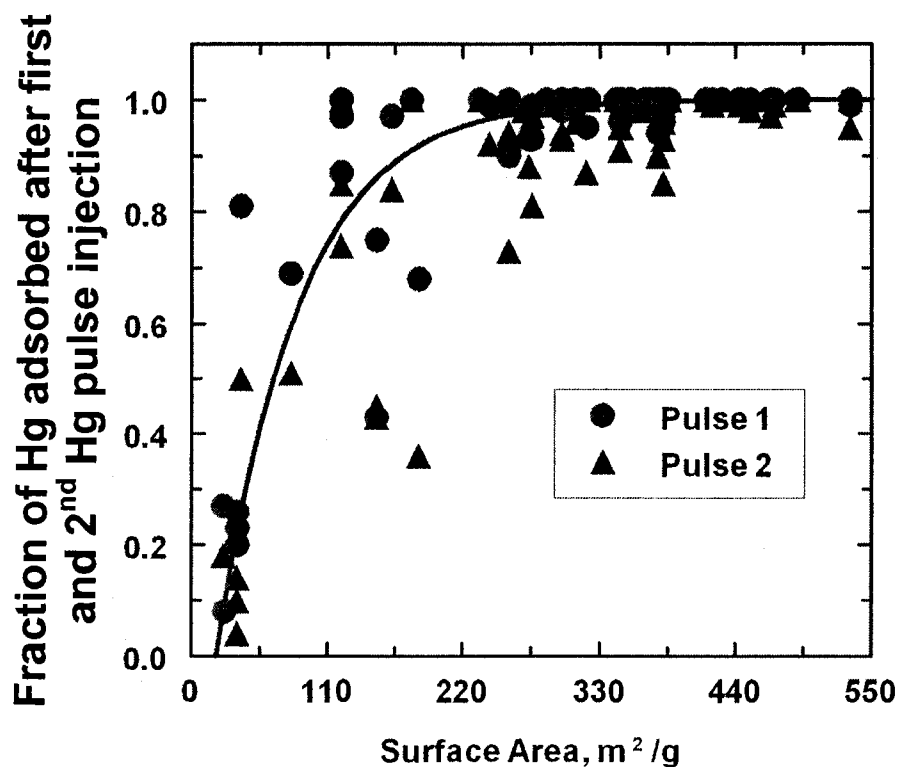


Figure 5-1. Effect of surface area on mercury adsorption by activated fluid coke at 140°C sorption temperature.

There is a strong correlation between mercury sorption and surface area of activated coke. Activated fluid coke samples with surface areas  $<100 \text{ m}^2/\text{g}$  did not capture mercury well; breakthrough of mercury occurred after Injection 1 for all samples with areas  $<100 \text{ m}^2/\text{g}$ . Most samples with areas  $>200 \text{ m}^2/\text{g}$  adsorbed all the mercury in the first pulse and all or most of the mercury in the second pulse. Some samples adsorbed all the mercury injected in 5 or 6 consecutive pulses. These results indicated that the steam-activated fluid coke samples are capable of adsorbing mercury in the temperature range found in the flue gases from coal fired electric power plants.

It can be seen in Figure 5-1 that samples with similar surface areas showed differences in mercury adsorption capacity. This might be due to the Hg injected/coke ratio, which varied among experiments from  $12$  to  $21 \times 10^{-9}$ . The same volume of mercury-saturated air was used for all the experiments, but the amount of Hg in each pulse varied because the temperature of the mercury reservoir varied from day to day. Another factor which might have influenced the results is the amount of coke loaded into sample holder; this quantity varied from  $40$  to  $50 \text{ mg}$ . The measured value of the mass was accurate to within  $\pm 0.5 \text{ mg}$ , but it was very difficult to always load the same amount because the sample was very small.

Another possible error is the possibility of channelling or by-passing which would give the appearance of breakthrough. Repeat experiments were done to determine the reproducibility of results. The results of repeat measurements on 20 activated fluid samples are shown in Figure 5-2. One to four repeat measurements were done; a fresh coke sample was used for each repeat measurement. It is evident that there are major differences in the amount of mercury captured in 6 of the 53 experiments. The most likely case of the low mercury capture for these runs is that some by-passing occurred in these experiments. Another interesting observation from these runs is that repeat runs showed essentially complete adsorption of the first pulse for all samples with surface areas  $>200 \text{ m}^2/\text{g}$ .

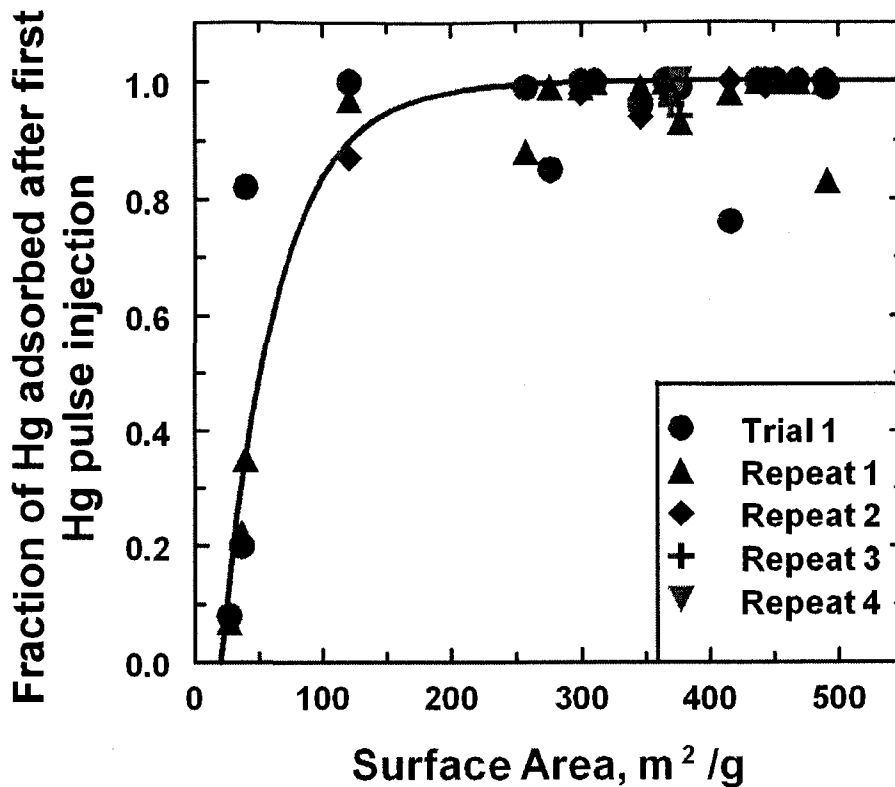


Figure 5-2. Results of repeat mercury capture experiments.

Figure 5-3 shows a comparison of the Hg adsorption capacities of samples with surface area higher than 200 m<sup>2</sup>/g. For many of these samples more than two pulses of Hg were injected before breakthrough occurred (the average amount of Hg in one pulse is about 800 pg, depending on the Hg reservoir temperature). The total amount adsorbed was calculated as the difference between the amount of mercury injected in all the pulses minus the amount of mercury eluted. Figure 5-3 shows that the amount of mercury adsorbed increases with increasing fluid coke surface area, as expected. However, the scatter is very large in these data. The correlation is poor because other factors, besides surface area, influence the mercury capture ability. As pointed out earlier, the differences between the samples with similar surface areas might be due to different Hg/carbon ratio. However, the activation conditions, activation temperature, H<sub>2</sub>O/CO<sub>2</sub> ratio during activation and H<sub>2</sub>O partial pressure, might play an important role in Hg capture because

these factors can result in activated coke with different surface properties. The pulse method is not a very reliable method for measuring adsorption capacities because adsorbed material (Hg) can desorb between the pulse additions. Further experiments in which Hg capture is a continuous mode must be done to obtain true adsorption capacities and to evaluate the most suitable activated cokes for Hg capture.

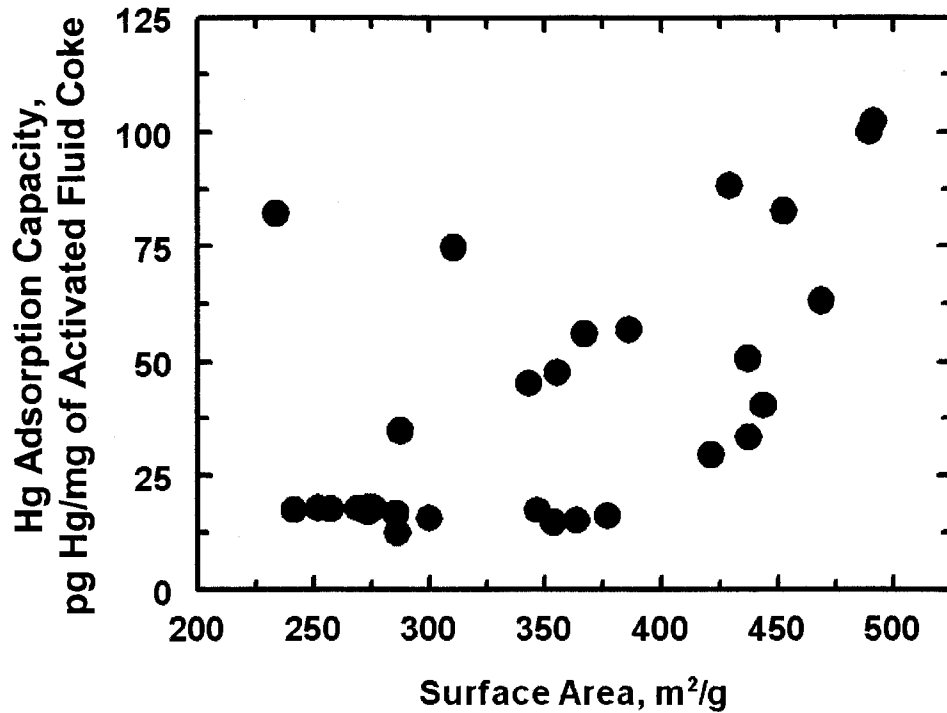


Figure 5-3. Variation of Hg adsorption capacity at 140°C as a function of surface area.

### 5.2. Mercury adsorption as a function of sorption temperature

Hg adsorption capacity of three activated carbons: SS10424, IC10474 and IC10482 were studied as a function of adsorption temperature. The activation conditions of raw coke and the properties of the resultant activated carbons are shown in Table 5-1. Hg adsorption was carried out at temperatures from 50 to 200°C. The experimental procedure for Hg adsorption experiments were described in Section 3.3. The results of the Hg adsorption experiments are shown in Figure 5-4.



Table 5-1. Activation treatment conditions and properties of activated carbons.

Sample I.D.	Treatment Temp., °C	Pressure, kPa	Treatment Length, h	Treat Gas Composition, mole, %		Treatment Gas Feed Rate, mmol/min	Surface Area, m <sup>2</sup> /g	Pore Volume, cm <sup>3</sup> /g	
				CO <sub>2</sub>	H <sub>2</sub> O			micro	meso
SS10424	782	100	4	30.6	69.4	10.2	415	0.159	0.042
IC10474	754	616	4	74.5	25.5	16.3	420	0.160	0.054
IC10482	754	344	4	34.6	63.6	19.6	490	0.182	0.080

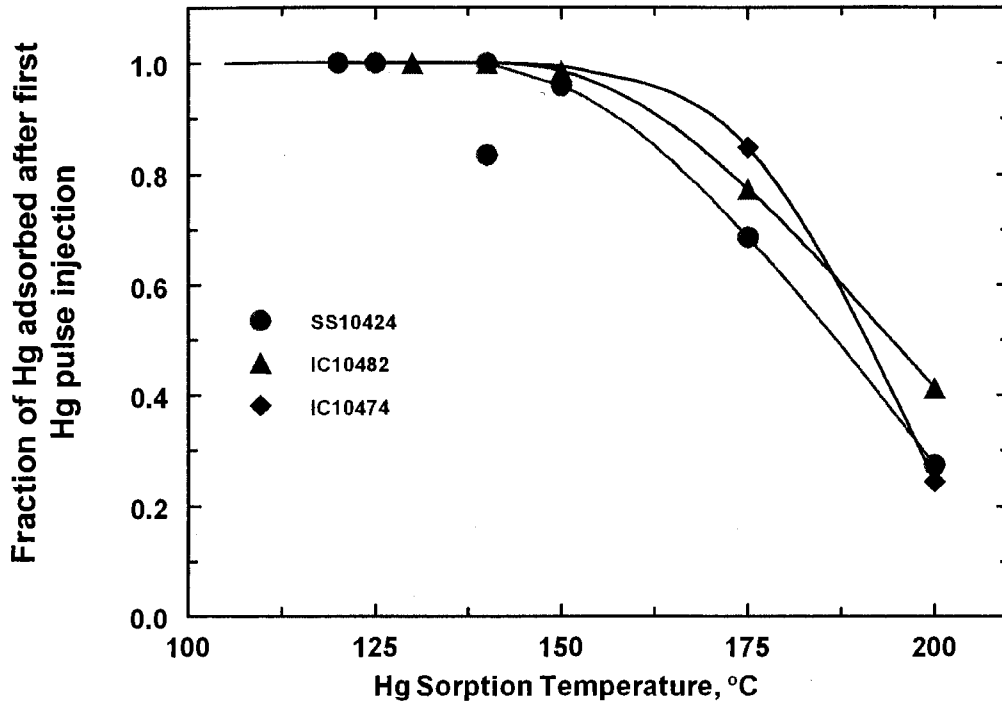


Figure 5-4. Mercury adsorption from first injected pulse as a function of adsorption temperature.

Mercury adsorption decreases significantly for adsorption temperatures above 140 to 150 °C for all three samples even though surface areas varied among the samples and mesopores volumes varied by about a factor of 2. Similar behaviour was reported in a study done by Krishnan et al. (1994); they studied the Hg adsorption capacity of two

thermally activated carbons FGD and PC100 at 23 and 140°C. The samples showed lower adsorption capacity with increasing temperature.

A small number of steam-activated carbon samples were heat treated in argon atmosphere at 200°C prior to Hg adsorption experiments. Measured amounts of samples were placed in sample U-tube and heated to 200°C in the oven under argon flow at 40 mL/min flow rate for approximately 15 h. After this, the oven temperature was decreased to 140°C and Hg adsorption experiments were performed, following the procedure described in Section 3.3. The results are showed in Table 5-2. A 75-88% reduction in Hg adsorption was observed, when compared with the Hg sorption capacity before heat treatment in argon. The highest decrease in Hg capture was recorded for IC10482, which was obtained by steam activation, using the highest H<sub>2</sub>O flow rate during activation process.

Table 5-2. The influence of heat treatment in argon of activated carbon on Hg adsorption capacity

Sample I.D.	Activation Temp., °C	Activation Pressure, ka	H <sub>2</sub> O flow rate, ml/h	Surface Area, m <sup>2</sup> /g	Hg adsorbed before heat treatment, pg/mg AC	Hg adsorbed after heat treatment, pg/mg AC	Hg ads Decrease, %
IC10473	764	472	4.5	437	50.8	11.8	76.8
IC10480	760	345	2.3	300	56.8	12.9	77.3
IC10482	754	344	13.5	491	102.6	12.3	88.0
IC10486	752	626	8.1	452	59	14.8	74.9
IC10499	697	625	8.1	121	52	12.7	75.6

A similar phenomenon was also reported by Krishnan et al. (1994) in their study on the adsorptive capacities of heat-treated activated carbons. They observed that the Hg adsorption capacities of activated carbons decreased if they were treated at 140°C in a N<sub>2</sub> atmosphere. They suggested that the reduction of Hg capture ability was probably caused by the removal of moisture from the carbon surfaces during the nitrogen treatment at 140°C. Y. Li et al. (2002), in their study on the effect of adsorbed water on Hg adsorption by activated carbons, found as 75 to 85% reduction in the Hg adsorption after heat treatment at 110°C.

This behaviour of activated carbons, unheated and heat treated, towards Hg capture raise questions regarding the mechanism of Hg adsorption. The decrease of Hg adsorption with the increasing temperature may be associated with a physical adsorption. Physical adsorption involves intermolecular forces (e.g. van der Waals forces) and the change in electronic state of adsorbent and adsorbate is minimal. During physical adsorption, equilibrium is established between the adsorbate and the fluid phase. In solid/gas systems the extent of physical adsorption increases with increases in gas pressure and decrease with increasing temperature.

However, chemisorption, which involves making of chemical bonds show similar adsorption behaviour, i.e. a decreases of adsorption uptakes with increasing adsorption temperature. The probable sites for chemisorption on activated carbons are carbon-oxygen surface complexes. According to Bansal et al. (1988), carbon-oxygen surface complexes are by far the most important structures influencing the surface characteristics and adsorption properties of activated carbons. It is believed that oxygenated functional groups are formed on the active sites when the carbon material, after being prepared at high temperatures, is placed in an atmosphere at lower temperature (Lahaye, 1998).

Oxygen complexes formed on the carbon surfaces may play an important role for Hg<sup>0</sup> adsorption. Krishnan et al. (1994) suggested that the alteration or depletion of these oxygen-surface complexes with increasing temperature might be one of the factors responsible for the lowering of sorptive capacity of these activated carbons. Li et al. (2002) suggested that the oxygen-complexes on the carbon surfaces form primary adsorption centres which bind H<sub>2</sub>O molecules by means of hydrogen bonding. Adsorbed water molecules then become secondary adsorption centres for Hg capture. The removal of the H<sub>2</sub>O from the carbon surface by heat-treatment reduces the number of active sites that can chemically bond Hg or eliminates the reactive surface conditions that favour Hg adsorption. In a later study, Li et al. (2003) found that oxygen surface complexes, possibly lactone and carbonyl groups are the active sites for Hg capture; they suggested that phenol groups may inhibit Hg adsorption.

X-ray photoelectron spectroscopy, XPS, showed that the activated fluid coke surfaces contained both carbon-oxygen complexes as well as carbon-sulphur compounds. XPS spectra were obtained for seven samples. These samples were embedded in epoxy,

sectioned and then argon sputtered before recording the XPS spectra. A summary of the results is given in Table 5.3 and sample plots of the O 1s and S 2p spectra for Sample SS10421 are shown in Figures 5-5 and 5-6. The binding energies were referenced to the binding energy of carbon 1s which was set at 284.6 eV (Niemantsverdriet, 2000).

Table 5-3. XPS results for various activated and cross-sectioned fluid coke samples.

Sample	Binding Energies, eV		Prior Activation Conditions				Surface Area, m <sup>2</sup> /g
	S, 2p line Maxima	O, 1s line Maxima	Temp °C	Time hr	H <sub>2</sub> O mL/h	CO <sub>2</sub> , mol %	
SS10415	163.50	532.6	800	6	2.3	64.0	234
SS10420	163.36	531.9	800	8	4.5	31.3	471
SS10521	163.62	532.4	800	4	4.5	31.3	273
SS10423	163.02	532.2	600	8	4.5	31.3	36
SS10424	163.10	532.1	800	4	9.0	18.5	416
SS10425	163.64	532.4	800	4	9.0	0 <sup>b</sup>	425
SS10429	163.34	532.8	800	4	12.0	14.6	444
Average	163.37	532.3					

<sup>b</sup> 18.5% N<sub>2</sub>, the remainder is H<sub>2</sub>O

Binding energies (B.E.) for oxygen 1s for water and hydroxides are typically in the 531 to 532 eV range, and for metal oxides the B.E, are ≤531 eV (Moulder et al., 1992; Dupin et al., 2000). B.E. of 532 to 533 eV for the O 1s line are typical of organic oxygen such as C-O-C, C-OOR, C=O and COOH (Xie et al, 1991). Hence, the detected oxygen in the samples indicates that the oxygen is complexed with carbon. The oxygen signal was strong, indicating that most of the surface is oxygenated (XPS is a surface sensitive technique).

A binding energy of <164 eV for sulphur indicates a negatively charged sulphur. Metal sulphides have binding energies of about 161 to 162 eV (Duan, 2006). Binding energies for S 2p of about 163 eV are attributed to aliphatic organic sulphides and a binding energy of about 164 can be attributed to thiophenic (aromatic) sulphur (George, 1991). The S 2p binding energies measured for the activated coke indicates that most of the detected sulphur is organic sulphur.

It is not known whether both the oxygen and the sulphur containing species interact with the  $\text{Hg}^{\circ}$  species. However, both chemisorption and physical adsorption are probably involved in the capturing of mercury by the activated fluid coke.

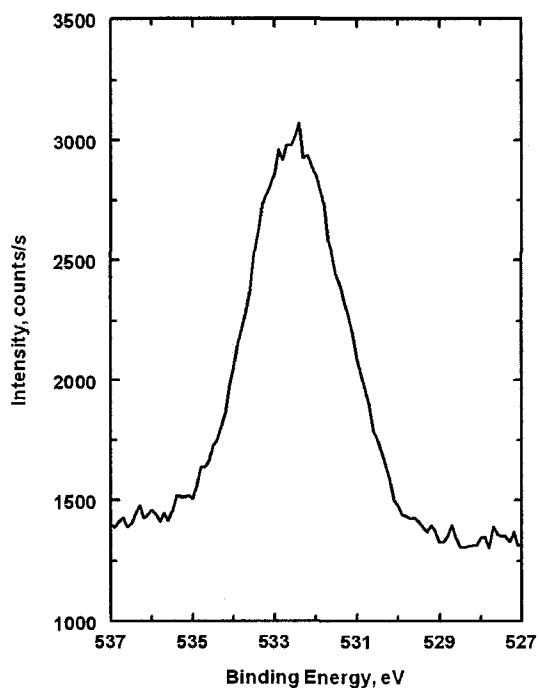


Figure 5-5. XPS spectrum of oxygen 1s 2p line for Sample SS10421.

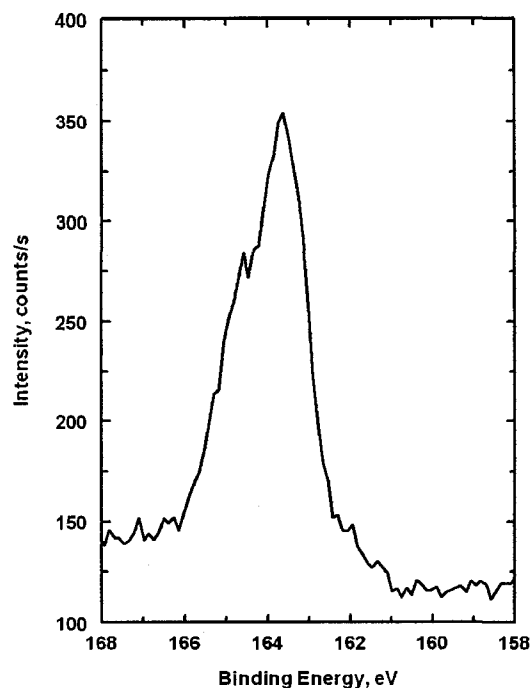


Figure 5-6. XPS spectrum of sulphur line for Sample SS10421.

### 5.3. Hg adsorption on $\text{H}_2$ -treated samples

Two activated coke samples, SS10432 and IC10489 were treated in  $\text{H}_2$  atmosphere and the Hg adsorption capacities of the treated samples were tested. About 2 g of each sample was placed in the reactor used for activation of fluid coke followed by treatment in pure hydrogen. The treatment temperature was  $400^\circ\text{C}$ , treatment time was 1 h and  $\text{H}_2$  flow rate was 10 mL/min. The treatment for both samples was done at two different pressures: 100 kPa and 345 kPa. The samples were exposed to the atmosphere after the hydrogen treatment.

The purpose of this treatment was to determine whether reduction in hydrogen permanently removed oxygen species from the coke. The effect of the hydrogen treatment on the mercury capturing ability is shown in Table 5-4. The results in Table 5-4 show that the hydrogen treatment resulting in a decrease in mercury capturing ability, but

the decrease was much less than the treatment in argon at 200°C discussed above; the average decrease in the amount of Hg captured as a result of the hydrogen treatment was about 30% while the average decrease resulting from the argon treatment was 79% (see Table 5-2).

Table 5-4. Hg adsorption results of activated and H<sub>2</sub>-treated activated coke samples.

Sample I.D.	Hydrogen Treatment Pressure, kPa	Hg Adsorbed Before Hydrogen Treatment, pg/mg of AC	Hg adsorbed After Hydrogen Treatment, pg/mg of AC	Decrease in Hg Captured as a Result of Hydrogen Treatment, %
10432	-	18.5	-	-
10432	100	-	12.14	34.4
10432	345	-	9.08	50.9
10489	-	17.8	-	-
10489	100	-	13.5	24.2
10489	345	-	15.2	14.6

The treatment in hydrogen at 400°C should have removed more of the oxygen containing species from the surface of the fluid coke compared to the 200°C treatment in argon, but the argon-treated samples were not exposed to the atmosphere after the argon treatment while the hydrogen treated samples were exposed to the atmosphere after hydrogen treatment. The exposure to air of the hydrogen-treated samples must have restored some of the adsorbed (complexed) oxygen as well as resulted in adsorption of water. These results show the exposure of ‘reduced’ activated fluid coke to the atmosphere reactivated the coke. If oxygenated species are partially responsible for the Hg capture, then treatments of activated fluid coke in oxidizing atmospheres, e.g. air, at temperatures below the combustion temperature may improve the mercury capture ability of the activated fluid cokes.

#### 5.4. Hg adsorption on sulphur impregnated activated coke

The addition of elemental sulphur to the surface of activated fluid coke should improve the mercury capturing ability of the fluid coke since it is well know that

elemental sulphur reacts with mercury. Activated fluid coke sample IC10474 was used as the starting material for vapour-phase sulphur impregnation. Sample IC10474 was obtained by activation of Coke 104, under the following treatment conditions:  $T=755^{\circ}\text{C}$ ; treatment time = 4 h; pressure = 614 kPa; total feed rate of treatment gas = 16.7 mmol/min; feed gas composition: 24.9 mole %  $\text{H}_2\text{O}$ , 72.9 mole %  $\text{CO}_2$ , 2.2 mole %  $\text{N}_2$ ). The properties of this activated fluid coke are: BET surface area:  $420\text{ m}^2/\text{g}$ , micropore volume =  $0.160\text{ mL/g}$ , mesopore volume =  $0.0545\text{ mL/g}$ , average pore radius =  $1.02\text{ nm}$ , sulphur content = 4.40 mass %.

Sulphur impregnation was carried out at  $100^{\circ}\text{C}$ ,  $200^{\circ}\text{C}$ ,  $300^{\circ}\text{C}$ ,  $400^{\circ}\text{C}$ ,  $500^{\circ}\text{C}$  and  $600^{\circ}\text{C}$ . High purity elemental sulphur powder was used for the impregnation of activated coke (treatment procedure described in Section 3.4). Figure 5-7 shows the sulphur concentration of sulphur-impregnated samples at different impregnation temperatures. The sulphur content increased with increasing sulphur treatment temperatures up to  $400^{\circ}\text{C}$ , followed by a decrease at temperatures above  $400^{\circ}\text{C}$ .

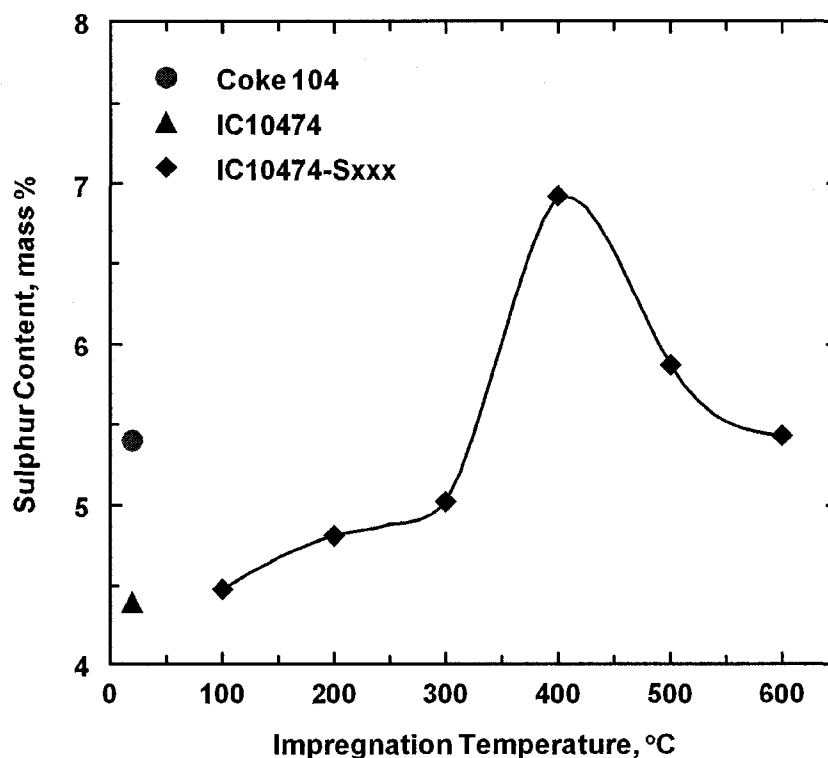


Figure 5-7. Sulphur content of sulphur-impregnated activated fluid coke (IC10474-Sxxx) as a function of impregnation temperature compared to sulphur content of unactivated (Coke 104) and activated fluid coke (IC10474).

The increase in sulphur content with increasing impregnation temperature for temperatures up to 400°C is largely due to the increase in sulphur vapour pressure with increasing temperature (see Figure 5-8). The reduction in amount of sulphur with impregnation temperatures above 400°C was due to the decrease in equilibrium adsorption capacity with increasing temperature, i.e. typical temperature dependence of adsorption.

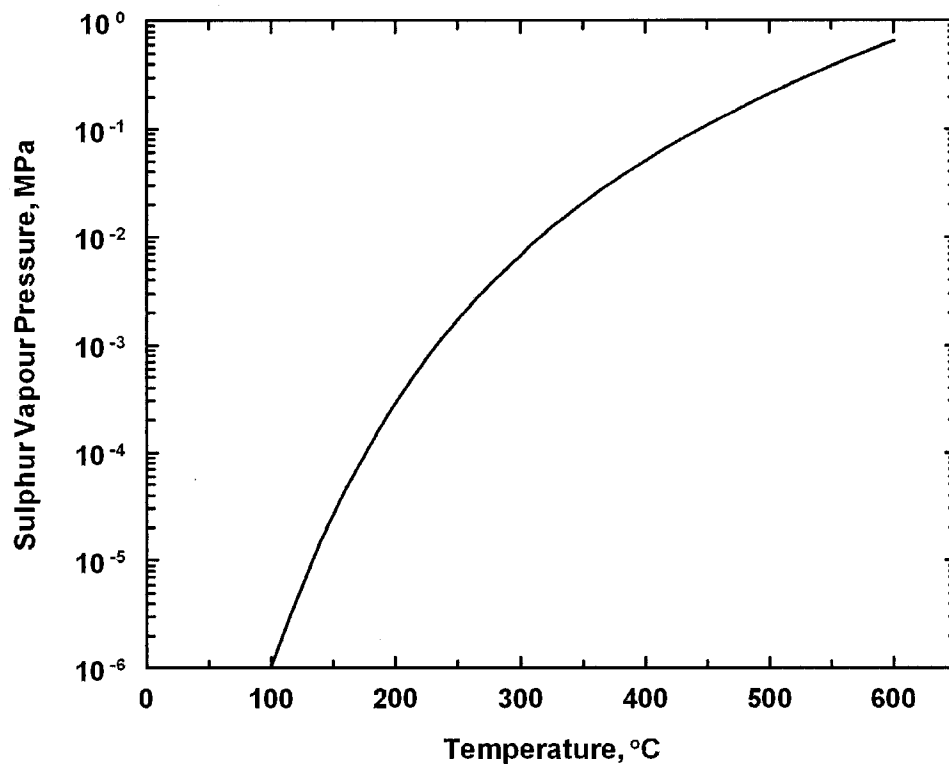


Figure 5-8. Variation of sulphur vapour pressure with temperature (Hampel, 1968).

The effect of sulphur addition on Hg capture of impregnated samples was evaluated as a function of sorption temperature and impregnation temperature. Sulphur impregnated samples, except the sample for which sulphur was added at 100°C, were tested for Hg capture following the same pulse adsorption procedure used for the activated coke. Sample IC10474-S100 was not tested because very little sulphur was added during the 100°C treatment (see Figure 5-7). The mercury sorption ability of the other sulphur treated samples was measured at temperatures of 100 to 250°C. Figure 5-9



shows the percentage of mercury adsorbed on sulphur treated samples after the first pulse injection, at different sorption temperatures. More than one mercury-containing pulse was injected for most of the sulphur treated samples. The total amount of Hg adsorbed for these multiple injections are shown in Figure 5-10. The maximum number of pulses injected was 6 and for some of the samples no Hg breakthrough had occurred. No breakthrough was observed for all the data points in Figure 5-10 for which the Hg uptake was above 50 pg/mg of activated fluid coke.

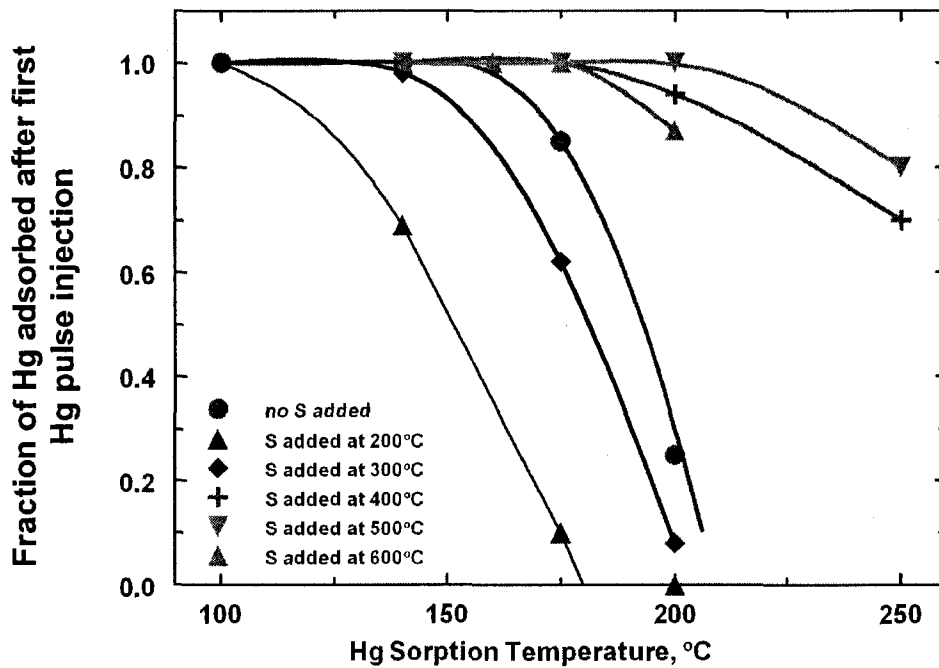


Figure 5-9. Effect of sulphur addition on Hg capture as a function of sorption temperature (for samples IC10474-Sxxx\*).

\*xxx- represents sulfur impregnation temperature

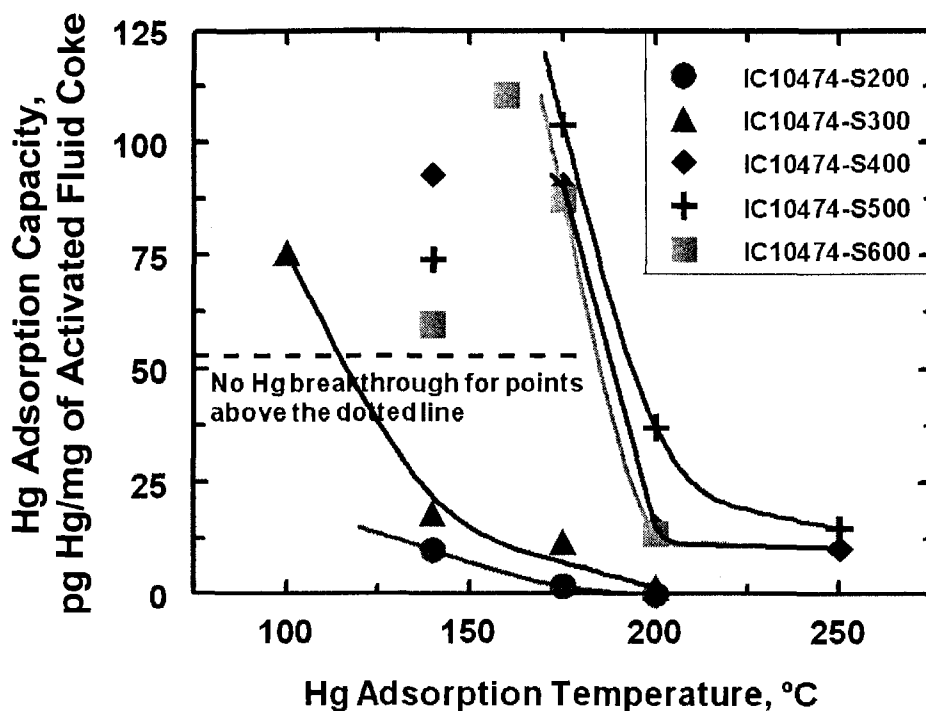


Figure 5-10. Mercury adsorption capacities as a function adsorption temperature for sulphur-treated samples of activated fluid coke IC10474.

The results in Figure 5-9 clearly show that the Hg sorption is a strong function of the temperature at which sulphur was added to the activated fluid coke. At sulphur addition temperatures of 200 and 300°C (IC10474-S200 and IC10474-S300), the mercury capture was less than without sulphur addition even though some sulphur was added at these temperatures. Sulphur addition at 400°C (IC10474-S400) increased Hg capture ability. Increasing the sulphur addition temperature to 500°C (IC10474-S500) resulted in a further increase in Hg capture even though the sulphur content of the fluid coke after the 500°C addition was considerably less than after the 400°C addition (see Figure 5-7). A further increase in the sulphur addition temperature to 600°C (IC10474-S600) resulted in a decrease in sulphur content as well as a decrease in Hg capture ability

The variation in the concentrations of sulphur allotropes with temperature along with the strong temperature dependence of the sulphur vapour pressure with temperature are probably the main factors responsible for effects of sulphur impregnation temperature on subsequent mercury adsorption capacity. Sulphur exists in several allotropes, including  $S_\lambda$  ( $S_8$  rings),  $S_\pi$  ( $S_8$  chains) and  $S_\mu$  (chains of variable length). At impregnation

temperatures up to 400°C, sulphur molecules will condense mainly in the form of S<sub>8</sub> and S<sub>6</sub> and form voluminous rings or long linear chains. The S<sub>6</sub>/S<sub>8</sub> molar ratio increases with the increasing temperature, as illustrated in Table 5-4 (Tuller, W. N., 1954). With increasing temperature, the concentration of small sulphur molecules increase and this has a significant effect on the structure of the sulphur-impregnated activated fluid coke. Hence, the effect of sulphur impregnation temperature on the mercury capture properties of the sulphur impregnated activated fluid coke samples is explained as follows:

1. At low sulphur impregnation temperatures ( $\leq 300^\circ\text{C}$ ) the amount of sulphur added to the activated fluid coke was small (low sulphur vapour pressure) and the type of sulphur added was almost all S<sub>8</sub> and S<sub>6</sub> and these molecules condense in even larger aggregates. At low temperature these sulphur species can easily block the micropores in the activated coke (average micropore diameter is  $< 2$  nm). This blocking of the pores is probably the reason for the low Hg sorption ability of IC10474-S200 and IC10474-S300 compared to the sample without sulphur treatment.
2. After sulphur impregnation temperature of 400°C, the sulphur content is the highest, but the mercury capture ability is not the highest. The high sulphur loading after the 400°C sulphur treatment is due to a combination of the higher vapour pressure and the high sorption capacity of the fluid coke at 400°C, but most of the sulphur is still present in large molecules. This means that many of the micropores are probably blocked. The somewhat improved Hg capture ability of IC10474-S400 compared to IC10474-S300 is due to the large amount of sulphur in IC10474-S400; it is well known that Hg is captured by elemental sulphur.
3. After sulphur impregnation temperature of 500°C (IC10474-S500) the sulphur content is less and the mercury capture ability is higher than that after sulphur impregnation at 400°C. This lower sulphur content is due to the lower equilibrium sulphur uptake by the activated fluid coke at the higher temperature and the higher sulphur capture ability is probably due to the presence of higher concentration of smaller sulphur molecules, such as S<sub>2</sub> (see Table 5-4) and less pore blockage. These smaller sulphur molecules can penetrate into the micropores and bind relatively strongly to the surface of the activated coke where they can subsequently capture mercury.

4. After sulphur impregnation temperature of 600°C (IC10474-S600) the sulphur content is less than sulfur content of the sample impregnated at 500°C and the mercury capture ability is also lower than that of the sample impregnated at 500°C. The lower sulphur content is again due to the decrease in equilibrium adsorption uptakes with increasing temperature and the decrease in mercury capture ability is probably associated with the decrease in the amount of sulphur on the surface of the pores after the 600°C impregnation.

Table 5-4. Molar composition of saturated sulphur vapour at various temperatures (Tuller, 1954)

Temperature, °C	Sulphur allotropes, mole %		
	S <sub>8</sub>	S <sub>6</sub>	S <sub>2</sub>
148.9	82.8	17.2	0.01
204.4	76.0	24.0	0.04
260	68.9	31.0	0.15
315.6	60.9	38.6	0.5
371.1	52.6	46.1	1.3
398.9	48.7	49.4	1.9
426.7	44.9	52.4	2.7
444.6	42.5	54.0	3.5
454.4	41.3	54.7	4.0
482.2	37.8	56.6	5.6
510	34.6	58.0	7.4
537.8	31.4	58.8	9.8
565.6	28.3	59.3	12.4
593.3	25.4	59.1	15.5
648.9	20.0	57.0	23.0

Based on these preliminary results, it can be concluded that the efficiency of mercury removal of sulphur-impregnated activated coke depends not on the total sulphur content, but rather on the nature of sulphur forms present in the coke matrix as well as on

the uniform distribution of sulphur in the coke matrix. These two factors are controlled by the impregnation temperature. These results further support the fact that materials with sufficient amounts of active adsorption sites (e.g. sulphur) and sufficient microporous structure are needed to achieve large mercury adsorption capacities. Additional work to optimize the sulphur impregnation conditions (time and temperature) is required.

Additional characterization of the sulphur-treated activated cokes is required to determine the homogeneity of sulphur concentration throughout the activated coke particles; EDX, in the same fashion as used to get the sulphur concentration in the activated coke particles (Section 4.1), can be used to obtain this information. Surface area measurements of the sulphur-impregnated fluid cokes should be done to determine whether the hypothesis that pore blocking is the main cause of the low mercury adsorption capacities after sulphur impregnation at 200 and 300°C.

## Chapter 6. Summary, Conclusions and Recommendations

This study showed that Syncrude fluid coke can be converted into high surface area activated carbon (surface areas in the 300 to 500 m<sup>2</sup>/g) by treatment in H<sub>2</sub>O/CO<sub>2</sub> at temperatures of 700 to 800°C. These activated fluid coke particles adsorb mercury from gas streams at temperatures up to 150°C. The mercury sorption capabilities are improved significantly if the activated fluid coke is impregnated with elemental sulphur at about 500°C. A detailed summary of the treatment conditions and observation on which the above general statements are based is given below. Some recommendations for future work are also made.

Physical activation of fluid coke was employed to increase the surface area. The conditions used for these activations were:

Size of sample used for each activation: 10 g

Size of fluid coke particles: 100 to 125 µm for most experiments

Temperature: 200 to 800°C

Pressure: 0.1 to 0.6 MPa

Length of treatments: 1 to 8 h

H<sub>2</sub>O feed rate: 0 to 70 mmol/min (0 to 18 mL/h)

CO<sub>2</sub> feed rate: 0 to 12.2 mmol/min

N<sub>2</sub> feed rate: 0 to 3.6 mmol/min

O<sub>2</sub> feed rate: 0 to 0.8 mmol/min

Most of the treatments were carried out in mixtures of H<sub>2</sub>O and CO<sub>2</sub>. A few runs with nitrogen in the feed treatment gas were done to determine whether the CO<sub>2</sub> played a significant role in the activation. Oxygen was added to the feed treatment gas in a few runs to determine whether the presence of oxygen would affect the pore structure.

The properties of the virgin fluid cokes as well as activated cokes were obtained by the following techniques:

- Laser light scattering for particle size determination (Malvern Mastersizer 2000);
- Nitrogen adsorption and desorption at liquid nitrogen temperatures for surface area and pore size distribution (Omnisorb 360);
- Scanning electron microscopy on whole and sectioned particles for determination of exterior and internal particle morphology (Hitachi S-2700);

- Energy dispersive x-ray analysis for the determination of sulphur distribution in particles (Princeton Gamma Tech Prism IG);
- X-ray photoelectron spectroscopy for the determination of oxidation states of sulphur and oxygen on the pore surfaces of activated fluid coke (Kratos Axis 165);
- Total sulphur analyses of particles (Horiba EMIA 320 and an Antek 9000NS).

A HP 5890 gas chromatograph was used to analyze the effluent gases.

The following observations and conclusions were made from the activation and characterization experiments:

1. Virgin fluid coke particles were roughly spherical in shape and the sphericity of the particles increased with increasing particle size;
2. The particle shapes did not change with activation and the size distribution did not change markedly with activation except when oxygen was present in the treatment gas;
3. Increases in surface areas were insignificant for treatment temperatures  $\leq 600^{\circ}\text{C}$  for all feed gas compositions examined;
4. Treatments at temperatures of 600 to  $800^{\circ}\text{C}$  resulted in increases in surface area, and the increases were very dependent on the composition of the treatment gas;
5. The maximum surface area obtained with pure  $\text{CO}_2$  as the treatment gas was  $60\text{ m}^2/\text{g}$  after treatment for 8 h at  $789^{\circ}\text{C}$ ;
6. Surface areas after treatments in a  $\text{H}_2\text{O}/\text{CO}_2$  mixtures at 750 to  $800^{\circ}\text{C}$  and treatment times of 4 h were in the  $400$  to  $500\text{ m}^2/\text{g}$  range, with one experiment resulting in a surface area of  $533\text{ m}^2/\text{g}$  (IC10486);
7. Replacement of  $\text{CO}_2$  with  $\text{N}_2$  in  $\text{H}_2\text{O}/\text{CO}_2$  mixtures did not result in significantly different surface areas; this leads to the conclusion that  $\text{CO}_2$  does not play a major role in the fluid coke activation in the temperature range studied, and the  $\text{H}_2\text{O}$  is the major activating agent;
8. The amount of  $\text{H}_2\text{O}$  fed and the partial pressure of  $\text{H}_2\text{O}$  affected the surface area; higher  $\text{H}_2\text{O}$  feed rates and higher  $\text{H}_2\text{O}$  partial pressures usually resulted in higher surface areas;
9. Using  $\text{N}_2/\text{O}_2$  mixtures as the treatment gas did not result in increases in surface area; the oxygen only causes combustion of carbon on the external surface of the particles;

10. Adding O<sub>2</sub> to H<sub>2</sub>O/CO<sub>2</sub> mixtures did not result in increases in surface area compared to treatment in H<sub>2</sub>O/CO<sub>2</sub> mixtures, but it did result in an increase in mass loss. The added O<sub>2</sub> did not result in an increase in pore size;
11. The average pore size in all activated fluid coke particles was about the same. The average pore radius was 1.0 ( $\pm$ 0.1) nm for all fluid coke samples with surface areas above 50 m<sup>2</sup>/g.
12. The sulphur content of the fresh coke was about 6 to 7 mass % and activation resulted in decreases in sulphur content to about 4 to 6 mass %.
13. The sulphur in the virgin fluid coke particles was distributed evenly throughout the particles as measured by EDX, while in activated fluid coke particles the sulphur concentration increased towards the interior of the particles;
14. XPS results lead to the conclusion that most of the sulphur in the fluid coke, virgin and activated, is present as organic sulphur;
15. XPS results also showed that there is a high concentration of oxygen on the surface of the activated coke and that the O 1s binding energies are in the range of oxygen in organic compounds.

The activated fluid coke samples as well as sulphur impregnated activated fluid coke samples were tested for their ability to remove mercury from an argon stream at various temperatures. A pulse adsorption apparatus was used for these studies. The following observations and conclusions are based on these measurements:

1. Activated fluid coke particles, with surface areas above 200 m<sup>2</sup>/g, adsorb mercury from a gas stream at temperatures up to about 150°C.
2. Surface oxygen groups, and possibly strongly adsorbed water are responsible for the mercury capture ability of the activated fluid coke particles as shown by in situ treatment at 200°C in flowing argon prior to Hg capture measurement;
3. The removal of surface oxygen and water is at least partially reversible as shown by ex situ treatment in hydrogen;
4. Impregnation of activated fluid coke with elemental sulphur at temperatures of 400 to 600°C increased the mercury capture ability significantly;



5. The optimum sulphur impregnation temperature is about 500°C. The sample impregnated with sulphur at 500°C adsorbed mercury at temperatures up to 250°C.

The above results have demonstrated that the sulphur-treated activated fluid coke is capable of removing mercury from gas stream at temperatures encountered in flue gases of coal-fired power plants. However, additional work is required to ensure that the sulphur-treated activated fluid coke is suitable for flue gas treatment. The following additional work is required:

1. The sulphur-impregnation conditions must be optimized (time of exposure and fine-tuning of the temperature) along with the determination of whether pore blocking is the cause for low Hg capture for sulphur impregnation temperatures  $\leq 400^\circ\text{C}$ .
2. The total mercury adsorption capacity of the sulphur-treated activated fluid coke must be determined. The pulse method does not yield good estimates of mercury sorption capacity and continuous mercury adsorption from a gas stream must be done;
3. The adsorption of mercury from actual flue gases should be measured to determine whether any components in the flue gas interfere, or possibly enhance, the mercury removal by sulphur-treated activated fluid coke. These studies require in-plant tests.
4. An economic analysis for the manufacturing of sulphur-treated activated fluid coke should be done to determine whether the use of sulphur-treated activated fluid coke is economically viable compared to alternate methods of mercury removal for flue gases of coal-fired power plants.

If the results of the above future work show that sulphur-treated activated fluid coke is economic for removal of mercury from flue gases than a use of a currently useless by-product of bitumen upgrading will have been found. The possibility of using activated fluid coke for other applications, such as water treatment, should also be explored.

## REFERENCES

- Bansal, R.C., Donnet, J.B., and Stoeckli, F., "Active Carbon", Marcel Deker, Inc., New York and Basel, (1988).
- Carpi, A., "Mercury from Combustion Sources: a Review of the Chemical Species Emitted and Their Transport in the Atmosphere", *Water, Air, and Soil Pollution*, **98**, 241-254, (1997).
- Chunlan, L., Shaoping, X., Yixiong, G., Shuqin, L., and Changhou, L., "Effect of Pre-carbonization of Petroleum Cokes on Chemical Activation Process with KOH", *Carbon*, **43**, 295-2301, (2005).
- Dietz, W.A., "Response Factors for Gas-Chromatographic Analyses", *Journal of Gas Chromatography*, **5**, 68-71, (1967).
- DiPanfilio, R. and Egiebor, N.O., "Activated Carbon Production from Synthetic Crude Coke", *Fuel Processing Technology*, **46**, 157-169, (1996).
- Duan, J., Hou, B., and Yu, Z., "Characteristics of Sulphide Corrosion Products of 316L Stainless Steel Surfaces in the Presence of Sulphate-Reducing Bacteria", *Materials Science and Engineering: C*, **26**, 624-629 (2006).
- Dubin, M.M., "Chemistry and Physics of Carbons", P.L.Walker (Editor), Vol.2, Marcel Deker, Inc., New York, (1966).
- Dupin, J-C., Gonbeau, D., Vinatier, P. and Levasseur. A., "Systematic XPS Studies of Metal Oxides, Hydroxides and Peroxides", *Phys. Chem. Chem. Phys.*, **2**, 1319-1324 (2000).
- Fairbridge, C., Palmer, A.D., Ng, S.H., and Furimsky, E., "Surface Structure and Oxidation Reactivity of Oil Sand Coke Particles", *Fuel*, **66**, 688-691, (1987).
- Fairbridge, C., Palmer, A.D., and Ng, S.H., "Fractal Analysis of Gas Adsorption on Syncrude Coke", *Fuel*, **65**, 1759-1761, (1986).
- Feng, W., Kwon, S., Feng, X., Borquet, E. and Vidic, R.D., "Sulphur Impregnation on Activated Carbon Fibers through H<sub>2</sub>S Oxidation for Vapour Phase Mercury Removal", *Journal of Environmental Engineering*, **132**(3), 292-300, (2006).
- Furimsky, E., "Gasification of Oil Sand Cokes – Review", *Fuel Processing Technology*, **56**, 263-290, (1998).
- Furimsky, E., "Characterization of Cokes from Fluid/Flexi-Coking of Heavy Feeds", *Fuel*

- Processing Technology, **67**, 205-230, (2000).
- George, G.N., Gorbaty, M.L., Keleman, S.R. and Sansone, M., "Direct Determination and Quantification of Sulphur Forms in Coals from the Argonne Premium Sample Program", *Energy & Fuels*, **5**, 93-97, (1991).
- Gregg, S.J. and Sing, K.S.W., "Adsorption, Surface Area and Porosity", 2<sup>nd</sup> Ed., London, Academic Press, (1982).
- Hall, B., Schager, P. and Lindqvist, O., "Chemical Reactions of Mercury in Combustion Flue Gases", *Water, Air and Soil Pollution*, **56**, 3-14, (1991).
- Hampel, C.A., "The Encyclopedia of the Chemical Elements", Reinhold Book Corporation, New York, (1968).
- Hsi, C. H., Chen, S., Rostam-Abadi, M., Rood, M., Richardson, C.F., Carrey, T.R. and Chang, R., "Preparation and Evaluation of Coal Derived Activated Carbons for Removal of Mercury Vapours from Simulated Coal Combustion Flue Gases", *Energy and Fuels*, **12**, 1061-1070, (1998).
- Ityokumbul, M., "Upgrading of Oil Sand Residues", *Fuel Processing Technology*, **38**, 127-138, (1994).
- Jack, T.R., Sullivan, E.A., and Zajic, E., "Comparison of the Structural and Composition of Cokes from the Thermal Cracking of Athabasca Oil Sands Bitumen", *Fuel*, **58**, 585-588, (1979).
- Krishnan, S.V., Gullett, B. K. and Jozewicz, W., "Sorption of Elemental Hg by Activated Carbons", *Environmental Science and Technology*, **28**, 1506-1512, (1994).
- Kwon, S., and Vidic, R.D., "Evaluation of Two Sulphur Impregnation Methods on Activated Carbon and Bentonite for the Production of Elemental Mercury Sorbents", *Environmental Engineering Science*, **17**, 303-313, (2000).
- Lahaye, J., "The Chemistry of Carbon Surfaces", *Fuel*, **77**, 6, 543-547, (1998).
- Lee, S.H. and Choi, C.S., "Chemical Activation of High Sulphur Petroleum Cokes by Alkali Metal Compounds", *Fuel Processing Technology*, **64**, 141- 153, (2000).
- Lee, S.H., Rhim, Y.J., Cho, S.P. and Baek, J.C., "Carbon-Based Novel Sorbent for Removing Gas-Phase Mercury", *Fuel*, **85**, 219-226, (2006).
- Li, Y.H., Lee, C.W., Gullett, B.K., "The Effect of Activated Carbon Surface Moisture on Low Temperature Mercury Adsorption", *Carbon*, **40**, 65-72, (2002).

- Li, Y.H., Lee, C.W., Gullett, B.K., "Importance of Activated Carbon's Oxygen Surface Functional Groups on Elemental Mercury Adsorption", *Fuel*, **82**, 451-457, (2003).
- Liu, W. and Vidic, R.V., "Optimization of Sulphur Impregnation Protocol for Fixed-Bed Application of Activated Carbon-Based Sorbents for Gas-Phase Mercury Removal", *Environmental Science and Technology*, **32**, 531-538, (1998).
- Liu, W., and Vidic, R.D., "Optimization of High Temperature Sulphur Impregnation on Activated Carbon for Permanent Sequestration of Elemental Mercury Vapours", *Environmental Science and Technology*, **34**, 483-488, (2000).
- Lowell, S. and Shields, J.E., "Powder Surface Area and Porosity", 3<sup>rd</sup> Ed., Chapman & Hall, London, (1991).
- Majid, A., and Sparks, B.D., "Potential Applications of Oil Sands Industry Wastes", *Journal of Canadian Petroleum Technology*, **38**, (11), 29-33, (1999).
- Modell, M. and Reid, R.C., "Thermodynamics and Its Applications", 2<sup>nd</sup> Ed., Prentice-Hall, Englewood Cliffs, N.J., p. 335, (1983).
- Moulder, J.F., Stickle, W.F., Sobol, P.E. and Bomben, K., "Handbook of X-Ray Photoelectron Spectroscopy", 2<sup>nd</sup> ed., (J. Chastain, Ed), Perkin-Elmer Corporation (Physical Electronics), (1992).
- Nabais V.J., Carrott, P.J.M., Carrott, M.M.L., Belchior, M., Boavida, D., Dially, T., Gulyurtlu, I., "Mercury Removal from Aqueous Solution and Flue Gas by Adsorption on Activated Carbon Fibers", *Applied Surface Science*, **252**, 6046-6052, (2006).
- Niemantsverdriet, J.W., "Spectroscopy in Catalysis, An Introduction", 2<sup>nd</sup> Ed, 50, Wiley-VCH, Weinheim, Germany, ( 2000).
- O'Grady, T.M., and Wennerberg, A.N., "High Surface Area Active Carbon", Petroleum derived carbons, Bacha D., John, Newman W., John, White L., J. (Editors), American Chemical Society, Washington, DC, (1986).
- Otaigbe, J.U., and Egiebor, N.O., "Athabasca Petroleum Coke Utilization: Coagglomeration with Sulphur Sorbents for Control of Sulphur Dioxide Emissions during Combustion", *Energy and Fuels*, **5**, 30-34, (1991).
- Otani, Y., Kanaoka, C., Uchijima, I., and Nishino, H., "Removal of Mercury Vapour

- from Air with Sulphur-Impregnated Adsorbents”, *Environmental Science and Technology*, **22**, 708-711, (1988).
- Otowa, T., Tanibata, R. and Itoh, M., “Production and Adsorption Characteristics of Maxsorb: High-Surface Area Active Carbon”, *Gas Separation and Purification*, **7**, 241- 245, (1993).
- Pavlish, J.H., Sondreal, E.A., Mann, M.D., Olson, E.S., Galbreath, K.C., Laudal, D.L., Benson, S.A., “Status Review of Mercury Control Options for Coal-Fired Power Plants”, *Fuel Processing Technology*, **82**, 89-165, (2003).
- Pavlish, J.H., Laudal, D.L., Holmes, M.J., Hamre, L.L., Musich, M.A., Pavlish, B.M., Weber, G.F., Hajicek, D.R., “Technical Review of Mercury Technology Options for Canadian Utilities – a Report to the Canadian Council of Ministers of the Environment”, March 2005.
- Shashkov, A.G., Kamchatov F.P. and Abramenko, T.N., “Thermal Conductivity of the Hydrogen-Helium Mixture”, *Journal of Engineering Physics and Thermophysics*, **24**, 461-464, (1973).
- Shawwa, A.R., Smith, D.W. and Sego, D.C., “Color and Chlorinated Organics Removal from Pulp Mills Wastewater Using Activated Petroleum Coke”, *Water Research*, **35**(3), 745-749, (2001).
- Sinha, R. K., and Walker, P.L., “Removal of Mercury by Sulphurized Carbons”, *Carbon*, **10**, 754-756, (1972).
- Tuller, W.N., “The Sulphur Data Book”, McGraw-Hill Book Company, Inc., New York, (1954).
- Wu, M., Zha, Q., Qiu, J., Han, X., Guo, Y., Li, Z., Yuan, A., and Sun X., “Preparation of Porous Carbons by Different Activation Methods”, *Fuel*, **84**, 1992-1997, (2005).
- Xie, Y., Wang, T., Franklin, O. and Sherwood, P.M.A., “X-Ray Photoelectron Spectroscopic Studies of Carbon Fiber Surfaces. Part XVI: Core-Level and Valance Band Studies of Pitch-Based Fibres Electrochemically Treated in Ammonium Carbonate Solution”, *Applied Spectroscopy*, **46**, 645-651 (1992).
- Zamora, R.M., Schouwenaars, R., Moreno, D.A., and Buitron, G., “Production of

Activated Carbon from Petroleum Coke and Its Application in Water Treatment for the Removal of Metals and Phenol”, *Water Science and Technology*, **42**, 119-126, (2000).

## **APPENDIX A**

This appendix contains summaries of the results of the fluid coke activation experiments (Table A-1) and of the mercury pulse adsorption experiments (Table A-2).

Table A-1. Summary of activation experiments.

Run <sup>a</sup>	Treatment Conditions				Treatment Gas Composition, mole %				Treat. Gas Feed Rate, mmol/min	Mass Loss <sup>c</sup> , %	Surface Area, m <sup>2</sup> /g		Pore Volume, cm <sup>3</sup> /g	
	Temperature <sup>b</sup> , °C		Pres. <sup>c</sup> kPa	Length h	CO <sub>2</sub>	H <sub>2</sub> O	N <sub>2</sub>	O <sub>2</sub>			micro	meso		
	Set	Actual												
SS10401	600	603 (0.7)	100	4	100				3.8	1.6	25.7	0.0091	0.0031	
SS10402	600	597 (1.1)	100	2	100				3.8	2.6	24.7	0.0091	0.0032	
SS10403	600	611 (1.0)	100	8	100				3.8	0.8	23.9	0.009	0.004	
SS10404	800	787 (1.5)	100	6	100				3.8	9.8	49.4	0.018	0.0044	
SS10405	800	793 (3.8)	100	4	100				3.8	8.1	37.2	0.013	0.0042	
SS10406	200	202 (0.4)	100	6	100				3.8	0.1	21.0	0.0086	0.0033	
SS10407	400	417 (0.9)	100	4	100				3.8	0.1	21.9	0.0087	0.0029	
SS10408	400	422 (0.8)	100	6	100				3.8	1	21.8	0.0081	0.0025	
SS10409	600	602 (1.2)	100	6	100				3.8	2.6	25.0	0.0092	0.0023	
SS10410	800	789 (1.9)	100	8	100				3.8	11.8	64.3	0.021	0.008	
SS10411	400	426 (0.8)	100	8	100				3.8	0.3	22	0.008	0.004	
SS10412	200	217 (3.4)	100	8	100				3.8	0.1	20.7	0.0077	0.0027	
SS10413	800	785 (1.9)	100	8	64.0	36.0			5.9	41.9				
SS10414	800	792 (23.7)	100	6	64.0	36.0			5.9	31.9				
SS10415	800	773 (96)	100	6	64.0	36.0			5.9	11	233.5	0.090	0.019	
SS10416	400	458 (21.2)	100	6	64.0	36.0			5.9	0	20.6	0.008	0.004	
SS10417	600	611 (18.5)	100	6	64.0	36.0			5.9	0.5	27.5	0.010	0.002	
SS10418	600	617 (6.6)	100	4	31.3	68.7			12.1	-2.6	26.4	0.010	0.004	
SS10419	600	621 (3.4)	100	8	47.6	52.4			8.0	-0.3	25.9	0.010	0.003	
SS10420	800	795 (1.5)	100	8	30.4	69.6			6.0	36.9	471.4	0.177	0.055	
SS10421	800	791 (1.0)	100	4	30.4	69.6			6.0	21.5	273.1	0.105	0.020	
SS10422	400	441 (0.8)	100	8	30.6	69.4			6.0	n.a.				
SS10423	600	623 (3.0)	100	8	30.6	69.4			6.0	1.2	36.4	0.014	0.002	
SS10424	800	782 (2.8)	100	4	18.5	81.5			10.2	31.1	415.8	0.159	0.042	
SS10425	800	786 (4.2)	100	4	81.5	18.5			10.3	27	424.5	0.165	0.033	
SS10426	700	706 (27.6)	100	4	31.3	68.7			6.0	8.7	59.1	0.019	0.039	
SS10427	800	803 (3.9)	100	4	52.9	47.1			4.1	19.2	203.4	0.078	0.014	
SS10428	800	794 (1.0)	100	5	47.1	52.9			4.0	21.4	319.3	0.124	0.030	
SS10429	800	796 (1.3)	100	4	14.6	85.4			12.9	40.1	443.9	0.169	0.052	
SS10430	700	704 (3.3)	100	4	31.3	68.7			6.0	9.5	79.7	0.028	0.013	



Run <sup>a</sup>	Treatment Conditions				Treatment Gas Composition, mole %				Treat. Gas Feed Rate, mmol/min	Mass Loss <sup>c</sup> , %	Surface Area, m <sup>2</sup> /g	Pore Volume, cm <sup>3</sup> /g	
	Temperature <sup>b</sup> , °C		Pres. <sup>c</sup> , kPa	Length, h	CO <sub>2</sub>	H <sub>2</sub> O	N <sub>2</sub>	O <sub>2</sub>				micro	meso
	Set	Actual											
SS10431	700	701 (1.6)	100	4	18.5	81.5			10.2	11.7	134.4	0.051	0.013
SS10432	800	796 (1.2)	100	4	47.1	52.9			4.0	22.9	275.9	0.107	0.027
MB10433	800	801 (2.2)	100	4			97.7	2.3	1.7	7.7			
MB10434	800	800 (1.1)	100	4			95.3	4.7	1.7	11			
MB10435	800	795 (1.0)	100	4			90.7	9.3	1.7	15			
MB10436	800	797 (2.1)	100	4			87.4	12.6	1.9	14.3			
MB10437	800	796 (4.9)	100	4			85.3	14.7	1.9	11.5			
MB10438	800	797 (1.4)	100	4			79.0	21.0	1.9	16.1	20.0	0.0068	0.0030
MB10439	800	799 (2.0)	100	5			87.8	12.2	3.6	23.3	20.4	0.0073	0.0032
MB10440	800	800 (2)	100	4			91.6	8.4	3.8	15.3	17.3	0.0062	0.0027
MB10442	800	797 (2.7)	100	4			98.1	1.9	4.2	9.3			
MB10443	800	795 (1.4)	100	4			79	21	1.9	20.8	19.1	0.0065	0.0035
MB10444	800	799 (1.3)	100	4			87.4	12.6	3.8	24.3	21.8	0.0078	0.0029
MB10445	800	798 (3.5)	100	4			27.7	1.4	5.9	24.2	235.7	0.0900	0.0273
MB10446	800	792 (22.4)	100	4		70.9	43.6	4.0	8.0	33	242.3	0.0925	0.0273
MB10447	800	785 (25.5)	100	4		52.4	28.6	2.6	12.1	41.5	320.9	0.1232	0.0356
MB10448	800	795 (4.1)	100	4		68.7	14.6	3.9	10.2	42.5	349.1	0.1318	0.0412
MB10449	800	795 (3.3)	100	4		81.5	24.7	6.6	12.1	65.2	286.2	0.1015	0.0358
MB10450	750	756 (4.7)	100	4		68.7	91.6	8.4	3.8	15.4	12.7	0.0048	0.0024
MB10451	700	710 (1.7)	100	4			91.6	8.4	3.8	13.5	12.1	0.0043	0.0023
MB10452	600	616 (1.0)	100	4			91.6	8.4	3.8	11.1	22.3	0.0083	0.0021
MB10453	400	435 (1.1)	100	4			91.6	8.4	3.8	9.1	30.8	0.0114	0.0045
MB10454	200	213 (0.7)	100	4			91.6	8.4	3.8	0.5			
MB10455	600	622 (8.3)	100	4		68.7	28.6	2.7	12.1	14.9	31.9	0.0126	0.0049
MB10456	400	435 (15.6)	100	4		68.7	28.6	2.7	12.1	11.6	31.4	0.0114	0.0026
MB10457	200	209 (3.4)	100	4		68.7	28.6	2.7	12.1	-1.4	22.4	0.0081	0.0027
MB10458	850	823 (17.6)	100	4		79.1	28.9		10.6	38.6	385.9	0.1429	0.0450
MB10459	800	789 (3.8)	100	4		100			3.8	9.8	44.3	0.0168	0.0025
MB10460	800	792 (2.2)	100	4		62.4	37.6		3.9	17.8	165.2	0.0632	0.0092
MB10461	700	702 (0.8)	100	4		62.4	37.6		3.9	7.9	44.0	0.0161	0.0007
MB10462	500	543 (3.9)	100	4		62.4	37.6		3.9	2.4	26.8	0.0106	0.0020
MB10463	750	754 (4.1)	100	4		62.4	37.6		3.9	12.7	104.2	0.0394	0.0026

Run <sup>a</sup>	Treatment Conditions				Treatment Gas Composition, mole %				Treat. Gas Feed Rate, mmol/min	Mass Loss <sup>c</sup> , %	Surface Area, m <sup>2</sup> /g	Pore Volume, cm <sup>3</sup> /g	
	Temperature <sup>b</sup> , °C		Pres. <sup>c</sup> , kPa	Length, h	CO <sub>2</sub>	H <sub>2</sub> O	N <sub>2</sub>	O <sub>2</sub>				micro	meso
	Set	Actual											
MB10301	800	767 (25.5)	100	4			91.9	8.1	4.0	16.2	12.9	0.0046	0.0033
MB10601	800	789 (0.9)	100	4			91.9	8.1	4.0	14.9	9.3	0.0028	0.0023
MB10701	800	794 (0.9)	100	4			91.9	8.1	4.0	14.3	8.2	0.0024	0.0026
MB10101	800	794 (1.0)	100	4			91.9	8.1	4.0	22.8	30.5	0.0117	0.0039
MB10501	600	--	100	5			91.9	8.1	4.0	12.1	15.2	0.0056	0.0029
MB10502	800	795 (1.4)	100	4			91.9	8.1	4.0	16.1			
MB10201	800	792 (0.8)	100	4			91.9	8.1	4.0	19.4	23.1	0.0085	0.0034
MB20701	800	792 (7.8)	100	4		69.2	28.3	2.5	12	31.4	159.8	0.0577	0.0169
MB20601	800	791 (2.3)	100	4		69.2	28.3	2.5	12	33.9	179.1	0.0662	0.0179
MB20501	800	794 (2.1)	100	4		69.2	28.3	2.5	12	36.5	251.7	0.0932	0.0253
MB20401	800	792 (1.8)	100	4		69.2	28.3	2.5	12	41.3	274.1	0.1017	0.0261
MB20301	800	788 (1.6)	100	4		69.2	28.3	2.5	12	55.4	292.5	0.1086	0.0290
MB20201	800	787 (4.5)	100	1		69.2	28.3	2.5	12	19.8	89.4	0.0325	0.0056
MB10464	600	781 (5.4)	118 (19)	4		68.1	31.9		6.1	19.3	211	0.0803	0.0098
MB10465	800	767 (2.9)	137 (17)	4		81	19		10.3	28.3	342.7	0.1317	0.0284
IC10466	800	788 (11.7)	113 (8)	4		52.2	47.8		4.1	18	161.9	0.0619	0.0074
IC10467	800	784 (7.1)	125 (14)	3		68.1	31.9		6.1	18.2	184.1	0.0697	0.0093
IC10468	800	784 (6.5)	120 (15)	4	30.6	69.4			6	23.6	268.9	0.1040	0.0172
IC10469	800	766 (38.6)	327 (17)	4	63.2	36.8			11.3	24.6	359	0.1396	0.0219
IC10470	800	738 (51.4)	177(21)	4	0	69.1	28.2	2.7	12.1	45.3	285.8	0.1099	0.0209
IC10471	800	710(146.4)	193 (36)	4	18.8	68	10.4	2.8	12.3	46.6	305.9	0.1183	0.0202
IC10472	800	684 (56.9)	341 (14)	4	63.2	36.8			11.3	12.5	149.7	0.0564	0.0024
IC10473	800	764 (59.1)	472 (6)	4	70	30			13.9	29.8	436.8	0.1680	0.0336
IC10474	800	754 (28.6)	616 (6)	4	74.5	25.5			16.3	30.2	421	0.1601	0.0545
IC10475	800	753 (60.8)	206 (7)	4	51.7	48.3			8.6	23.4	321	0.1239	0.0202
IC10476	800	608 (3.6)	343 (12)	4	63.2	36.8			11.3	4.7	36.7	0.0137	0.0012
IC10477	800	725 (9.9)	344 (7)	4	63.2	36.8			11.3	17.9	257.1	0.0998	0.0086
IC10478	800	509 (23.5)	345 (8)	4	63.2	36.8			11.3	2.4	26.8	0.0104	0.0026
IC10479	800	752 (39.1)	348 (7)	4	46.2	53.8			15.5	32.7	443.4	0.1710	0.0383
IC10480	800	764 (11)	345 (3)	4	77	23			9.3	19.9	299.6	0.1160	0.0173
IC10481	800	760 (16.4)	348 (8)	4	30	70			23.8	39.4	489.3	0.1861	0.0510
IC10482	800	754 (4)	344 (61)	4	36.4	63.6			19.6	38.2	491.1	0.1818	0.0801

Run <sup>a</sup>	Treatment Conditions				Treatment Gas Composition, mole %						Treat. Gas Feed Rate, mmol/min	Mass Loss <sup>c</sup> , %	Surface Area, m <sup>2</sup> /g	Pore Volume, cm <sup>3</sup> /g	
	Temperature <sup>b</sup> , °C		Pres. °C	Length	CO <sub>2</sub>	H <sub>2</sub> O	N <sub>2</sub>	O <sub>2</sub>	micro	meso					
	Set	Actual												kPa	h
IC10483	800	740 (56.9)	350 (8)	4	30	70			23.8	43.5	532.9	0.1980	0.0688		
IC10484	800	667 (31)	624 (8)	4	61.9	38.1			19.7	28.3	241.3	0.0928	0.0058		
IC10485	700	476 (5.1)	624 (8)	4	61.9	38.1			19.7	0.6	25.5	0.0097	0.0025		
IC10486	800	752 (9.3)	626 (7)	4	61.9	38.1			19.7	32.7	452.2	0.1744	0.0408		
IC10487	600	578 (9.9)	625 (8)	4	61.9	38.1			19.7	2.6	39.4	0.0143	0.0011		
IC10488	750	715 (6)	627 (9)	4	61.9	38.1			19.7	22.2	376.8	0.1476	0.0198		
IC10489	800	770 (5.1)	345 (7)	4	63.2	36.8			11.3	25.2	346.4	0.1339	0.0251		
IC10490	600	608 (1.4)	347 (4)	4	63.2	36.8			11.3	3	33.4	0.0122	0.0015		
IC10491	800	773 (1.5)	346 (5)	4	77	23			9.3	17.6	310.2	0.1197	0.0177		
IC10492	800	756 (22.9)	344 (3)	4	63.2	36.8			11.3	-2.5	221.8	0.0859	0.0133		
IC10493	800	766 (2.4)	347 (10)	1.7	63.2	36.8			11.3	41.6	234.5	0.0883	0.0343		
IC10494	800	771 (1.5)	346 (4)	4	63.2	36.8			11.3	34.5	353.4	0.1376	0.0278		
IC10495	800	766 (23.2)	346 (5)	4	63.2	36.8			11.3	28	355	0.1361	0.0267		
IC10496	800	761 (38.3)	348 (7)	4	63.2	36.8			11.3	29.3	363.4	0.1406	0.0277		
IC10497	800	770 (18.1)	346 (3)	4	63.2	36.8			11.3	22.8	437.1	0.1350	0.0266		
IC10498	800	764 (40.2)	348 (6)	4	63.2	36.8			11.3	26.6	178.1	0.0688	0.0139		
IC10499	700	697 (6.2)	625 (8)	4	61.9	38.1			19.7	15.1	120.7	0.0472	0.0045		
IC104100	800	771 (5.5)	625 (8)	4	61.9	38.1			19.7	34.5	428.9	0.1636	0.0434		
IC104101	750	738 (3.4)	624 (7)	4	61.9	38.1			19.7	22.3	370.3	0.1448	0.0186		
IC104102	800	767 (12.6)	351 (8)	4	36.4	63.6			19.6	37.4	468.4	0.1770	0.0489		
IC104103	750	734 (20.8)	348 (8)	4	63.2	36.8			11.3	17	285.2	0.1109	0.0124		
IC104104	800	762 (66.3)	348 (4)	4	68.7	31.3			13.3	25	366.6	0.1423	0.0274		
IC104105	800	766 (17.1)	243 (6)	4	68.9	31.1			13.4	22.2	287.2	0.1113	0.0189		
IC104106	800	767 (37.7)	625 (9)	4	69.1	30.9			13.5	26.5	310.9	0.1204	0.0203		
IC20401	800	789 (1.9)	108 (6)	4	27.7	72.3			5.8	18.0	222.9	0.0841	0.0159		
IC20402	800	776 (29.9)	209 (5)	4	56.9	43.1			18.7	18.7	234.0	0.0878	0.0210		
IC20403	800	802 (1.4)	348 (3)	4	68.0	32.0			28.7	28.7	295.6	0.1116	0.0244		
IC20404	800	783 (13.2)	485 (3)	4	73.9	26.1			26.2	26.2	304.2	0.1154	0.0250		
IC20405	800	767 (24.1)	497 (186)	4	78.2	21.8			14.8	14.8	97.5	0.0361	0.0058		
IC20407	800	789 (1.9)	208 (3)	4	18.5	81.5			20.8	20.8	188.8	0.0695	0.0154		
IC20408	800	787 (1.8)	346 (3)	4	57.7	42.3			24.7	24.7	255.2	0.0965	0.0187		
IC20410	800	778 (0.8)	623 (4)	4	75.4	26.5			19.1	19.1	255.5	0.0974	0.01292		

Run <sup>a</sup>	Treatment Conditions				Treatment Gas Composition, mole %				Treat. Gas Feed Rate, mmol/min	Mass Loss <sup>c</sup> , %	Surface Area, m <sup>2</sup> /g		Pore Volume, cm <sup>3</sup> /g	
	Temperature <sup>b</sup> , °C		Pres. <sup>c</sup> kPa	Length h	CO <sub>2</sub>	H <sub>2</sub> O	N <sub>2</sub>	O <sub>2</sub>			micro	meso		
	Set	Actual												
IC20411	800	720 (130.8)	132 (11)	4	2.9	97.1			29.2	340.8	0.1286	0.0357		
IC20412	800	776 (3.4)	210 (5)	4	13.2	86.8			24.5	390.2	0.1464	0.0441		
LW104114	800	777 (1.7)	143 (21)	4	13.2	86.8			14.4	275.0	0.1063	0.0136		
LW104115	800	776 (1.3)	141 (8)	2	13.2	86.8			14.4	169.4	0.0655	0.0048		
LW104116	800	773 (1.4)	147 (12)	0.5	13.2	86.8			14.4	54.9	0.0205	0.0013		
LW104117	800	773 (0.9)	137 (24)	8	13.2	86.8			14.4	433.7	0.1640	0.0395		
LW104118	800	774 (0.9)	138 (7)	1	13.2	86.8			14.4	100.1	0.0379	0.0023		
LW104119	800	777 (1.5)	141 (15)	2		86.8	13.2		14.4	176.8	0.0640	0.0047		
LW104120	800	777 (1.0)	140 (14)	1		86.8	13.2		14.4	104.9	0.0377	0.0022		
LW104121	800	778 (1.6)	143 (16)	4		86.8	13.2		14.4	306.2	0.1183	0.0163		
LW104122	800	779 (1.6)	137 (12)	8		86.8	13.2		14.4	411.8	0.1570	0.0339		
LW104123	800	774 (1.4)	141 (27)	0.5		86.8	13.2		14.4	46.3	0.0172	0.0013		

<sup>a</sup> The format of the Run Numbers is XYYZZ, where XX are the initials of the person who did the, YYY identifies the starting coke samples, i.e. 104 refers to Coke104, and ZZ or ZZZ is the sequential run number; the runs are listed in chronological order.

<sup>b</sup> The **Set** temperature is the temperature set on the controller and the **Actual** temperature is the average of the temperature acquired, at intervals of 1 min or less, from the thermocouple located on top of the coke particles; the values in brackets are the standard deviation of these temperatures.

<sup>c</sup> The pressure is the average inlet pressure; for runs MB20201 and prior, was not monitored and the listed inlet pressure of about 100 kPa corresponds to an exit pressure of atmospheric pressure; for subsequent runs the inlet pressure was recorded by the data acquisition system at 1 minute or shorter intervals. The values listed for these runs are the average values and the values in brackets are the standard deviation of these pressures.

<sup>d</sup> The initial mass for all the treatments was about 10 g.

Table A-2. Summary of pulse mercury adsorption results.

Sample ID	Sample Size, mg	Sorption Temp, °C	Avg. Hg injected through detector, pg	Avg. Area of Calibration Injections, a.u.	Average Standard Response	No of Hg pulses injected	Hg B.T. after pulse no.	Total Hg injected, pg	Area of first BT pulse, a.u.	Fraction of First Pulse adsorbed	Hg adsorbed, pg Hg/mg AC
SS10424	43	125	821.9	755314.3	821.9	10	2	1663.9	6493	1.00	38.7
SS10424	43.1	120	898.4	807872.7	898.4	10	2	1801.6	6111	1.00	41.8
SS10424	48.3	140	898.4	846615	900.8	10	1	908.2	140031	0.83	17.2
SS10410	42.2	50	810.1	727525	898.1	5	0	4067.2	0	1.00	96.4
SS10410	46.6	75	820.2	762313	929.5	5	3	2490.8	1671	1.00	53.4
SS10410	45.3	100	837.1	794188.3	948.7	5	1	830.3	17469	0.98	18.2
SS10410	42.3	150	812.3	654485.7	805.7	4	1	816.8	107399	0.84	18.1
IC10482	42.1	150	833.7	691003.3	828.9	5	1	837.1	10501	0.98	19.8
IC10482	41.8	140	846.3	744324	879.6	5	0	4289.3	0	1.00	102.6
IC10482	46.2	130	806.8	701659	869.7	5	0	4104	0	1.00	88.8
IC10482	46.4	175	848.6	716253.3	844.8	5	1	857.9	162639	0.78	16.3
IC10482	41	200	899.6	749702.7	833.4	3	1	908.2	440969	0.42	8.5
SS10424	44.6	150	863.7	721331.5	868.4	5	1	879.1	29890	0.96	19.5
SS10424	44	175	805.7	679655.3	805.7	3	1	803.5	213237	0.67	14.7
SS10424	41.7	200	619.6	487288	619.6	3	1	631.9	354200	0.10	5.9
IC10482	45.5	150	673.6	538113.3	798.9	6	0	4138.1	0	1.00	90.9
IC10470	45.2	150	660.6	573733.3	868.5	5	1	675.5	171409	0.71	12.5
IC10471	41.5	150	710	592794.7	834.9	5	1	710	82547	0.86	16.3
SS10403	44.8	140	830.5	624845.3	752.4	1	1	830.3	554158	0.11	1.2
SS10416	42.8	140	857.9	672043.3	783.4	1	1	857.9	614096	0.09	-0.7
SS10419	45.2	140	893.5	707364.3	791.7	1	1	886.3	563932	0.20	2
SS10428	40.7	140	796.1	629619.5	790.9	2	1	803.5	31417	0.95	19.5

Sample ID	Sample Size, mg	Sorption Temp, °C	Avg. Hg injected through detector, pg	Avg. Area of Calibration Injections, a.u.	Average Standard Response	No of Hg pulses injected	Hg B.T. after pulse no.	Total Hg injected, pg	Area of first BT pulse, a.u.	Fraction of First Pulse adsorbed	Hg adsorbed, pg Hg/mg AC
SS10430	45.4	140	818.9	637048.7	777.9	2	1	823.5	198431	0.69	15.1
SS10415	41.5	140	849.8	674306.3	793.5	4	0	3413.9	0	1.00	82.3
SS10420	41.5	140	858.7	674563.3	785.5	4	2	1701.7	3718	1.00	41
SS10423	42.6	140	800.2	634206.7	792.6	2	1	806.8	474291	0.26	4.3
SS10432	42.7	140	785	674315.7	859	2	1	787.2	50527	0.93	18
SS10429	42.6	140	771.1	662445	859.1	4	0	3075.1	0	1.00	72.2
SS10421	44.5	140	771.1	656788.3	851.7	2	1	771.2	46050	0.93	17
SS10424	42.5	140	764.8	643444.7	841.3	2	2	1520.2	2996	1.00	35.8
MB10458	40.9	140	777.5	638980.3	821.8	3	3	2338	21463	0.99	57
MB10460	46.4	140	802.4	641934.3	800	2	1	806.8	157670	0.76	15.3
IC10478	46.6	140	834.8	625148.3	748.8	2	1	826.9	567215	0.08	0.5
IC10477	45.6	140	857.9	647667.3	755	2	1	857.9	1981	1.00	18.8
IC10476	46.5	140	888.7	648870	730.2	2	1	889.9	518080	0.20	3.9
IC10472	42.8	140	779.2	596278.8	765.2	1	1	793.7	345402	0.43	9.9
IC10468	44.8	140	801.3	624677	779.6	2	1	803.5	11298	0.98	17.9
IC10467	42.4	140	802.4	630768.3	786.1	2	1	796.9	197925	0.68	15.5
MB10465	45.3	140	688.7	579035.7	840.8	4	3	2066.2	24841	0.99	45.5
IC10466	49.2	140	726	554917	764.4	3	1	727.9	16323	0.97	14.7
IC10464	48.2	140	746.2	567529	760.6	3	1	752.3	15994	0.97	15.5
MB10463	45.7	140	794.7	528386	664.9	2	1	793.6	79352	0.85	16.7
MB10462	44.8	140	685.9	528299	770.3	2	1	686.8	384930	0.27	5.3
MB10461	42.6	140	694.5	528845.3	761.5	2	1	695.4	402414	0.24	4.9
IC10469	45.5	140	599.2	444022.7	741.1	2	1	741.1	4929	0.99	16.3

Sample ID	Sample Size, mg	Sorption Temp, °C	Avg. Hg injected through detector, pg	Avg. Area of Calibration Injections, a.u.	Average Standard Response	No of Hg pulses injected	Hg B.T. after pulse no.	Total Hg injected, pg	Area of first BT pulse, a.u.	Fraction of First Pulse adsorbed	Hg adsorbed, pg Hg/mg AC
IC10480	42.3	140	602.6	453915.7	753.3	4	4	2405.9	10478	0.99	56.8
IC10480	41.8	140	578.5	453885.3	784.6	2	1	578.5	86959	0.81	12.9
IC10481	43.2	140	581.8	428413	736.4	4	2	1169.3	2627	1.00	27.1
IC10473	46.1	140	590	443452.7	751.7	4	0	2341	0	1.00	50.8
IC10473	42.4	140	579.1	406142.5	701.3	2	1	578.5	140559	0.65	11.8
IC10482	45.4	140	591.7	442642.3	748.1	2	1	590.8	19229	0.96	12.9
IC10499	46.6	140	603.4	450004.7	745.8	4	0	2423.6	0	1.00	52
IC10499	45.8	140	597.7	482338.3	807	4	1	595.8	24081	0.95	12.9
IC10486	41.4	140	607.2	474098.5	780.8	4	0	2444	0	1.00	59
IC10486	43.8	140	656.1	471372.7	718.5	2	1	658.8	24547	0.95	14.9
IC10488	42.6	140	671.8	495817	738	4	1	669.9	4023	0.99	15.7
IC10488	40.7	140	628	457355	728.3	4	2	629.2	32358	0.93	15.2
IC10487	45.2	140	671.8	522033.3	777	2	1	672.7	101524	0.81	13.8
IC10485	42.4	140	680.2	536444	788.7	2	1	681.1	390187	0.27	5.2
SS10424	40.7	140	677.4	528589.3	780.4	3	0	2029.3	0	1.00	49.9
IC10479	41.8	140	627.5	459436.3	732.2	3	0	1892.9	0	1.00	45.3
IC10494	43.7	140	644.3	481945	748.1	4	1	645.2	4688	0.99	14.7
IC10495	42	140	665.3	484340	728	3	0	2006.9	0	1.00	47.8
IC10474_S_600	45.2	140	669.9	531550.7	793.5	4	1	669.9	9664	0.98	14.8
IC10496	45.4	140	689.7	528777.7	766.7	3	1	692.6	5641	0.99	15.2
IC10497	42.5	140	706.1	486916	689.6	3	2	1423	2458	1.00	33.5
IC104106	42.6	140	731.8	537793.3	734.9	4	2	1474	5290	1.00	34.6
IC104105	41.1	140	707.2	535290.5	757	4	0	3034.2	0	1.00	73.8

Sample ID	Sample Size, mg	Sorption Temp, °C	Avg. Hg injected through detector, pg	Avg. Area of Calibration Injections, a.u.	Average Standard Response	No of Hg pulses injected	Hg B.T. after pulse no.	Total Hg injected, pg	Area of first BT pulse, a.u.	Fraction of First Pulse adsorbed	Hg adsorbed, pg Hg/mg AC
IC10474	45.1	140	659.8	421655	639.1	4	0	2567.4	0	1.00	56.9
IC104104	48.6	140	697.4	463270	664.3	4	0	2657.2	0	1.00	54.7
IC10489	45.3	140	700.7	462894.7	660.6	4	0	2640.7	0	1.00	58.3
IC10498	45.4	140	695.1	443504.7	638.1	4	2	1277	1453	1.00	28.1
IC10474_S_600	46.6	140	666.2	474105.7	711.7	4	0	2665.6	0	1.00	57.2
IC 104106	42.5	140	674	454011.3	673.6	4	2	1351	1269	1.00	31.8
IC 10488	41.9	140	734.2	444771.3	605.8	4	0	2428.7	0	1.00	58
IC10474_S_600	44.8	200	640.7	458382.7	715.4	2	1	637.2	59295	1.00	13.8
IC10474_S_600	45.5	175	669.4	490739.7	733.1	6	2	1306.7	0	1.00	28.7
IC10474_S_600	41.5	160	763.2	538367.5	705.4	6	4	3059.2	0	1.0	73.7
IC104100	43	140	705.5	539526.3	764.8	4	0	3059.2	0	1.00	71.1
IC104101	45.2	140	707.3	519046.7	733.9	6	0	4415.6	0	1.00	97.7
MB10450	46.6	140	706.8	518727.3	733.9	2	1	733.9	24670	0.95	15.6
MB10451	43.5	140	720.7	528919.3	733.9	2	1	733.9	44223	0.92	16.6
MB10452	42.1	140	734.9	536356.3	729.9	1	1	727.9	253444	0.52	12.3
MB10453	43.3	140	733	531340.7	724.8	1	1	724.9	209335	0.60	13.2
MB10454	46.3	140	694	510757.3	735.9	1	1	740	538544	0.01	-0.2
MB10440	47.1	140	674.8	510480	756.5	1	1	758.6	561259	0.02	-0.7
MB10450	45.9	140	704.1	515463	732	1	1	737	107654	0.80	14.9
IC104102	42.2	140	697.5	547446.7	739	4	0	2969.2	0	1.00	70.4



Sample ID	Sample Size, mg	Sorption Temp, °C	Avg. Hg injected through detector, pg	Avg. Area of Calibration Injections, a.u.	Average Standard Response	No of Hg pulses injected	Hg B.T. after pulse no.	Total Hg injected, pg	Area of first BT pulse, a.u.	Fraction of First Pulse adsorbed	Hg adsorbed, pg Hg/mg AC
IC104103	47.4	140	753.8	483249	726.2	2	1	727.9	53897	0.90	15
IC10490	46	140	687.2	485886.3	703.2	1	1	713	259100	0.48	10.7
IC10491	42.8	140	682.4	532483.3	712	6	0	4286.6	0	1.00	100.2
IC10469	43.2	140	741.7	452142.3	717.9	4	0	2857.7	0	1.00	66.2
IC10487	49	140	674	492073	670.8	1	1	713	543726	-0.14	-0.9
IC10483	41.8	140	685.9	473661.3	717.4	6	0	4149.6	0	1.00	99.3
IC10481	44	140	690.6	448558.8	685.9	6	0	4152.4	0	1.00	94.4
IC10469	44.1	140	692.5	459317	647.7	2	1	1396.6	10200	0.99	31.6
IC10489	46.9	140	723.8	490468.3	634.6	2	1	721.9	17728	0.96	15.3
IC10477	40.8	140	744.1	500868	659.2	2	1	740	48264	0.90	17.8
IC10472	44.7	140	733.9	497146.7	682.5	2	1	733.9	125611	0.75	14.9
IC10476	46.1	140	734.9	480286.7	676.5	2	1	733.9	385485	0.22	6.1
IC10486	44.5	140	734.2	351706	654.1	5	0	3687.8	0	1.00	82.9
IC104100	42	140	721.7	495219.3	487.3	5	0	3709.2	0	1.00	88.3
IC10488	45.9	140	745.1	504477	664.6	2	1	746.2	5566	0.99	16.2
IC104101	49	140	747.2	468828	675.2	5	0	3727.7	0	1.00	76.1
IC10499	46.5	140	717.9	476227.7	653.1	2	1	721.9	15946	0.97	15.5
IC10487	47.3	140	723.8	498984	657.9	1	1	724.9	307899	0.35	9
IC10488	43.1	140	725.9	455937.7	687.4	2	1	727.9	28968	0.94	16.7
IC10491	46.1	140	686.8	463593	663.9	5	0	3451.3	0	1.00	74.9
IC104102	44.2	140	696.4	522971.3	665.7	4	0	2793.2	0	1.00	63.2
IC10474_S_400	42.6	175	638	438705.7	687.6	6	0	3838.9	0	1.00	90.1

Sample ID	Sample Size, mg	Sorption Temp, °C	Avg. Hg injected through detector, pg	Avg. Area of Calibration Injections, a.u.	Average Standard Response	No of Hg pulses injected	Hg B.T. after pulse no.	Total Hg injected, pg	Area of first BT pulse, a.u.	Fraction of First Pulse adsorbed	Hg adsorbed, pg Hg/mg AC
IC10474_S_400	41.8	200	618.7	433381.3	700.5	2	1	618.8	25961	0.94	14.6
IC10474_S_400	42	250	614.4	479832	780.9	1	1	616.2	146275	0.70	12.9
IC10474_S_200	41.2	200	599.2	478621.7	798.8	1	1	600.9	569177	-0.19	0.4
IC10474_S_200	40.6	140	576.9	522106	905.1	1	1	576.1	161996	0.69	12.1
IC10474_S_400	40	140	577.7	521185.7	902.2	7	0	4049.5	0	1.00	101.2
IC10474_S_600	46.4	140	634	577034	910.1	6	2	1277	2139	1.00	27.5
IC10474_S_200	42.1	175	693.5	537906.7	775.6	1	1	698.3	486723	0.10	5.9
IC10474	43.4	140	640.6	623595.3	973.5	6	2	1287.7	4475	1.00	29.6
IC10474	43.4	175	642.5	593344	923.5	1	1	642.5	90888	0.85	13.9
IC10474	43.7	200	647	581638.3	899	1	1	653.4	439854	0.25	6.3
IC10480	47.4	140	746.1	589630	790.2	2	1	746.2	7177	0.99	15.7
IC10483	41	140	821.3	733889.3	893.6	3	1	820.2	4223	0.99	20
IC10490	47.6	140	830.3	710487.3	855.8	1	1	830.3	534169	0.25	6.4
IC10498	47.3	140	817.9	696406.3	851.5	4	0	3277.2	0	1.00	69.3
IC104103	42.4	140	823.5	708309	860.1	1	1	823.5	194939	0.72	16.8
IC104105	47.3	140	829.1	697577	841.4	3	2	1653.7	7694	0.99	34.9
IC104104	43.9	140	819	715866	874.1	3	0	2460.5	0	1.00	56
IC10484	44.7	140	787.2	687033	872.7	3	1	790.4	7996	0.99	17.6

Sample ID	Sample Size, mg	Sorption Temp, °C	Avg. Hg injected through detector, pg	Avg. Area of Calibration Injections, a.u.	Average Standard Response	No of Hg pulses injected	Hg B.T. after pulse no.	Total Hg injected, pg	Area of first BT pulse, a.u.	Fraction of First Pulse adsorbed	Hg adsorbed, pg Hg/mg AC
IC10477	44.5	140	793.7	673119.7	848.1	3	1	793.7	9652	0.99	17.8
IC104104	48.3	140	749.2	654200.5	873.2	9	7	5250.7	9105	1.00	108.6
MB10440	46.5	140	793.7	672584.8	847.4	1	1	803.5	777779	-0.14	-4.8
MB10450	41	140	820.2	685532	835.9	1	1	823.5	39743	0.94	19.7
MB10451	46	140	820.1	697136.3	850	1	1	823.5	238960	0.66	14.7
MB10452	47.8	140	811.2	698461	861	1	1	810.1	500400	0.28	7.1
MB10453	42.9	140	803.5	708614.7	881.9	1	1	803.5	200771	0.72	16
MB10454	42	140	800.2	678126	847.5	1	1	796.9	680424	-0.01	3.2
IC104106	41	140	799	684436	856.6	2	1	803.5	7889	0.99	19.5
IC10497	46.1	140	789.3	714246	904.9	2	1	790.4	3092	1.00	17.1
IC10489	47.7	140	838.2	715347.3	853.4	2	1	837.1	7890	0.99	17.5
IC10475	43.2	140	864.9	752963.7	870.6	4	2	1729.7	1721	1.00	40
IC10472	46.9	140	889.9	768277.3	863.4	1	1	889.9	460367	0.40	11.7
IC10476	45.7	140	891.1	779965	875.3	1	1	889.9	625957	0.20	7
IC10469	45.9	140	900.8	790004.7	877	4	2	1801.6	3597	1.00	39.2
IC10478	47.2	140	910.5	776359.3	852.6	1	1	908.2	716441	0.07	3.7
IC10479	45.1	140	910.6	790307	867.9	3	2	1827.4	5282	1.00	40.5
IC104101	43.3	140	876.7	769109.7	877.3	8	0	7043.2	0	1.00	162.7
IC10488	40.3	140	882.7	780523.3	884.3	4	2	1765.3	3308	1.00	43.8
IC10474_S_500	42.6	140	772.1	576475.3	746.6	4	0	3155.2	0	1.00	74.1
IC10474_S_500	43.6	200	806.8	578253.3	716.7	4	2	1620.2	2676	1.00	37.1

Sample ID	Sample Size, mg	Sorption Temp, °C	Avg. Hg injected through detector, pg	Avg. Area of Calibration Injections, a.u.	Average Standard Response	No of Hg pulses injected	Hg B.T. after pulse no.	Total Hg injected, pg	Area of first BT pulse, a.u.	Fraction of First Pulse adsorbed	Hg adsorbed, pg Hg/mg AC
IC10474_S_500	43.9	250	812.3	622677.3	766.5	2	1	813.5	125178	0.80	16.6
IC10474_S_300	44.3	200	815.7	613484	752.1	1	1	817.8	564390	0.08	2.6
IC10474_S_300	44.6	140	816.8	625320.7	765.6	2	1	816.8	9581	0.98	18.2
IC10474_S_300	43.2	100	815.7	634479.7	777.9	4	0	3267	0	1.00	75.6
IC10474_S_300	43.4	175	816.8	635976.7	778.6	1	1	816.8	243237	0.62	14.3
IC10474_S_500	44.9	175	781.8	641077.7	820	6	0	4665.2	0	1.00	103.9
MB20501	41.9	140	757.5	582170	768.5	2	1	755.4	8167	0.99	17.9
MB20701	42.4	140	762.7	588876	772.1	1	1	764.8	231416	0.61	13.7
MB20301	43.2	140	773.5	599109.5	774.5	2	1	771.2	17329	0.97	17.6
IC10491	44.6	140	860.2	777218.3	903.6	3	1	861.4	1486	1.00	19.3
IC10489-H2-13psi	46.4	140	805.7	753130.7	934.7	1	1	810.1	258486	0.66	13.5
IC10489-H2-50psi	45.6	140	831.4	750786.3	903	1	1	833.7	207162	0.72	15.2
IC10489	46.3	140	848.6	769438	906.7	1	1	850.9	44436	0.94	17.8
SS10432-H2-50psi	45.5	140	856.7	778433.7	908.7	1	1	857.9	500420	0.36	9.1
SS10432-H2-13psi	45.1	140	866.6	816716	942.4	1	1	864.9	392354	0.52	12.1
IC104102	44.6	140	744.1	681247.3	915.5	2	2	1495.4	4593	1.00	33.5
IC104102	45.2	140	839.4	729334.7	868.9	2	1	840.5	1382	1.00	18.6

Sample ID	Sample Size, mg	Sorption Temp, °C	Avg. Hg injected through detector, pg	Avg. Area of Calibration Injections, a.u.	Average Standard Response	No of Hg pulses injected	Hg B.T. after pulse no.	Total Hg injected, pg	Area of first BT pulse, a.u.	Fraction of First Pulse adsorbed	Hg adsorbed, pg Hg/mg AC
SS10432	45.4	140	848.1	760576.7	896.9	2	1	845.8	5850	0.99	18.6
IC10479	45.6	140	848.4	790683.7	932	3	2	1699	11580	0.99	37.1
IC10469	44.8	140	848	771519.3	909.8	2	1	851.5	32621	0.96	18.6
IC10480	45.3	140	851.7	799371.7	938.6	2	1	856.1	17375	0.98	18.7
IC10486	45.6	140	853.9	779109	912.4	2	1	854.5	1932	1.00	18.7
IC10499	44.8	140	831.4	761841.3	916.4	2	1	830.3	98783	0.87	17.2
MB20401	43.1	140	781	731770.3	937	2	1	776.4	3305	1.00	18
MB20301	42.1	140	773.5	725455	937.8	3	2	1544.1	3657	1.00	36.6
MB20501	42.4	140	772.1	731075.7	946.9	2	1	772.1	7706	0.99	18.1
MB20701	42	140	743.1	704250.3	947.7	1	1	746.2	339803	0.52	11.5